1993-09

Analysis of radiation damaged and annealed gallium arsenide and indium phosphide solar cells using deep level transient spectroscopy.

Bruening, Joseph A.

Monterey, California. Naval Postgraduate School

Approved for public release; distribution is unlimited.

Analysis of Radiation Damaged and Annealed Gallium Arsenide and Indium Phosphide Solar Cells Using Deep Level Transient Spectroscopy

by

Joseph A. Bruening
Lieutenant United States Navy
B.S., The Ohio State University, 1982

Submitted in partial fulfillment
of the requirements for the degree of

MASTER OF SCIENCE IN ASTRONAUTICAL ENGINEERING
(SPACE SYSTEMS)

from the

NAVAL POSTGRADUATE SCHOOL
September 1993

REPORT DOCUMENTATION PAGE

a Report Security Classification: Unclassified		1b Restrictive Markings	
a Security Classification Authority		3 Distribution/Availability of Report	
b Declassification/Downgrading Schedule		Approved for public release; distribution is unlimited.	
Performing Organization Report Number(s)		5 Monitoring Organization Report Number(s)	
a Name of Performing Organization aval Postgraduate School	6b Office Symbol 31	7a Name of Monitoring Organization Naval Postgraduate School	
c Address *(city, state, and ZIP code)* Ionterey CA 93943-5000		7b Address *(city, state, and ZIP code)* Monterey CA 93943-5000	
a Name of Funding/Sponsoring Organization	6b Office Symbol *(if applicable)*	9 Procurement Instrument Identification Number	
ddress *(city, state, and ZIP code)*		10 Source of Funding Numbers	
		Program Element No	Project No / Task No / Work Unit Accession No

Title *(include security classification)* ANALYSIS OF RADIATION DAMAGED AND ANNEALED GALLIUM ARSENIDE AND NDIUM PHOSPHIDE SOLAR CELLS USING DEEP LEVEL TRANSIENT SPECTROSCOPY

Personal Author(s) BRUENING, Joseph, A.

a Type of Report	13b Time Covered	14 Date of Report *(year, month, day)*	15 Page Count
laster's Thesis	From To	1993 September	126

Supplementary Notation The views expressed in this thesis are those of the author and do not reflect the official policy or position f the Department of Defense or the U.S. Government.

Cosati Codes			18 Subject Terms *(continue on reverse if necessary and identify by block number)*
eld	Group	Subgroup	Radiation damage in solar cells; DLTS; Annealing; Heterojunction; gallium arsenide; indium phosphide

Abstract *(continue on reverse if necessary and identify by block number)*

ower loss in spacecraft solar cells due to radiation damage was investigated. The mechanisms behind the degradation and covery is based on deep-level defects in the crystalline lattice structure of the solar cell. Through a process known as Deep evel Transient Spectroscopy (DLTS), a correlation can be made between damage/recovery and trap energy of the cell. Gallium rsenide (GaAs/Ge) and Indium Phosphide (InP) solar cells were subjected to 1 MeV electron irradiation, to fluences of 1E16 ectrons/cm^2. Attempts at recovery included thermal annealing, alone, and with an applied forward bias current, and hotoinjection annealing. Various cycles of irradiation, annealing and DLTS were performed, in an attempt to correlate damage to ap energy level and growth.

The results show that DLTS cannot be performed on GaAs/Ge, and no recovery was apparent in these cells. DLTS nalysis of InP indicated excellent photoinjection annealing recovery at a variety of temperatures. Lower energy level defects are ssociated with the recovery of the cells while the higher energy traps are indicative of permanent degradation in the InP solar ells. Applying this information to future research could increase satellite mission life, and significantly reduce space mission osts.

Distribution/Availability of Abstract X unclassified/unlimited __ same as report __ DTIC users	21 Abstract Security Classification Unclassified	
a Name of Responsible Individual IICHAEL, Sherif	22b Telephone *(include Area Code)* 408-656-2252	22c Office Symbol EC/Mi

D FORM 1473,84 MAR 83 APR edition may be used until exhausted security classification of this pag
All other editions are obsolete Unclassifie

ABSTRACT

Power loss in solar cells due to radiation damage was investigated. The mechanisms behind the degradation and recovery is based on deep-level defects in the crystalline lattice structure of the solar cell. Through a process known as Deep Level Transient Spectroscopy (DLTS), a correlation can be made between damage/recovery and trap energy of the cell. Gallium Arsenide (GaAs/Ge) and Indium Phosphide (InP) solar cells were subjected to 1 MeV electron irradiation, to fluences of 1E16 electrons/cm^2. Attempts at recovery included thermal annealing, alone, and with an applied forward bias current, and photoinjection annealing. Various cycles of irradiation, annealing and DLTS were performed, in an attempt to correlate damage to trap energy level and growth.

The results show that DLTS cannot be performed on GaAs/Ge, and no recovery was apparent in these cells. DLTS analysis of InP indicated excellent photoinjection annealing recovery at a variety of temperatures. Lower energy level defects are associated with the recovery of the cells while the higher energy traps are indicative of permanent degradation in the InP solar cells. Applying this information to future research could increase satellite mission life, and significantly reduce space mission costs.

TABLE OF CONTENTS

I. INTRODUCTION

A. BACKGROUND

The fundamental requirements for a spacecraft power supply are low cost, long-term power generation with a high power-to weight ratio. Solar arrays are uniquely suited to meet these requirements, and the standard power source for spacecraft continues to be photovoltaic arrays. For the last thirty years, spacecraft missions have grown more diverse and complex; with a corresponding increase in power requirements. Spacecraft solar arrays are specifically sized to provide mission end-of-life (EOL) power requirements. The design and performance of an array are thus determined by the efficiency of the solar cells that comprise the array.

Solar cells are the semiconductor devices which convert solar energy to electrical power through a process known as the photovoltaic effect. The actual photovoltaic conversion efficiency of a solar cell is limited by operating environment factors, such as temperature, incident photon energy, and radiation damage. Array engineering design considerations can effectively minimize thermal and quantum efficiency losses. Radiation damage to solar cells is the primary factor in determining spacecraft EOL power. In an effort to optimize their performance, solar cells have been the subject of extensive research to increase their

efficiency, radiation tolerance, and sustainability in the space environment.

An earth-orbit exposes spacecraft to radiation effects that cause damage to the solar cell crystal lattice structure that reduce the cell's p-n junction conversion efficiency. Solid state design attempts to compensate for radiation damage have progressed slowly. The n-on-p junction silicon cell is more resistant to radiation damage than the standard p on n. As shown in Figure 1-1, protective cell coverglass, of varying thicknesses in compromise for weight considerations, provides adequate shielding from bombarding protons. However, these efforts have not extended the life of silicon solar cells to any appreciable extent. Development of other III-V compound type cells (gallium arsenide and indium phosphide) provided greater radiation hardness to incident electrons. Until recently, high manufacturing costs for these materials have discouraged large scale production. Current advances in the solid state electronics industry have greatly increased the demand for III-V materials, with a corresponding decrease in manufacturing costs. Gallium arsenide has been discovered to have a particularly wide range of applications, and is rapidly becoming more economically attractive.

However, radiation damage to solar cells reduces their theoretical conversion efficiency (Figures 1-2 and 1-3), and what is needed is a process which would actually reverse the degradation in the cells.

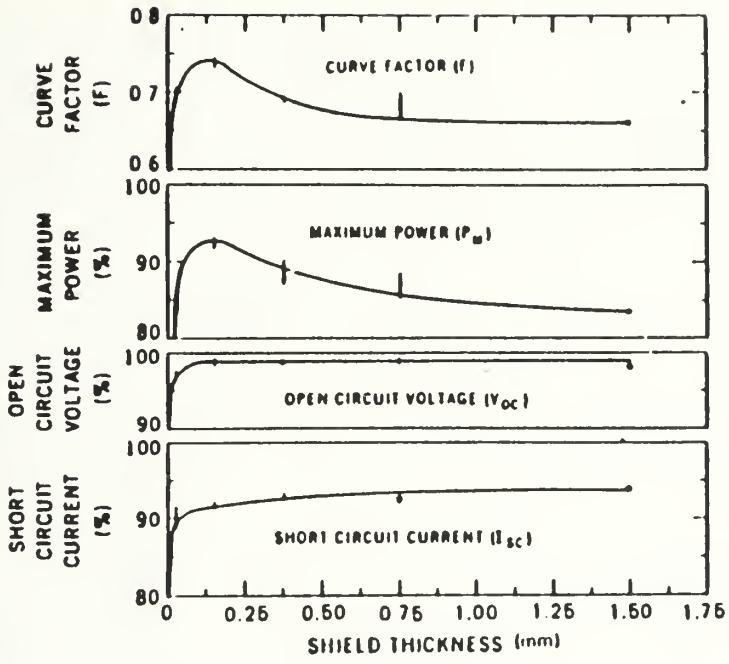

Figure 1-1 A.

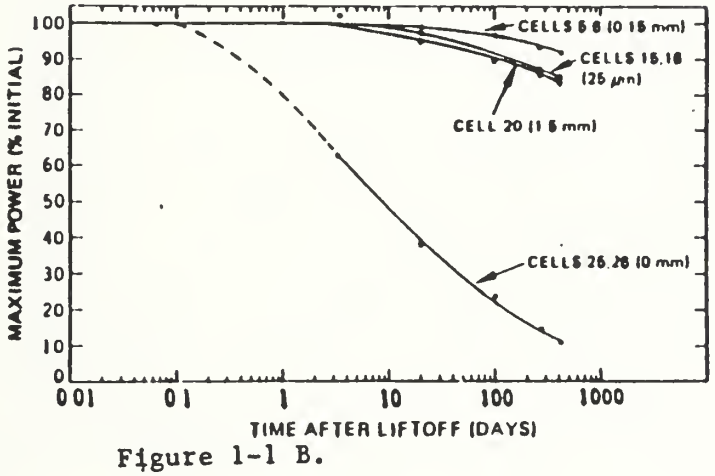

Figure 1-1 B.

Figure 1-1. The protective effect of coverglass shielding on the performance parameters of Silicon solar cells. (A.) After 417 days in orbit; and (B.) Normalized maximum power conserved by additional shielding. The coverglass screens primarily proton damage. [Ref 1: p. 11.13-5]

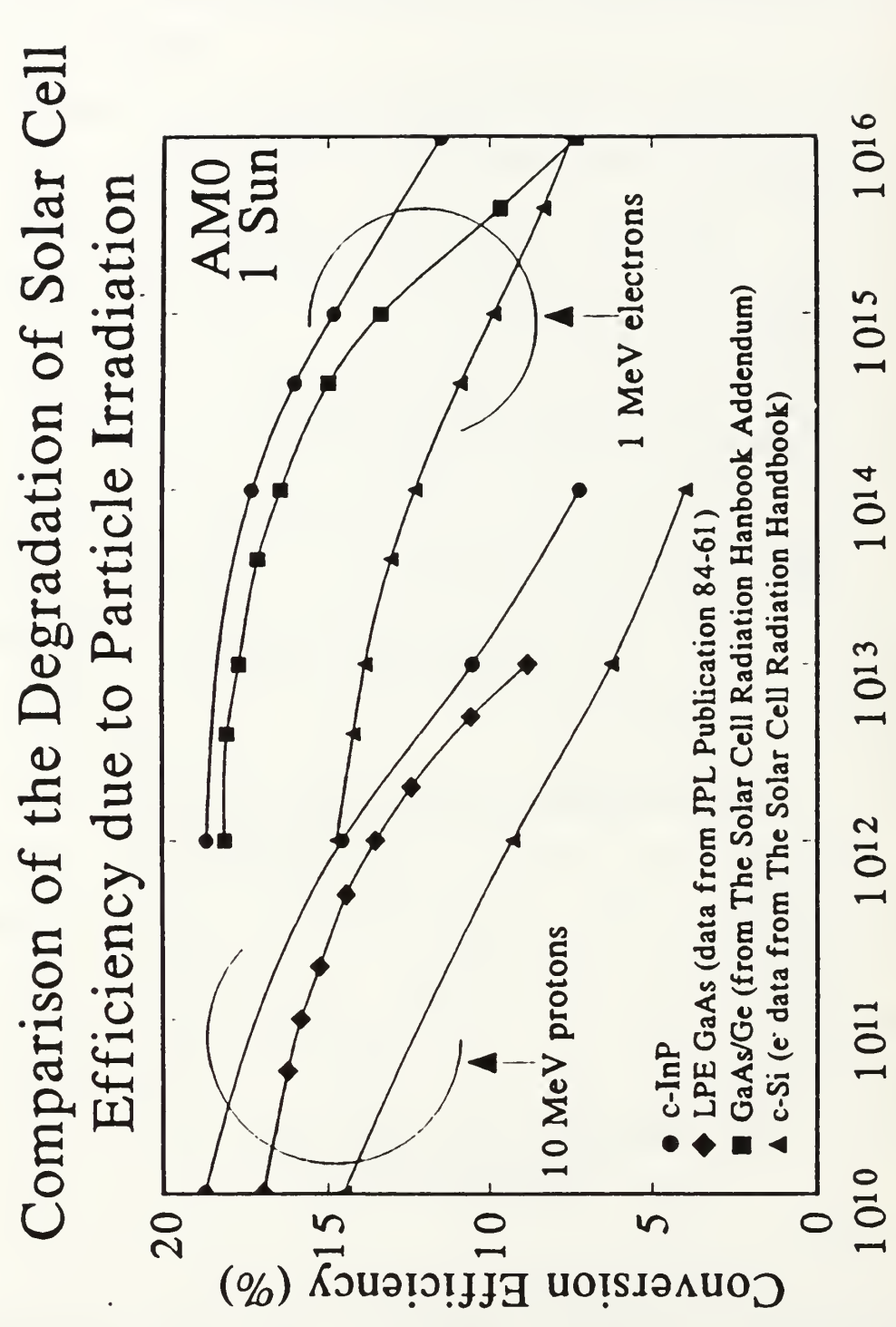

Figure 1-2. The degradation of Silicon, Gallium Arsenide, and Indium Phosphide solar cells due to electron and proton irradiation. [Ref 2: p. IV-9]

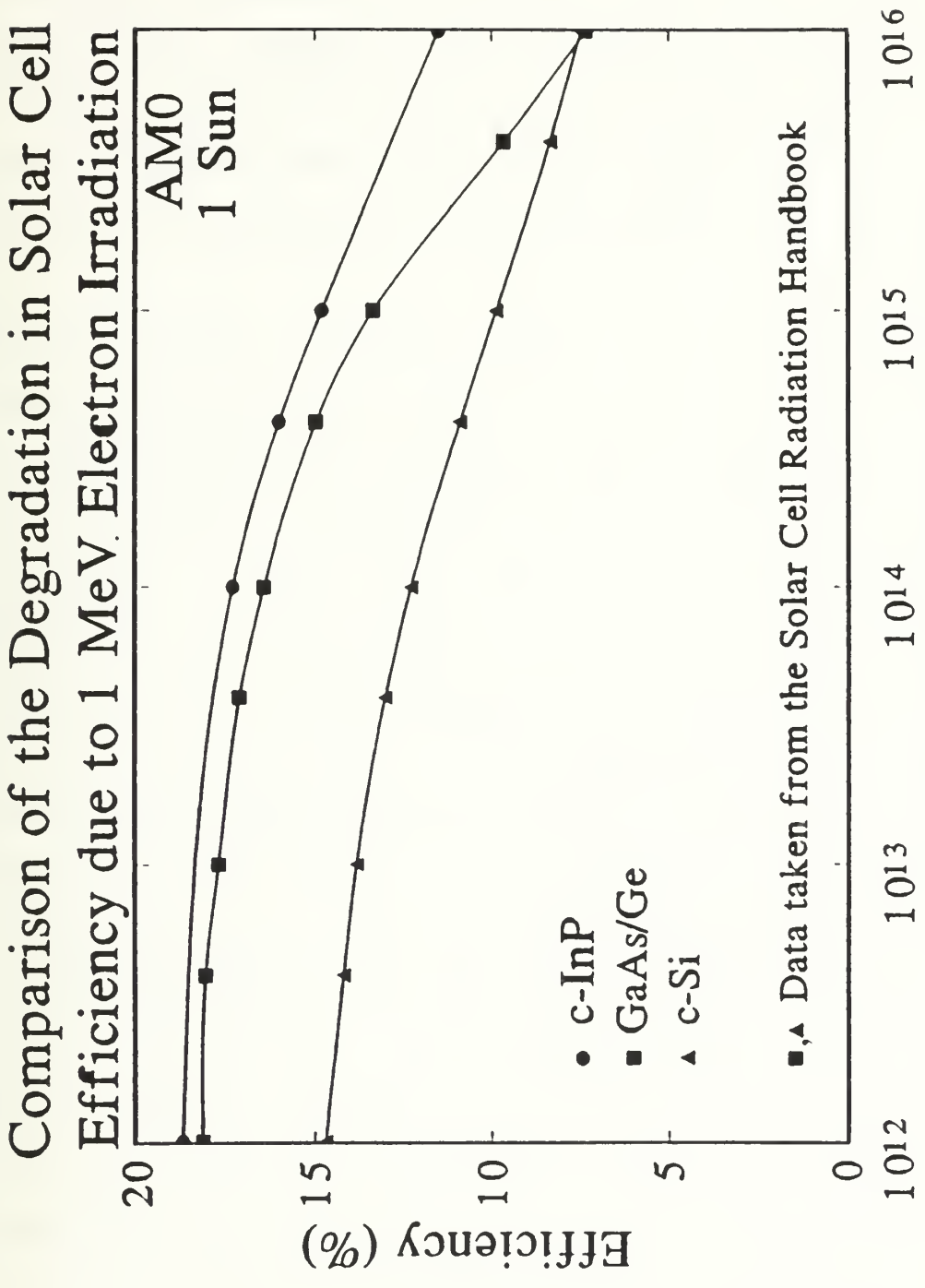

Figure 1-3. The predicted degradation of Silicon, Gallium Arsenide, and Indium Phosphide solar cells due to 1 MeV electron irradiation. [Ref 2: p. IV-34]

If this could be accomplished while on orbit, the process would present the most attractive alternative spacecraft missions lost to inadequate power supply. Cell damage recovery would extend the life of the spacecraft, decrease array design mass and size requirements, and increase payload. The economic advantages promise great potential for research in this area.

The potential for on-orbit radiation damage recovery became apparent when an annealing process was found to restore the electrical power generation loss experienced when the cells were subjected to radiation damage. The recovery was significant enough that the end of life (EOL) of a spacecraft could be extended well beyond present capability, and greatly reduce the size of the deployed array. Currently, a spacecraft will experience about a 30 percent reduction in power after 10 years in geosynchronous orbit and designers correct for this by deploying an array that initially generates 130 percent of EOL power (Figure 1-4). Reducing the beginning of life (BOL) array size has extraordinary financial implications not only because excess solar cells would no longer have to be purchased and assembled, but more so from the great savings realized in lifting less mass into orbit. Thus, with an effective power recovery process, the overall financial benefits are significant.

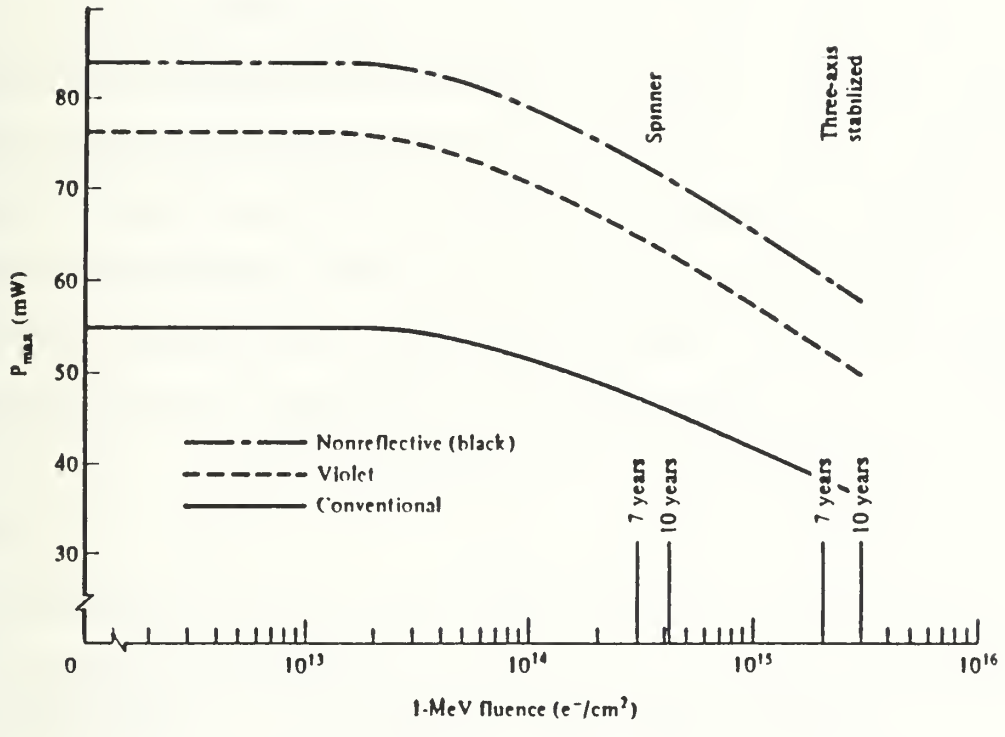

Figure 1-4. Maximum power output of conventional, violet, and nonreflective silicon solar cells as a function of 1-MeV electron irradiation. [Ref 3: p. 336]

B. SOLAR CELL TECHNOLOGY

To date, virtually all spacecraft solar arrays have been constructed using silicon solar cells. Many design methods have been implemented to improve the orbital life of silicon cells: coverglass, vertical junctions, back-surface-fields, thin cells, etc. Little satisfactory improvement has been made in extending the life of silicon arrays. The fundamental problems of silicon technology are its bandgap, responsible for its low conversion efficiency, and intolerance for radiation. This has made deployment of solar arrays that are over-designed (in size and mass) the only acceptable solution to meeting spacecraft end-of-life power demands. Silicon has significant advantages in cost, demonstrated performance, and simplicity [Ref. 4]. Table 1-1 indicates the comparative advantages of the most promising materials for replacing silicon as the predominant solar cell substrate.

TABLE 1-1
ELECTRICAL PROPERTIES OF COMMON PHOTOVOLTAIC MATERIALS

Solar Cell	Bandgap Eg (eV)	Efficiency BOL (%)		Specific Power BOL (W/kg)		Annealing Temp (°C)
		25°C	60°C	25°C	60°C	Note (1)
Silicon	1.14	15	12.7	113	96	400
GaAs	1.42	19	17.9	131	123	230
InP	1.35	18	16.4	126	115	25

(1) Minimum demonstrated temperatures for recovery with no minority carrier injection.

Gallium arsenide has recently been found to have many applications in the micro-electronics industry and is expected to replace silicon in many areas. The cost of gallium arsenide has dropped to a level where it is becoming competitive with silicon for space solar array applications. Not only are gallium arsenide solar cells more radiation tolerant than silicon, it has a higher conversion efficiency, and a lower thermal annealing temperature.

The most attractive parameters in a spacecraft solar cell, other than low cost, are radiation tolerance and high photoelectric conversion efficiency. Minimizing the deployed mass of the solar array is also a critical issue due to the high launch costs associated with getting the spacecraft into orbit. Launch costs are generally measured in thousands of dollars per kilogram, but fail to include the additional expenses of array assembly, array stowed size, and additional attitude control fuel to suppress the dynamic response of the deployed array.

C. RESEARCH PURPOSES

This research is seeks to investigate the solid state mechanisms involving the lattice structure degradation and recovery of gallium arsenide (GaAs) and indium phosphide (InP) solar cells through the use of Deep Level Transient Spectroscopy (DLTS). Preliminary investigation into the feasibility of annealing electron-damaged solar cells has been widely accepted for several years. Research has established

that after irradiation at a fluence level of between 1E14 and 1E15 el/cm^2, the effects of damage caused by trapped electrons was reversed in GaAs and InP solar cells.

Previous research conducted single annealing experiments to determine the optimum mechanism for recovery of radiation-damaged GaAs cells. Cypranowski [Ref. 5] continued the research for InP cells as well as investigating multiple cycles of radiation and annealing on GaAs and InP cells. Pinzon [Ref. 6] explored the forward biased current and heat annealing of GaAs and InP cells that have been electron damaged by looking into the lattice structure, via DLTS, to determine the mechanisms that affect the damage and annealing process. The purpose of this investigation was to reproduce the research of Cypranowski and Pinzon, in an effort to determine the optimum parameters for annealing gallium arsenide and indium phosphide solar cells.

Beginning with Chapter II, fundamentals of semiconductor theory and the photovoltaic effect are introduced. This information provides a foundation on which the thesis is based. Other important concepts such as p-n junction and carrier transport are also discussed. Chapter III deals with radiation effects on solar cells, the environment in which the cells must operate and outlines previous annealing research. Chapter IV continues to explain the mechanisms behind damage and recovery through a discussion of deep level transient spectroscopy and its relationship to solar cell measurement

parameters. The experiment is discussed in detail for GaAs in Chapter V, and InP in Chapter VI, with conclusions and recommendations following in Chapter VII.

II. PHOTOVOLTAICS

A. PHOTOVOLTAIC EFFECT

To understand how a solar cell converts light energy to electricity, it helpful to first consider the effect of putting a great many atoms close together in a solid. The behavior of the bulk material can be regarded as a cumulative effect of what is occurring in the individual atoms. In a solar cell incident light photons collide with atomic electrons, losing energy with each collision. The electrons that gain sufficient energy from these collisions can change to a higher energy band.

1. Energy Bands and Band Gap

In solids the potential energy experienced by a valence electron is discretely quantized as a function of its position in the atomic lattice. When atoms are brought close enough together that their wave functions overlap, the energy level of each system splits into two distinct energy levels (Figure 2-1), and the splitting increases as the separation between atoms decreases. Crystallographic symmetry effects force the energy levels of the atom to form two major energy bands, the valance band and the conductor band; each one with its own distinct levels of permissible electron energy. Figure 2-2 represents the energy band bending caused by equilibrium of Fermi levels across the junction.

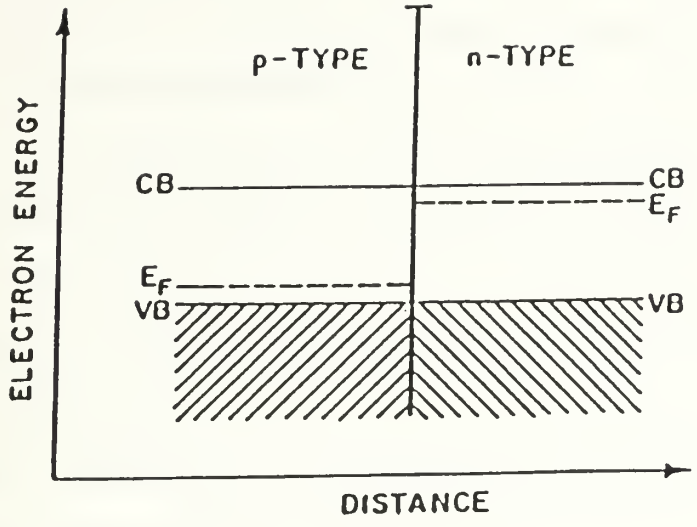

Figure 2-1. Schematic of a p-n junction immediately after formation. [Ref. 8: p. 138]

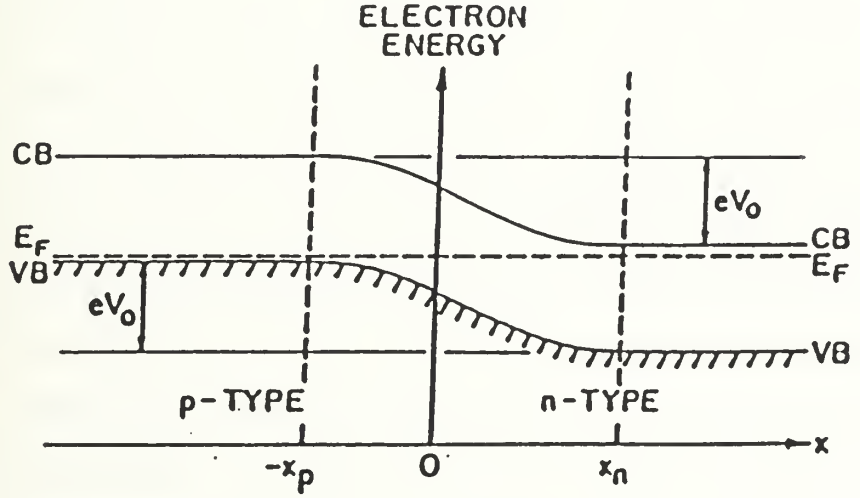

Figure 2-2. Schematic of a p-n junction at equilibrium. [Ref. 8: p. 141]

Semiconductors are covalent solids that may be regarded as "insulators" because the valence band is completely full and the conduction band is empty of electrons at 0°K . Thus, at 0°K, a semiconductor has no delocalized electrons; all electrons are bound to individual atoms, leaving none available to carry current.

Separating the two energy bands is a gap of forbidden energy levels, better known as the bandgap (E_g). In order for an electron to escape the valence band and cross the band gap into the conduction band to carry current, it must absorb enough energy to raise its energy level to that of the conduction band. It must absorb enough energy to jump the bandgap. The energy gap (band gap) for semiconductor devices ranges from 0 to 2.5 eV.

In situations where all the levels of an isolated band are filled except for those near the very top, the donor level, it is convenient to think in terms of holes representing the absence of electrons in an otherwise completely filled band. Since the absence of a negatively charged electron is equivalent to the presence of a positive charge, holes behave as if they are positively charged. Once electrons cross the gap to the conduction band, they move freely and thereby carry current. Each electronic excitation into the conduction band leaves behind a hole in the valence band. These holes , acting as positive charge carriers, also

contribute to the conductivity. The net result is that current carried through the semiconductor.

2. Semiconductor Doping

Semiconductors are distinguishable from insulators by the fact that the bandgap energy is small ($0 < E_g < 2.5eV$). A narrow bandgap allows electrical conduction with small inputs of energy. The conductivity of semiconductors arising from thermal excitation as called intrinsic conductivity. Another way to enhance conductivity is photoexcitation in semiconductors with a bandgap equivalent to the energy of incident photons, also known as photoconduction.

Extrinsic semiconductors lower the bandgap energy margin by the introduction of impurity atoms or dopants into the semiconductor. If a donor atom is introduced into the crystal lattice (an atom with an excess of one valence electron), then little energy is required to boost the extra electron to the conduction band. If an acceptor atom is introduced (an atom with fewer valence electrons than the host lattice, causing excess holes) then little energy is required to move electrons in the valence band to the hole site. The net effect is less energy required for conduction. Therefore, a semiconductor's electrical properties can be improved by adding impurities to the material. Figure 2-3 is a representation of what happens to the bandgap when impurities, either donor or acceptor are introduced. Note that the quantum state of the excess electron is located slightly below

the conduction band while the energy level associated with a hole is located just above the valance band.

Doping a semiconductor with either impurity donor (excess valence electrons) or acceptor (deficient valence electrons) atoms classifies the material now as either n-type or p-type, respectively. When these two types of material are placed in contact with each other, a p-n junction forms.

B. P-N JUNCTION

P-n junction semiconductors (Si, GaAs, InP) have a region doped to different conductivity levels. At the junction there is a change from n- to p-type material over a region of space. The structure shown in Figure 2-3 is an ideal abrupt junction in which the transition takes place suddenly. However, the graded, or diffused, junction is more characteristic of real junctions. The degree of grading depends on the fabrication process. The GaAs/Ge samples studied in this thesis were fabricated by metal-organic chemical vapor deposition (MOCVD) which can produce an almost perfectly abrupt junction. The Indium Phosphide samples used were thermally diffused and can be expected to have a less distinct transition at the junction. The following discussion will consider an n^+p junction which the n-side is much more heavily doped than the p-side (i.e. $N_D >> N_A$), since this is the configuration of the Indium Phosphide samples that were more extensively investigated.

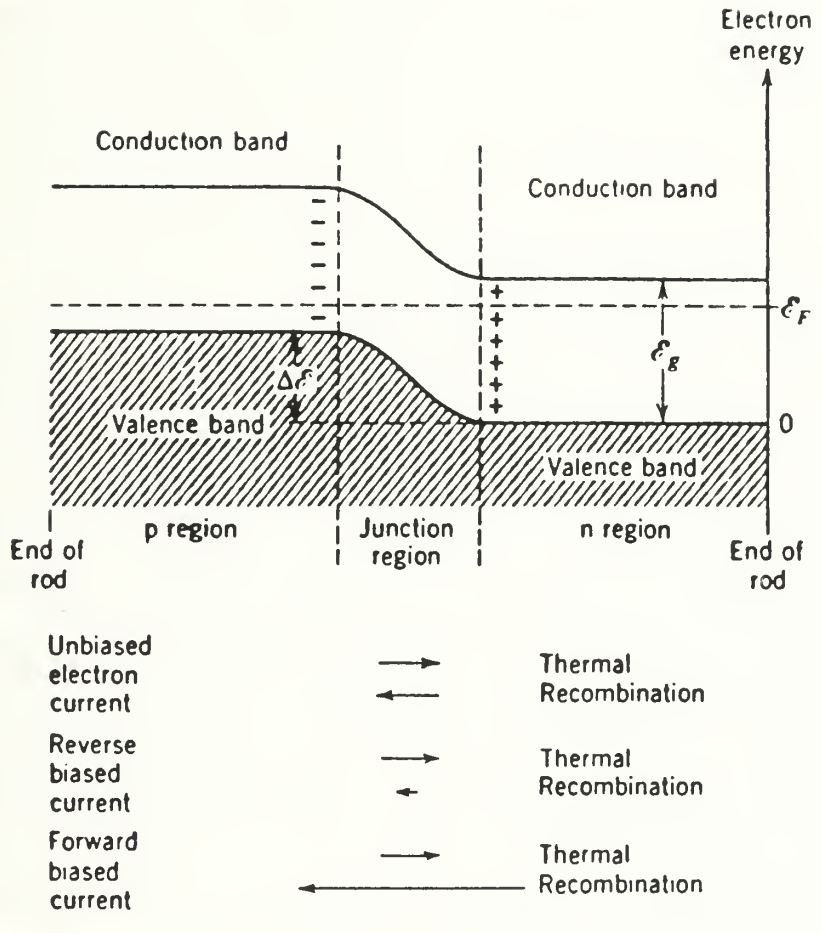

Figure 2-3. Electron energy -level diagram for an unbiased p-n junction. [Ref 9: p. 387]

When n- and p-type semiconductors come into contact, a non-equilibrium charge state exists. There will initially be an excess of electrons in the n-side relative to the p-side and an excess of holes in the p-side relative to the n-side. Charge concentration gradients across the junction cause diffusion to occur. Electrons will diffuse across the junction into the p-side and holes will diffuse into the n-side. A region in the p-side, near the junction, thus becomes deficient in free holes. Similarly, diffusion of electrons from the n-side of the junction leads to a loss of electrons. The p-side, therefore, has an excess of negatively charged ionized acceptor centers, and the n-side has an excess of positively charged ionized donors. Since these ionized atoms are at a fixed position in the lattice, a region of positive space charge (with concentration N_D) is created in the n-side near the junction and one of negative space charge (with concentration N_A) is created on the p-side. This gives rise to a layer depleted in carriers, which is known as a depletion layer. The width of the depletion layer (W) is given by

$$W = \left[\frac{2 \epsilon V(N_A + N_D)}{qN_AN_D} \right]^{\frac{1}{2}} \qquad (2.1)$$

where V is the potential difference across the junction, q is the electronic charge, and ϵ is the permittivity of the junction material [Ref. 8]. The magnitude of the potential barrier depends upon the width of the forbidden-energy gap,

the impurity concentration of dopant, and the temperature. Equations 2.2, and 2.3 give the depletion widths ($x_{n,p}$) of each side of the junction (i.e. $W = x_p + x_n$). For the n^+p junction, since $N_D >> N_A$, one can see that the width will be mostly comprised of the p-material.

$$x_n = \frac{N_A}{N_A + N_D} W \qquad (2.2)$$

$$x_p = \frac{N_D}{N_A + N_D} W \qquad (2.3)$$

The creation of the two space charge regions of opposite sign establishes a built-in electric field. The resultant electric field is directed from the n-side to the p-side. The force exerted by this field opposes the further diffusion of carriers and, in this way, the development of this field brings about a condition of equilibrium in the junction. The built-in electric field depends directly on the doping levels present in the junction (the higher the doping levels are, the higher the electric field is). This effect can lead to junction breakdown if the concentrations are high enough. The doping levels which we will consider ($\approx 10^{17} cm^{-3}$ on the p-side and $\approx 10^{18}$ cm^{-3} on the n-side) produce electric fields of the order of 10^7 V/m. Charge concentration gradients lead to variations in electric field causing the field to be non-uniform over junction width. Electric fields of this strength

can often mask the electronic properties of the junction, particularly when measuring the junction capacitance.

The initial electron concentration gradient across the junction induces a diffusion current from the n^+ into the p-region. This diffusion results in the ionization of a region of dopant atoms about the junction which constitutes a fixed space charge. The space charge creates an electric field in opposition to the diffusion current. The end result is an equilibrium situation where the current induced by the electric field of the ionized dopant atoms balances the diffusion current, and a potential gradient exists across the junction increasing from the p into the n^+ region. The magnitude of this potential difference is referred to as the built in voltage- V_{bi}. This potential creates an energy barrier against charge migration.

As a result of the energy barrier created by V_{bi}, a portion of the diode near the junction is depleted of free charge carriers and is referred to as the depletion region. The depletion region may be visualized as a parallel plate capacitor.

The potential barrier opposes the crossing of majority charge carriers but minority carriers are not hindered from crossing. Minority carriers are in fact driven by the field to the opposite side of the junction. Thus, when a light-generated electron-hole pair is formed, the electron is driven to the n-type side, and the hole is driven to the p-type side.

Once the electrons are on the n-type side and the holes are on the p-type side, they can move around without being prevented by the recombination process from reaching the surface contacts of the cell. Since a charge imbalance now exists in the cell, current can flow through a connected external circuit.

C. P-N JUNCTION CAPACITANCE

The p-n junction is a double layer of oppositely charge carriers separated by a small distance (the depletion region) and thus has the properties similar to a parallel plate capacitor. The junction capacitance can be expressed using the simple parallel-plate capacitor equation (since there are no free charge carriers in the depletion layer of the junction) and is given by

$$C = \frac{\epsilon A}{W} \tag{2.4}$$

where A is the area of the junction in the solar cell, ϵ is the permittivity of the cell ($\epsilon = K\epsilon_o$ where K is the dielectric constant of the cell), and W is the width of the depletion region.

The acceptor or donor density in the p-type or n-type region adjacent to the depletion region can be related to the capacitance per unit area by

$$\frac{C}{A} = \left[\frac{q\epsilon N}{2(V_b - V_a)}\right]^{1/2} \tag{2.5}$$

or

$$N = \frac{2(V_b - V_a)C^2}{qEA^2} \qquad (2.6)$$

where N is the smaller value of acceptor density N_A or donor density N_B, and V_a is the applied voltage (positive for forward bias), and V_b is barrier voltage. Using N_a assumes heavily doped n-region while N_D assumes heavily doped p-region.

Equation (2.6) illustrates that the capacitance varies with the applied voltage. Therefore, measuring C as a function of reverse bias to a solar cell and plotting $1/C^2$ versus V_a will allow N, the doping density on the lightly doped side of the cell to be found. These expressions assume an abrupt junction which is characteristic of conventional solar cells. When an external voltage is applied, equation (2.4) is modified to become

$$W^2 = \frac{2\,\epsilon(V_{bi} - V)}{q\,N_A} \qquad (2.7)$$

where V_{bi} is the built-in (diffusion) potential, V is an applied bias potential (negative for reverse bias) across the junction, ϵ is the dielectric constant of the junction, q is the electronic charge, and N_A is the doping level of the p-material. This gives rise to the junction capacitance

$$C^2 = \frac{q\,\epsilon\,N_A\,A^2}{2\,(V_{bi} - V)} \qquad (2.8)$$

In summary, a reverse bias will increase the depletion width and so decrease the capacitance. The effect of an applied bias voltage on the depletion region's capacitive properties is critical in the study of solar cells, and their photoelectric conversion behavior.

III. SOLAR CELLS

A. THEORY OF SOLAR CELLS

When a solar cell is illuminated, the photon energy is either absorbed, transmitted, or reflected. Absorbed photons that do not have sufficient energy to form electron-hole pairs simply contribute to lattice phonon energy as heat. Electron-hole pair formation requires photons with a minimum threshold energy. Due to the narrow range of photon energies acceptable for photoconduction, most sunlight that strikes the cell is lost before it can be converted to electricity. Some photons do result in electron-hole pairs, but if no electric field is present, the electrons will eventually recombine with the holes. The net effect of the absorption process being nothing more than a heating up of the semiconductor.

The solar cell p-n junction introduces an internal electric field which separates and collects the electron-hole pairs before they recombine. A charge field is created which sets up a barrier for further net charge movement. In other words, the barrier prevents other free charges from migrating across the junction. This barrier known as the potential barrier or depletion region, plays an important role in the generation of electricity. As electron hole pairs become available, the potential barrier separates them, forcing electrons from the p-region where they are called minority

carriers to the n-region where they are known as majority carriers. Light incident on the cell creates electron-hole pairs, which are separated by the potential barrier, creating a voltage that drives a current through an external circuit. The holes transport from the n-region to the p-region. An electron in the n-region is called a majority carrier and a hole in the n-region is called minority carrier. For the p-region, the opposite is true (holes are majority carriers and electrons are minority carriers). It is the minority carrier which must pass through the barrier. Since there are fewer carriers of opposite charge to recombine with, the minority carrier, has a high probability of reaching the respective region surface. The net result is a voltage difference between either end of the cell. The high number of available pairs at the solar cell junction will generate a current flow.

1. Conversion Efficiency

In order for a photon to be of significant use in the conversion process, it must have transfer sufficient energy to an electron in order for the electron to breach the bandgap. A photon collision transfer of energy slightly greater than the bandgap is preferred, to ensure the transition of the electron to the conduction band. Since, in space, the energy spectrum of sunlight is fixed, the photovoltaic material must be selected with an optimum bandgap. Figure 3-1 illustrates the relative bandgaps of various materials.

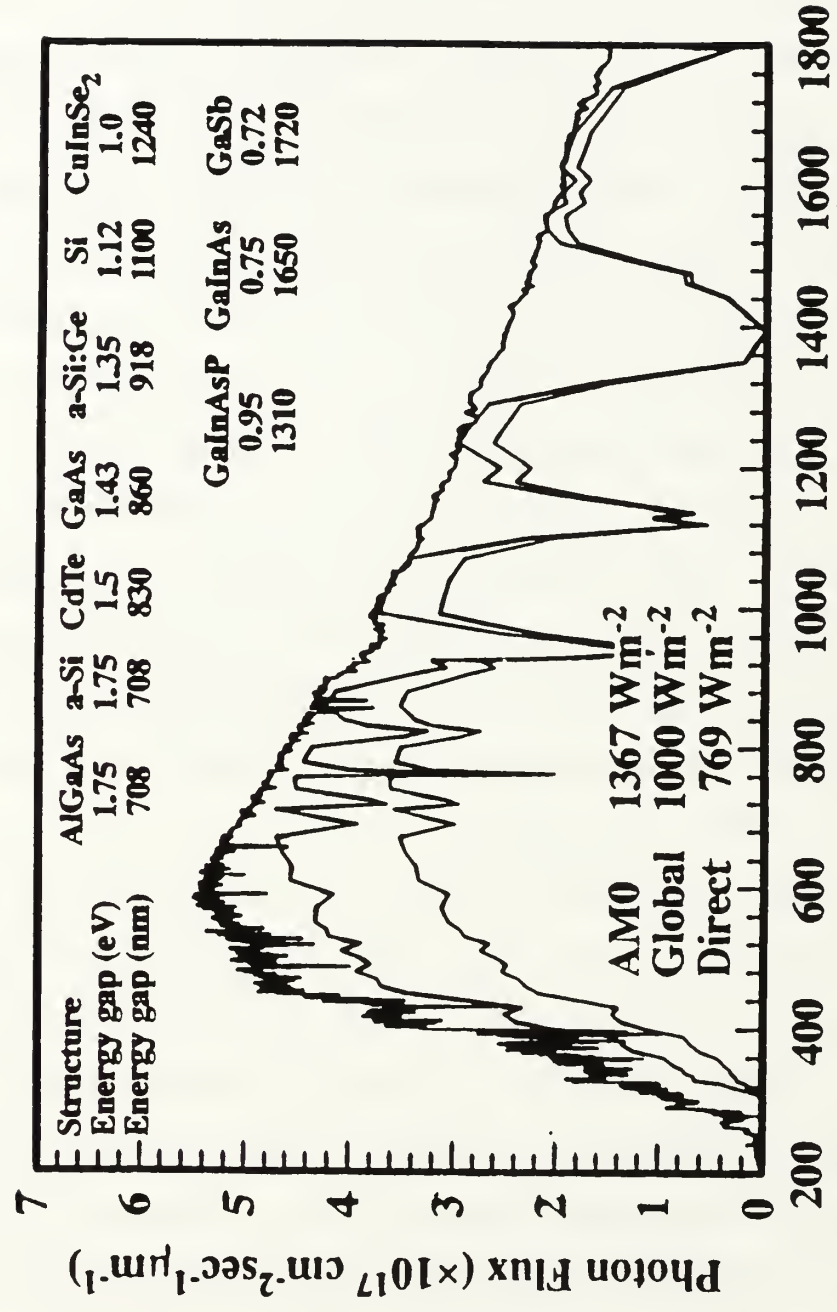

Figure 3-1. Energy density vs. optimum wavelength for various semiconductor materials. The curves are the nominal solar energy spectrum available at Earth orbit. [Ref 10: p. 213]

The maximum efficiency bandgap for space solar cells (Air Mass Zero) is about 1.4 eV, at room temperature (300 K). The bandgaps of silicon (1.12 eV), and indium phosphide (1.35 eV), are below this theoretical threshold, and gallium arsenide (1.42 eV) has a significant advantage.

The parameters that characterize the performance of a p-n junction solar cell are:

open circuit voltage	V_{oc}
short circuit current	I_{sc}
fill factor	FF

The efficiency of a cell is the ratio of the cell's maximum output power to the power incident on the cell from radiant energy. The theoretical maximum power P_T of a cell is

$$P_T = V_{oc}\ I_{sc} \qquad (3.1)$$

With the conversion losses mentioned above the maximum practical (P_m) power is somewhat less than P_t. The I-V curve of Figure 3-2 shows the maximum output power (P_m), occurs for zero series resistance, and infinite shunt resistance. Another solar cell parameter is the Fill Factor (FF) and is defined as:

$$FF = \frac{P_m}{V_{oc}\ I_{sc}} = \frac{P_m}{P_T} \qquad (3.2)$$

For orbiting spacecraft, at air mass zero (AMO) conditions, sunlight nominal incident power is 1.36 Kw/m^2.

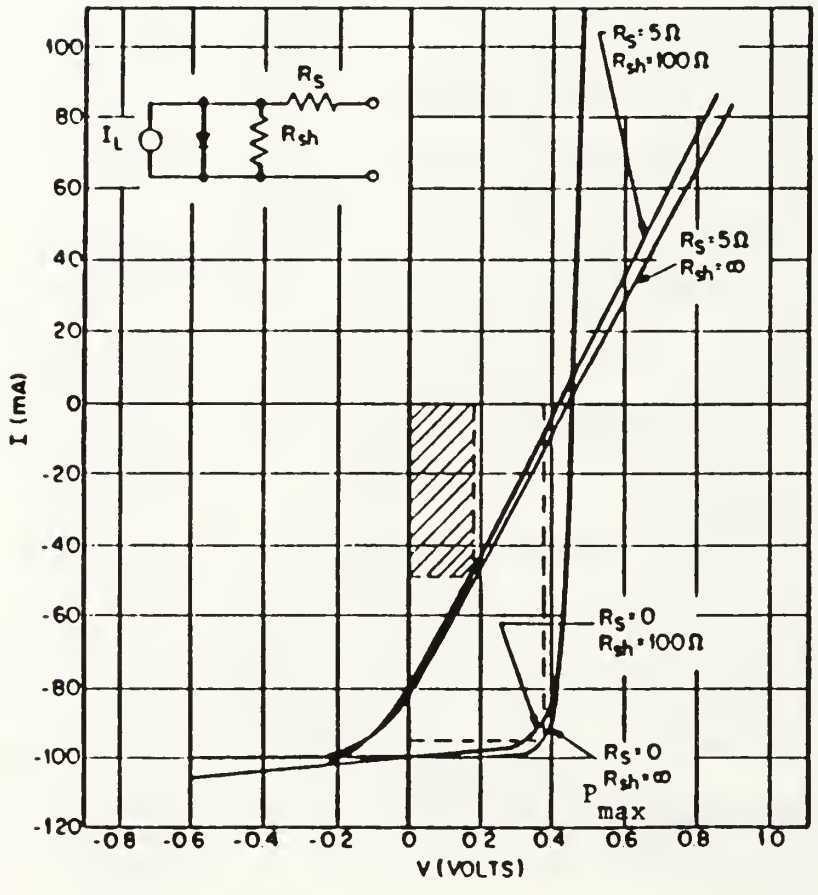

Figure 3-2. Theoretical current-voltage (I-V) characteristics for solar cells that includ series and shunt resistances. Inset shows the equivalent circuit. [Ref. 8:p. 243]

Solar cell efficiency can be calculated as

$$EFF = \frac{P_m}{P_{incident}} = \frac{V_{oc}\ I_{sc}\ FF}{\text{Sunlight Incident Power}} \qquad (3.3)$$

In order to achieve high conversion efficiency, the requirements are high V_{oc}, I_{sc}, and FF (sharp corner in the I-V curve). Energy conversion efficiencies of standard solar cells range between 12 and 20 percent, due primarily to limited material absorbtivity. In the solar spectrum, 26 percent of the energy is in photons having photon energy of less than 1.1 eV (bandgap for silicon). From Figure 3-1, it can also be seen that approximately 40 percent of the energy is in photons having photon energy less than 1.45 eV (bandgap for GaAs). Of the remaining 60 percent (those photons with energy greater than 1.45 eV), any energy greater than the 1.45 eV required to generate an electron-hole pair is absorbed by the atomic structure and produces heat in the form of atomic vibrations. Thus, approximately 25 percent of the energy in these photons is wasted. Solar cell efficiency of 15 to 18 percent for standard GaAs is typical.

2. Factors Affecting Efficiency

The upper limits of solar cell efficiency are bound by several factors. Radiant energy passing through the cell, as well as reflection, produce no effect in the photovoltaic conversion process. Sunlight is not monochromatic, much of the radiant energy absorbed produces heat. The remaining

energy causes the electron-hole pairs to generate current. The factors affecting the production of electron-hole pairs to generate current are discussed. Although some of the factors are inherent to the cell, improvement is achieved through good design and material selection.

a. Bandgap Energy

As noted earlier, the smaller the bandgap of the cell, the greater the number of available photons there are with enough energy to create electron-hole pairs. However, should the bandgap be too small, most of the radiant energy would be wasted as heat. The most desirable range for the bandgap would be the range that matched the peak of the solar spectrum. Silicon's bandgap energy is 1.1 eV while GaAs and InP are 1.42 and 1.35 Ev respectively. Note from Figure 3-1 that Gallium Arsenide's bandgap almost coincides with the peak photon bandgap associated with the solar spectrum.

b. Temperature

Figure 3-3 shows how solar cell efficiency decreases with increasing temperature, despite the fact that conductivity in semiconductors characteristically increases with increasing temperature. Two predominant factors cause efficiency to drop as temperature rises (as intrinsic conductivity increases): 1) lattice vibration phonon energy contributes to random electron energy levels, interfering with charge carrier migration; and 2) the junction electric field becomes less effective in separating pair charges. [Ref. 12]

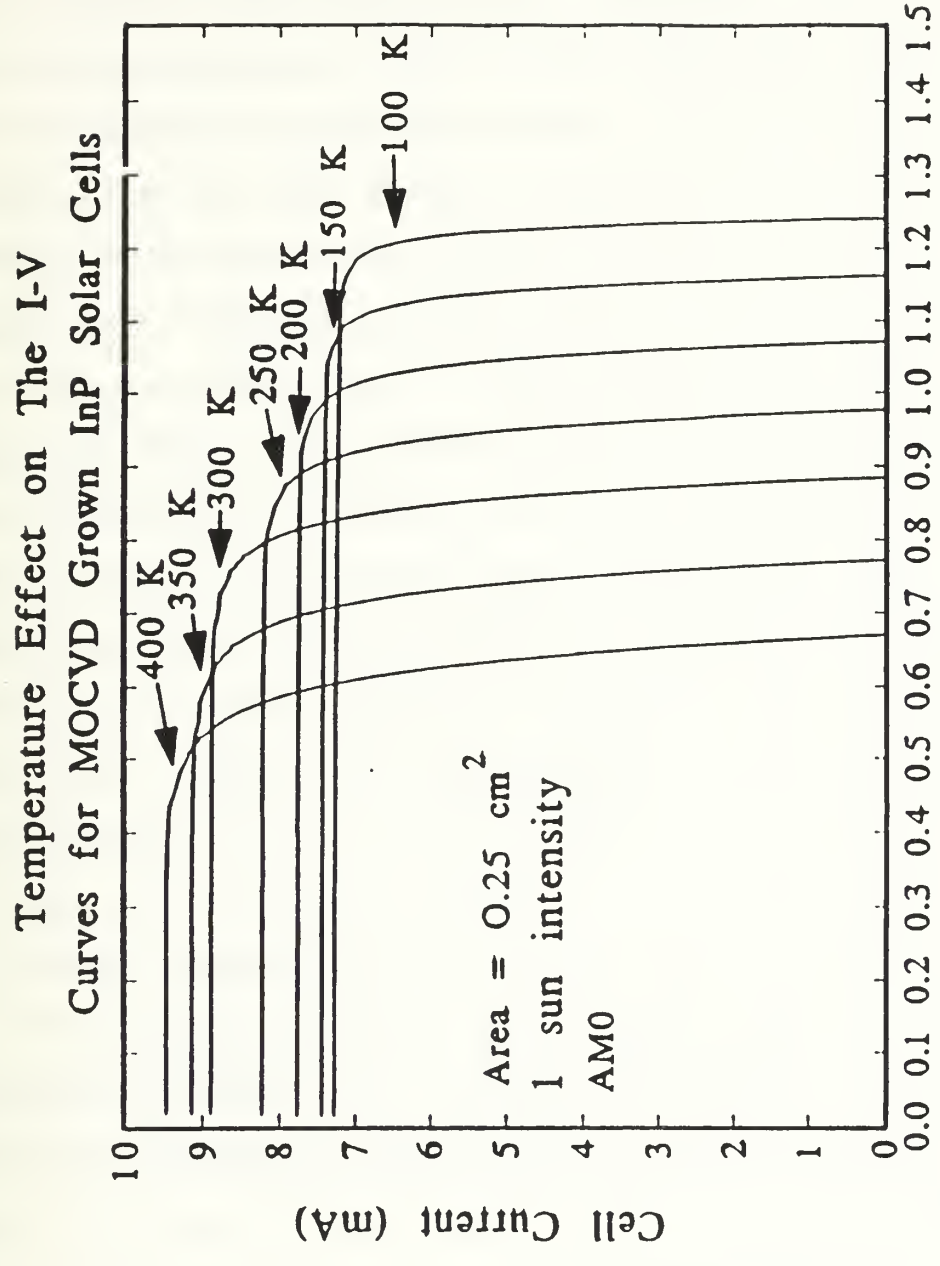

Figure3-3. The effect of operating temperature on the conversion performance of an InP solar cell .
[Ref. 11: p.43]

The first factor degrades performance even at room temperature. As temperature increases, the second phenomenon is predominant in reducing the electric field gradient at the p-n junction. At higher temperatures, as many electrons are freed from their bonds. These electrons outnumber the free electrons supplied by dopants. Also created are electron-hole pairs, formed by the thermal excitation. The n-type material begins to lose its n-type characteristics. The same process occurs on the p-type side which loses its p-type characteristics. The effect is 1) the thermally excited charge carriers have sufficient energy to freely cross over the p-n junction in both directions as if the barrier field were not there, and 2) ultimately, the depletion region disappears because there are no longer n- and p-type sides to create the barrier. These losses in junction efficiency eventually lead to a complete failure of the photoelectric effect. [Ref. 12]

Thermal effect degradation can be reduced by selecting a larger bandgap, to provide a wider response to variations at the depletion region. Thus, GaAs cells are only about half as sensitive to increasing temperature as silicon cells. [Ref. 9]

c. Recombination

The photon generated electron-hole pairs can randomly recombine before they contribute to current generation. Recombination occurs by either direct or indirect

methods. Direct recombination occurs when an electron and a hole randomly encounter each other. The electron rebinds with an atom when it encounters a hole, emitting energy as heat. Random recombination generally occurs before the electron has time to cross the depletion barrier. Once across, direct recombination is rare. Recombination can also occur when a free charge carrier has a collision, reducing its energy and increasing the probability that it will fall into a bond.

Indirect recombination occurs when an electron-hole recombination is encouraged by other influences, such as empty, or dangling bonds present from impurities or defects (traps) which capture the free electrons. This is the predominant mechanism associated with radiation degradation in solar cells, since radiation introduces defects into the crystalline lattice, and thus increases the opportunity for recombination.

C. SOLAR CELL RADIATION DAMAGE

1. Space Environment

A spacecraft in the earth's orbital environment is constantly exposed to magnetically-trapped electrons and protons, solar-flare protons, and cosmic rays. The cumulative effect is a dynamic environment causing degradation of solar cell efficiency on-orbit. In lower earth-orbits, both geomagnetically trapped electrons and protons play significant roles in cell damage. At higher altitudes (near geosynchronous orbit) the high energy trapped electrons are

the primary cause of damage, except during periods of high solar activity, when solar flare protons add significantly to the total cell-damaging effect. The effect variations in trapped radiation at different orbital altitudes can be seen in Figure 3-4. The use of solar cell coverglass effectively screens out most protons (Figure 1-1), and trapped electrons are the principle cause of solar cell degradation in the space environment.

2. Radiation Effects

The performance of solar cells is represented in terms of engineering output parameters. The effect of radiation on the cells can then be described in terms of changes in these performance parameters. These parameters deal with both the physical and electrical characteristics of the cell and give insight into the mechanisms involved. Dopant impurity concentrations, recombination, diffusion lengths and minority carrier lifetimes are the physical aspects of cell behavior while the electrical parameters include short circuit current (I_{sc}), open circuit voltage (V_{oc}) and power output (P). The damage phenomena can be categorized by two major types of radiation damage: ionization and atomic displacement.

Ionization occurs mainly in the solar cell cover glass. There is a reduction of transmittance of the cover glass due to its darkening. When ionizing radiation excites an orbital electron to the conduction band, the electron may become

Figure 3-4. The effect of orbital altitude (cumulative radiation exposure) on spacecraft solar cells. [Ref. 11: p.31]

trapped by impurity atoms in the glass, forming color centers. The subsequent result is a darkening of the cell cover glass, which reduces the illuminization of the cell.

Ionizing radiation will also excite the electrons in the cell from the valance band to the conduction band, creating electron-hole pairs similar to the photovoltaic process. This is the beneficial effect of ionization. However, much greater energy is required from the ionizing radiation than from the solar photon to create the same number of charge pairs. The interaction with the ionizing radiation and the atomic electron is inelastic; therefore, the electron experiences a transition to an excited state. If the energy transfer between the two is not sufficient to move the electron to the conduction band, the effect will be temporary. The electron will eventually recombine with a hole, losing its energy as heat. The net effect would be an increase in temperature.

3. Lattice Structure Damage

Considerable lattice damage takes place as radiative particles strike a solar cell. This damage is usually in the form of crystal defects (vacancies, interstitials, vacancy-impurity complexes, defect clusters). The creation of these defects in the crystal lattice introduces additional energy states which are found in the band gap. The defects then can act as additional recombination centers, causing a reduction in minority carrier lifetime and diffusion length; or they can

act as additional impurities, changing the net impurity concentration of the cell. In either case, the damage results in a deterioration on the cell's performance over time. Figure 3-6 shows the effect of several types of radiation on a single defect type.

High energetic, fast moving particles are capable of causing atomic displacements within the crystal lattice structure of solar cells. These displaced atoms and their associated vacancies will eventually form permanent stable defects within the crystal lattice. These defects produce the significant changes within the cell which affect the equilibrium carrier concentrations and the minority carrier lifetime and subsequently cell efficiency.

The displacement energy required to eject an atom from its lattice site is on the order of 13 eV for silicon and 25 eV for GaAs. Because the displacement of an atom involves the formation of a vacancy, the formation of an interstitial atom and other electronic and vibrational losses, the displacement energy can be expected to be much higher than the energy of formation for a vacancy. [Ref. 12]

The principal effect of radiation damage is the damage caused to the crystal lattice. Radiation induced displacement defects create additional recombination centers causing a reduction in minority carrier diffusion length (minority carrier lifetime).

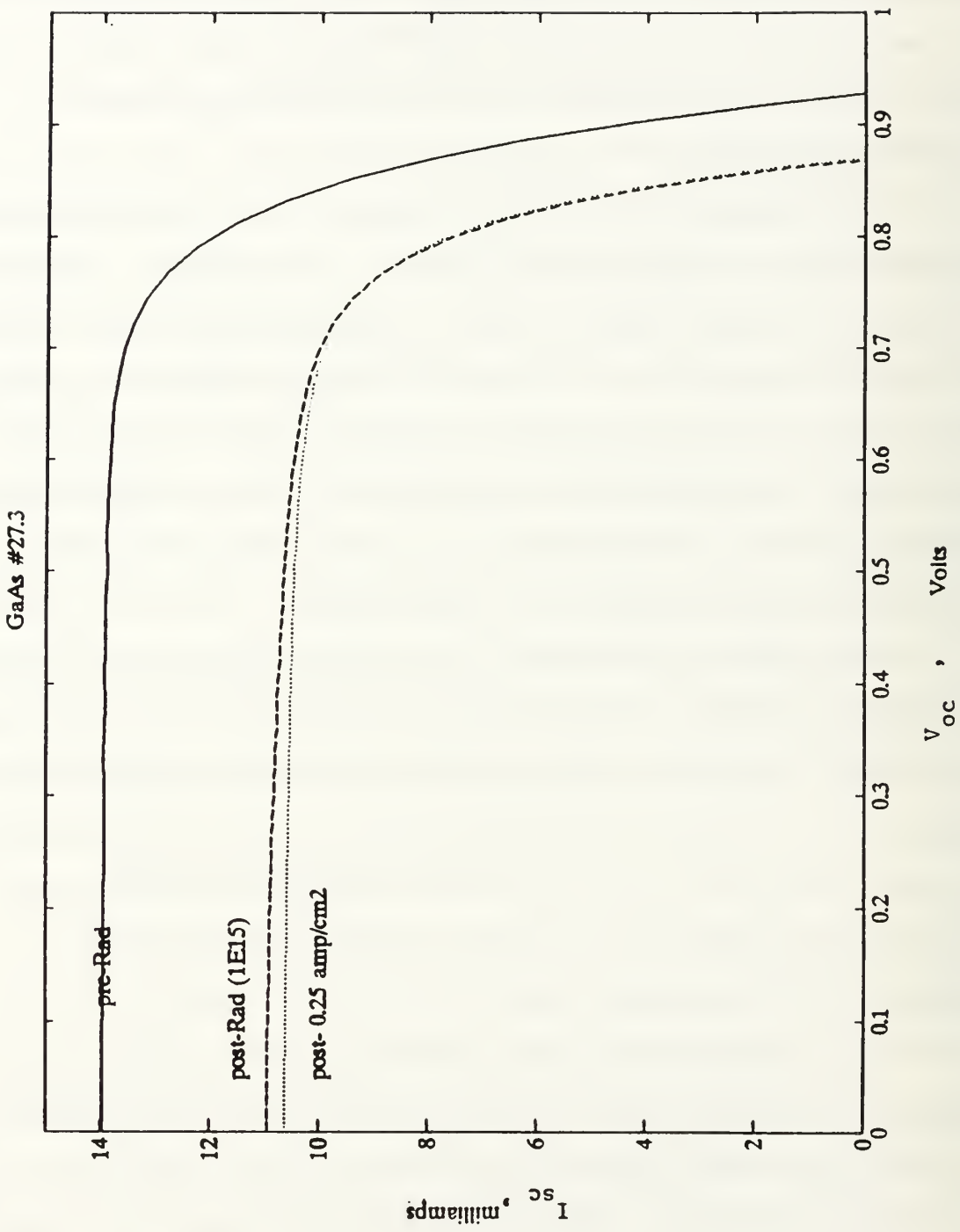

Figure 3-5. The effect of 1 MeV electron radiation exposure on the current-voltage (I-V) curve for Gallium Arsenide (GaAs/Ge). Post-Rad curve resulted from a single exposure to a fluence of 1E15.

Figure 3-6. The effect of displacement damage in InP caused by different energies of incident radiation. The damage is measured by the growth rate of a single type of defect (the trapping center known as H4). [Ref. 11:p. 45]

The diffusion length can be measured experimentally. It is a measure of the amount of displacement damage in the base of the solar cell. Limitations do exist. Low energy protons do considerable displacement damage within the junction depletion region without changing the cell's diffusion length, but seriously reducing solar cell I_{sc} and V_{oc}. In addition, the relationship between diffusion length and I_{sc} and V_{oc} are not well defined, and diffusion length is more difficult to measure than I_{sc} or V_{oc}. Therefore, to better evaluate the mechanism, radiation effects are expressed in terms of the electrical power generation parameters, rather than solid state effects.

Radiation will cause significant degradation in base resistivity, short circuit current (I_{sc}), open circuit voltage (V_{oc}) and subsequently the maximum power point (P_{max}). The degradation in I_{sc} and V_{oc} will result in a decreased I-V curve as shown in Figure 3-5. The maximum power (P_{max}) is found using equation: $P_{max} = (FF)\ I_{sc}\ V_{oc}$. The fill factor is relatively unaffected by electron radiation. The reduction in solar cell spectral response due to radiation induced defects is shown in Figure 3-7.

The direct result of electron displacement damage, which is of primary interest to this research, is the creation of vacancies and interstitials. Once an interaction occurs, the radiative particle may have sufficient energy to produce

Figure 3-7. The effect of radiation induced defects on the spectral response of an InP solar cell. The 1 MeV fluences shown are routinely encountered by spacecraft in Earth orbit. [Ref. 11:p. 33]

secondary displacements within the crystal. Therefore, the distribution of vacancies will not be uniform because the vacancies from secondary displacements will be relatively close to the associated primary vacancy. The interstitials, on the other hand, will move randomly throughout the crystal until it loses its energy and comes to rest in the interstices of the atom. It therefore seems reasonable that the interstitials will have a more uniform distribution within the crystal.

Vacancies and interstitials are extremely mobile and unstable at room temperature. Displacement damage is caused by the various combinations available to a vacancy within the crystal. A vacancy can combine with another atom such as impurity atoms forming close coupled vacancy-oxygen pairs, vacancy donor pairs, or vacancy-acceptor pairs. In the case of vacancy-oxygen and vacancy-donor pairs, the defects are electrically active and can become negatively charged by accepting an electron from the conduction band. The energy levels of these defects are slightly below the conduction band. For vacancy-acceptor pairs, the defects can become positively charged by accepting a hole from the valance band (giving up an electron to the valance band). The energy level of this defect is slightly above the valance band.

If a vacancy combines with an interstitial, the damage is functionally eliminated. The combination returns the

crystal to its original lattice structure formation. This would be the ideal condition for irradiated cells.

The major effect these defects have is the formation of additional recombination centers which affect the lifetime and diffusion lengths in the cell. The diffusion constant (D) is significant because it relates the mean distance that a minority carrier travels before recombination, or diffusion length (L), and the mean time of recombination (T), or minority carrier lifetime by the expression

$$L^2 = DT \tag{3.4}$$

The concept of diffusion length is used to describe the theory of operation of semiconductors and to calculate the effect of radiation. As will be discussed later, the effects of radiation on solar cell performance is due to the change in minority carrier lifetime which decreases the diffusion length.

4. Damage Equivalence

The energies associated with electrons and protons within the space environment vary over a wide range. In order to evaluate the effects of radiation damage in solar cells, it is necessary to describe the various types of radiation in terms of an environment that can be reproduced under laboratory conditions. The concept of damage equivalence is, therefore, based on the 1 MeV electron fluence for solar cell degradation. The damage produced in solar cells by electrons of various energies is related to the damage produced, under

laboratory conditions, by 1 MeV electron by the damage coefficients ϕ_c = critical fluence, and K_L = diffusion length damage coefficient. Similarly, the damage produced by protons of various energies is standardized to 10 MeV protons which have the approximately same penetration range in silicon as 1 MeV electrons. It is thus possible to construct a model in which the various source components of a radiation environment can be described in terms of an equivalent fluence.

a. NIEL

The many variables involved when measuring radiation damage to materials result in wide variations in predicting specific performance degradation. A preferred method of modeling radiation damage is that of Nonionizing Energy Loss (NIEL).

> NIEL is the amount of energy a primary knock-on atom can impart into displacements. The ratio of the NIEL for 3 MeV protons to 1 MeV electrons in InP is about 750. This agrees with the ratio of the H4 defect introduction rates, suggesting a linear dependency of displacement damage on NIEL for p-type InP. The effect of irradiation in proton and electron environments is usually discussed in terms of an equivalent 1 MeV fluence. This equivalent fluence is determined by first reducing the proton spectrum to an equivalent 10 MeV proton fluence, which is then reduced to an equivalent 1 MeV electron fluence by a damage equivalency factor. The measured equivalency factor for p-type Si is about 3500, and about 1000 for GaAs. From the present results, the equivalency factor for p-type InP is expected to be equal to the ratio of the NIEL for 10 MeV protons to 1 MeV electrons, which is about 300. [Ref. 2:p. 50]

The effect of nonionizing energy loss for various energy ranges of incident radiation is shown in Figure 3-8 for silicon, and in Figure 3-9 for InP.

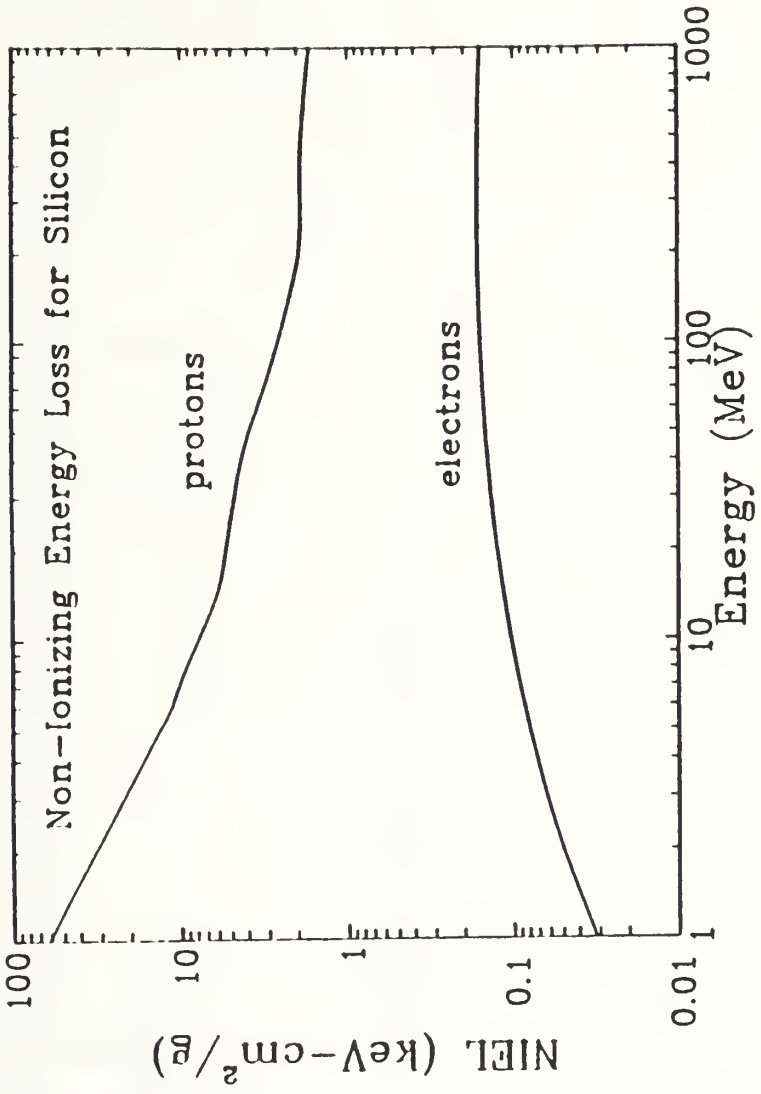

Figure 3-8. The calculated energy dependence of the nonionizing energy loss (NEIL) for protons and electrons in Silicon. [Ref. 2:p. 39]

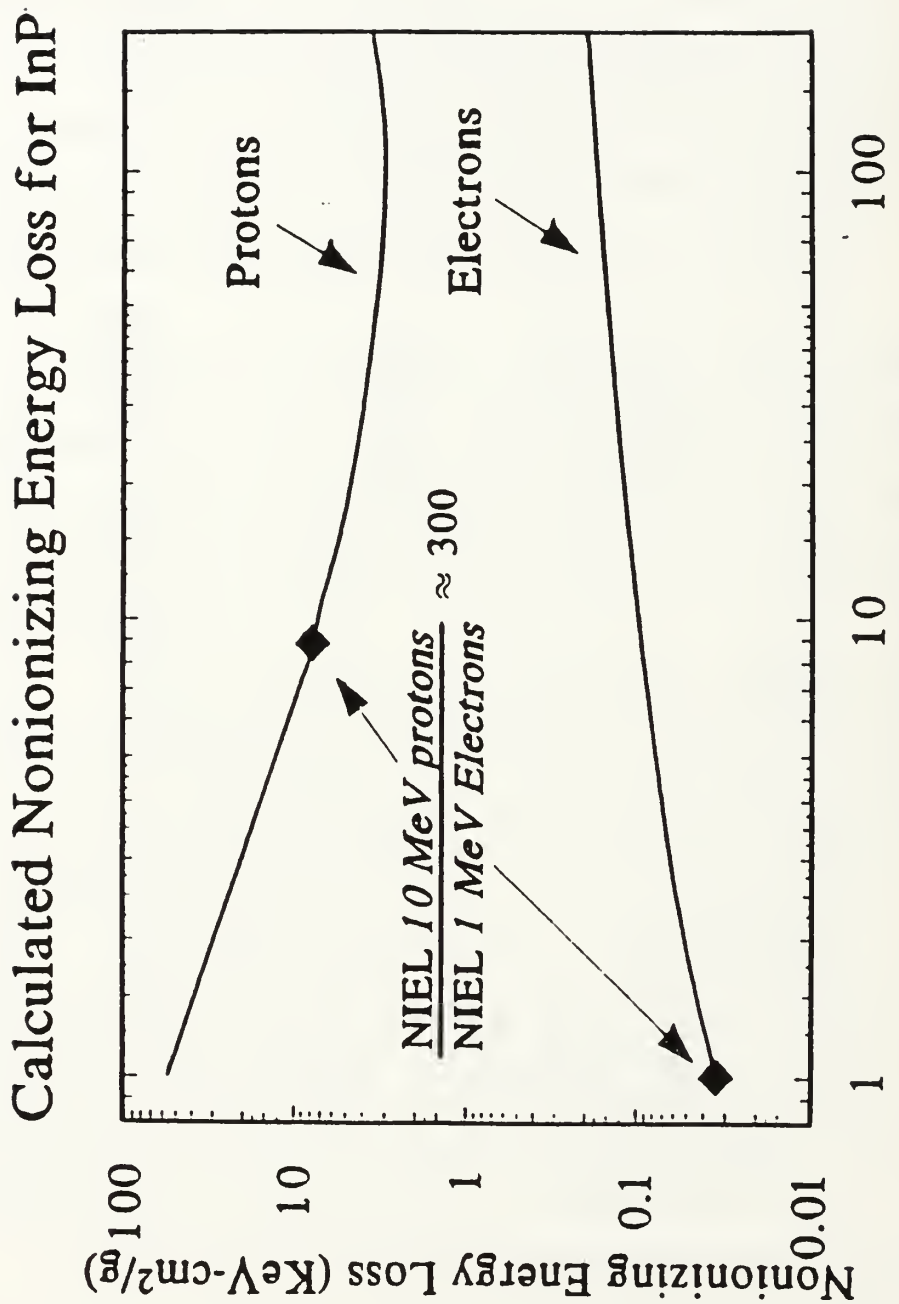

Figure 3-9. The calculated energy dependence of the nonionizing energy loss (NIEL) for protons and electrons in Indium Phosphide. [Ref. 2:p. 50]

C. SOLAR CELL ANNEALING

Lattice damage and associated electrical degradation of radiation-damaged solar cells can, to some extent, be reversed. This is done by thermal and/or electrical defect annealing -- a process by which heat and/or current is introduced to the cell, causing the energy level of the cell to increase. The recovery is due to atomic movement within the crystal causing the lattice structure to return to its original condition. Although the crystal is not 100% restored, the annealing process achieves sufficient recovery to extend the life of the cell's usefulness (Figure 3-10). This is accomplished via : 1) recombination of crystal vacancies and interstitials are effected, creating fewer atomic dislocations and 2) the rearrangement of dislocations to a lower energy configuration without changing in the actual number of dislocations present. Both processes provide a more stable crystal with a partial elimination of the radiation induced lattice defects and a decrease in recombination centers within the depletion region.

Increasing the temperature of the bulk solar cell through the addition of heat is known as thermal annealing. It is the most common method of defect annealing. The energy level increase is a function of annealing temperature. Research conducted by Loo, et al [Ref. 17], shows that periodic thermal annealing at temperatures as low as 200°C considerably reduces the radiation damage to GaAs cells.

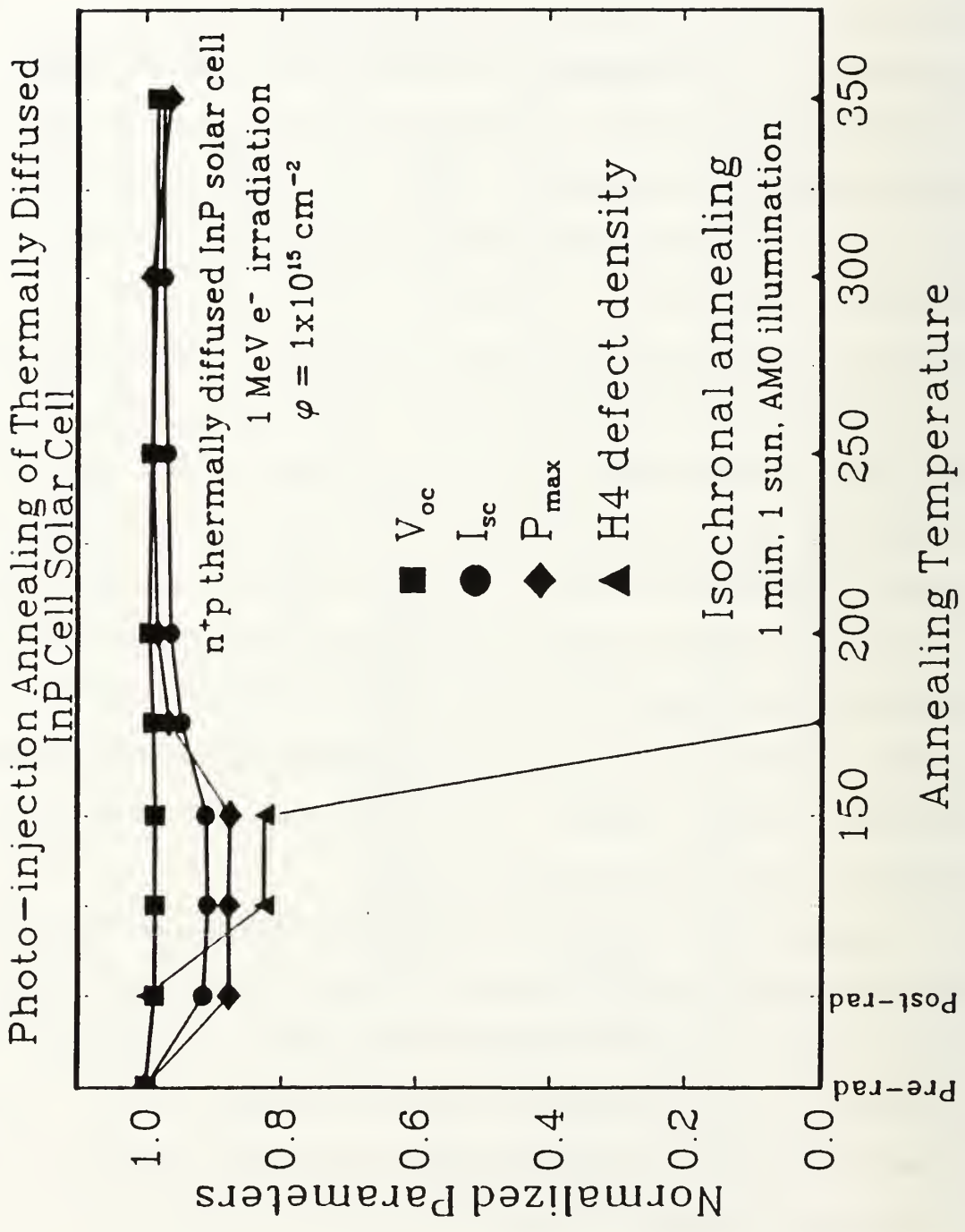

Figure 3-10. The effect of annealing on the photovoltaic parameters of an Indium Phosphide solar cell. [Ref. 11: p.37]

The use of minority carrier injection annealing has provided another method for cell damage recovery. Minority carrier injection can be provided either through photo-injection (exposure to light), or by applying a forward bias current. Here, a forward-biased potential is created across the cell, forcing current through. The forward current passed increases exponentially as the potential increases. The effect is an increase in cell temperature and minority carrier concentrations. The objective is to have some of the minority carriers attach to the additional recombination centers, forming a more stable lattice. Room temperature annealing using applied minority carrier injection (forward bias or photo-injection) has been repeatedly demonstrated, but the degree of recovery is not well demonstrated. [Ref. 13-18]

Lang [Ref. 14] discovered an accelerated annealing rate of defect states when a forward bias was applied in GaAs at a temperature of 100°C. Thus, a combination of thermal and electrical annealing appears to provide an optimizing process for damage recovery. The magnitude of the applied forward bias used in this experiment for the gallium arsenide cells , 0.5 Amps per square centimeter, is about one thousand times I_{sc} , the current density available from photo-injection.
This experiment also investigated the annealing of indium phosphide, using only photo-injection at various temperatures.

IV. DEEP-LEVEL TRANSIENT SPECTROSCOPY

A. DEEP-LEVEL TRANSIENT SPECTROSCOPY

Deep Level Transient Spectroscopy (DLTS) is a measurement technique which analyzes the capacitance transient of a semiconductor p-n junction following a voltage pulse to determine the characteristics of defect energy levels lying within the band gap (i.e. deep levels) existing in a semiconductor junction. The technique is spectroscopic in that the temperature dependence of the transient allows a precise determination of the energy of the defect level. The magnitude of the capacitance transient gives a measurement of the density of the defect in the crystal lattice. Thus, from a typical DLTS measurement, both the electronic properties and the concentration of any defects in the semiconductor device may be obtained.

1. Defect Levels and Traps

Since lattice structure damage is known to take place as radiative particles strike a solar cell, it is desirable to understand the characteristics of the defects that occur. These defects have significant impact on the cell's performance by creating additional recombination centers, or traps, within the bandgap of the semiconductor material. These traps cause a reduction in minority carrier lifetime and diffusion length, which, in turn, degrade the photovoltaic conversion process. Investigation into the energy levels of

the traps (called deep-levels), their concentration, and the effect of annealing, provide a clearer understanding into the mechanisms of solar cell damage, and an insight into reversing the deteriorating effects.

B. DLTS THEORY

Defect characterization and identification is accomplished by measuring the change in capacitance of a semiconductor when carriers (minority or majority) are injected into the sample by a bias pulse. This changes the electron occupation of a trap from an initial state. Because free carriers can interact with electronic defects through a thermal process, a charge exchange takes place and establishes the thermal capture and emission rates. Based on these rates, the electron occupation will return to an equilibrium state and the capacitance will return to its quiescent value. If a deep-level trap exists within the depletion region of the sample, a capacitance transient will be detected. Figures 4-1 and 4-2 illustrate an injection pulse used to produce a capacitance transient for the case of minority-carrier (electron) traps. The sign of the capacitance change depends on an increase or decrease in the electron occupation of the trap caused by the pulse. An increase in trapped minority carriers causes a decrease in junction capacitance. The capacitance transient due to minority carrier traps is always positive, and is induced only by injected minority carriers, The transient due to majority-carrier traps is always negative

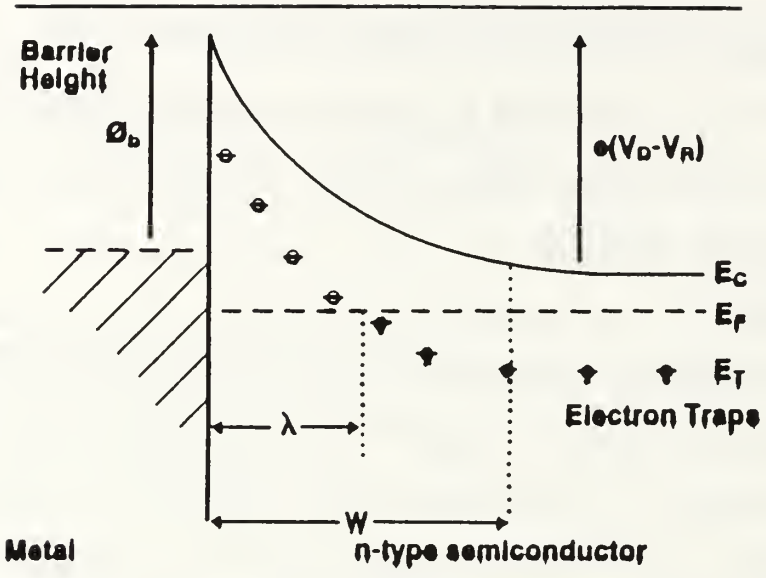

a) A Schottky barrier on n-type material. Deep level E_T crosses the fermi level at λ. A quiescent reverse bias V_R is applied across the barrier.

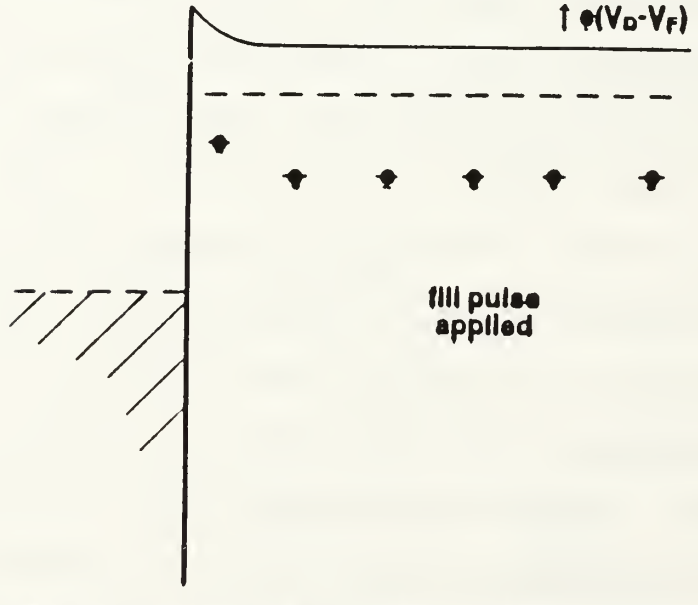

b) A forward bias pulse V_F fills all the traps.

Figure 4-1. Fill pulse effect on a Schottky barrier with a single deep level electron donor trap. [Ref. 16: p. 5]

and is induced only by majority carriers. [Ref. 19:p. 1730]

DLTS uses the capacitance transient and emission rate to uniquely identify traps. This is done by the rate window concept. The capacitance sampling interval provides a thermal emission rate for that time interval, Figure 4-3. The rate window is set such that the measurement system responds only to transients with an emission rate within a particular window. Since the emission rate, and thus the capacitance transient, is temperature dependent, the system will measure a peak at the temperature where the trap emission rate is within the window as shown. Thus, the temperature will uniquely define the trap responsible for the transient. A double boxcar sampling method (Figure 4-4) is used to sample the capacitance transient at two time intervals (the rate window), and the difference between the two signals determines the magnitude of the DLTS peak. It is from these peaks that much of the information concerning the trap is determined. The decay constant of the capacitance transient is changed by slowly varying the sample temperature. The rate window is then selected to generate a maximum DLTS signal. A full DLTS analysis will thus generate a spectrum of peaks at different temperatures until a maximum is found, as in Figure 4-5.

To capture free charge carriers, the defects must be flooded with free charge carriers. This is accomplished by momentarily forward biasing a reverse biased diode. Both the majority and minority carrier pulses are generally referred to

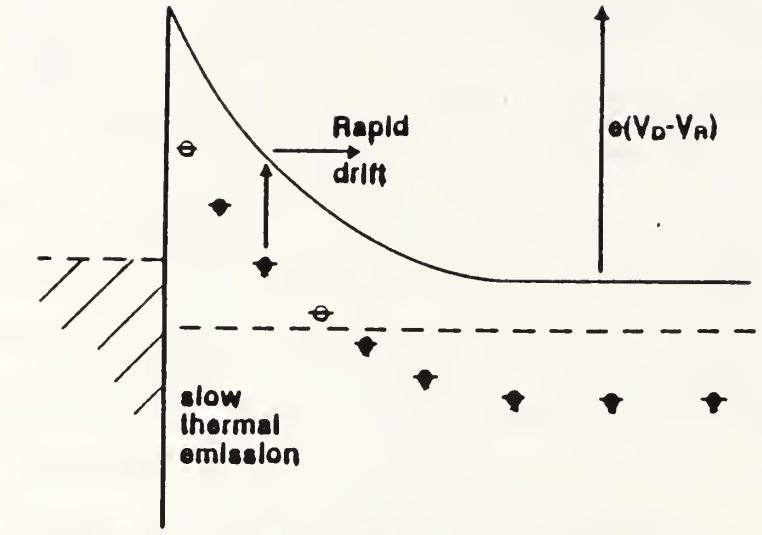

c) When the pulse ends the deep levels emit the trapped electrons. This increases the positive space charge which is observed as a capacitance transient.

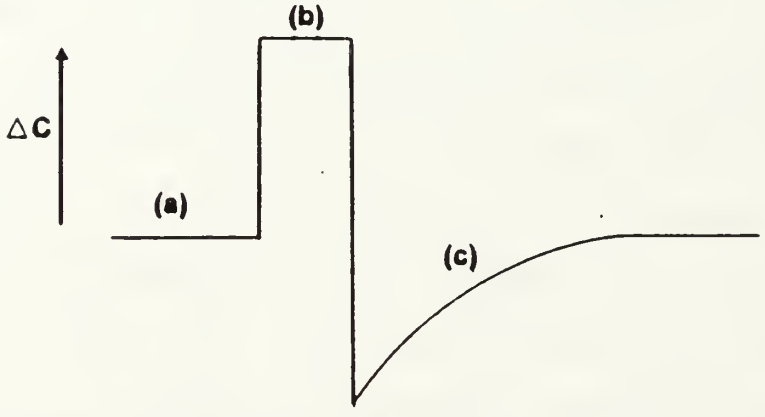

d) Observed capacitance variation corresponding to Figs a, b, & c.

Figure 4-2. The resultant capacitance transient from the applied fill pulse of Figure 4-1. [Ref. 16: p. 5]

as the "fill pulse". Defining time zero as the instant the reverse bias is restored, the capacitance at t=0 is seen to plunge lower than the quiescent value. This occurs because the trapped majority carriers neutralize a portion of the ionized acceptor atoms in the depletion region. The capacitance then exhibits a transient as the trapped charge is thermally emitted and the space charge recovers to its quiescent value.

Considering a minority carrier trap, the effects are similar except that the trapped minority charge carriers will be of the same sign as the ionized acceptor atoms, thus the capacitance at t=0 will be larger than the quiescent value. The capacitance will then decrease down to the quiescent value as the defects emit the trapped charge.

The DLTS technique provides information concerning thermal emission rates, activation energy, density and capture cross section by recombination centers that come about from the presence of deep levels in the bandgap of the semiconductor. These effects are now quantified for the case of a majority carrier trap (which in the present model is a hole so the subscript p will be used).

The formation of the p-n junction gives rise to a depletion layer of width W. When an external voltage is applied, (1) is modified to become:

$$W^2 = \frac{2\,\epsilon\,(V_{bi} - V)}{q\,N_A} \qquad (4.2)$$

where V_{bi} is the built-in (diffusion) potential, V is an applied bias potential (negative for reverse bias) across the junction, ϵ is the dielectric constant of the junction, q is the electronic charge, and N_A is the doping level of the p-material. This gives rise to the junction capacitance

$$C^2 = \frac{q\,\epsilon\,N_A\,A^2}{2\,(V_{bi} - V)} \qquad (4.3)$$

Hence, a reverse bias will increase the depletion width and so decrease the capacitance. If the charge emission is controlled by a single, thermal process,the time dependent trap occupation will be given by:

$$n(t) = N_t \exp(-e_p t) \qquad (4.4)$$

$N_t \equiv$ defect concentration
$e_p \equiv$ thermal emission rate of the defect level

Notice that this equation assumes that at t=0, all of the defects are filled with charge which is the case if the fill pulse is long enough to permit filling of all available defect levels. If it is further assumed that each defect captures a single charge carrier, Equation 4.3 may be used to adjust Equation 4.4 to include the effect of defects. An expression for the emission rate, e_p, may be derived from the principle of detailed balance. At thermal equilibrium, the capture rate

must equal the emission rate. The result is that the emission rate is given by:

$$e_p = g\ \sigma_p\ v_{th}\ N_v\ \exp-(E_a/kT) \qquad (4.5)$$

where: $E_a \equiv E_t - E_v$

$E_a \equiv$ activation energy of the defect
$g \equiv$ the degeneracy of the defect level
$\sigma_p \equiv$ the capture cross-section of the defect
$v_{th} \equiv$ the electron thermal velocity
$N_v \equiv$ density of states in the valence band

It is the activation energy which is used to identify a particular defect level and to aid in determining its origin and electronic properties. The activation energy can be determined as the slope of an Arrhenius plot of the emission rate e_p/T^2 vs. $1/T$. This requires a method of determining e_p at various temperatures.

The effect of an applied bias may be seen immediately by replacing the built-in voltage, V_{bi}, with an effective voltage, V, given by:

$$V = (V_{bi} - 2kT/q) \pm V_{appl} \qquad (4.6)$$

where V_{appl} is the applied bias. The effect of an applied bias is to either add or subtract from V_{bi}. If the bias is such that it subtracts from V_{bi}, it is called a forward bias since it will act to reduce the deletion layer and create a current through the junction. A forward bias will increase the depletion layer capacitance. A reverse bias is one which adds to V_{bi} and increases the depletion layer width which decreases the depletion layer capacitance.

Any free charge carriers captured by defects in the depletion region will either decrease (majority carriers) or increase (minority carriers) the space charge and hence the capacitance, and the occupation of the defect level will be controlled by the thermal emission rate of the defect. The emission rate will depend on the type of charge carrier being emitted, so either an n or p subscript is used in denoting the emission rate for a certain defect.

During a DLTS measurement, the diode is initially held at a constant reverse bias so that all of the defects in the depletion region are empty of charge carriers. Then, the diode is momentarily pulsed with a voltage bias, which decreases the depletion layer width, W, and allows the defects to capture charge. This is called the fill pulse because it floods the depletion region with charge thus filling the defects. The diode is then returned to its quiescent reverse bias state. Defining time zero to be at the end of the fill pulse, the capacitance is measured twice, at times t_1 and t2, and the output signal is the difference between these two capacitances:

$$\delta C \equiv C(t_2) - C(t_1) \tag{4.7}$$

$$\delta C^2 \propto N_t(\exp-(e_p t_1) - \exp-(e_p t_2)). \tag{4.8}$$

From Equation 4.8, it is clear that δC will change when the temperature of the diode changes because the emission rate is exponentially dependent on the temperature. So, for a given set of sampling times, t_1 and t_2, there must be a

temperature which gives an emission rate which will create a maximum δC. Taking the derivative of δC with respect to e_p and setting the result equal to zero gives:

$$e_{max} = \frac{\ln(t_1/t_2)}{t_1 - t_2} \qquad (4.9)$$

e_{max} is the emission rate which produces a maximum change in capacitance for a given set of sampling times. Thus, when the δC vs. temperature DLTS signal passes through a maximum, the emission rate of the defect level must equal the emission rate from Equation 4.9.

In this way, the DLTS measurement sequence may be considered as having an emission rate of its own defined by the sampling times t_1 and t_2. The maximum δC must then occur at the temperature at which the defect emission rate equals the DLTS emission rate. By ramping the temperature of the diode and determining the temperature at which the maximum δC occurs, the value of e_p and T are determined. These two values may then be put into Equation 4.5, to solve for the activation energy of the defect, E_a.

To calculate E_a with just a single pair of (T,e_p), the values of the variables in Equation 4.5 would need to be known, which usually is not the case, especially for the capture cross-section. Instead, the DLTS technique generates many data pairs of T and e_p by determining the temperature of maximum δC for many different sampling times, t_1 and t_2. A semilogarithmic plot is then made of e_p vs. 1/T.

In DLTS, the junction is initially kept at a constant reverse bias. Thereafter, a short pulse of forward bias (called a fill pulse) is applied which collapses the junction and thus fills the defect levels (traps) which are present. The trapped charge carriers are then emitted thermally, giving rise to a capacitance transient.

In studying deep-levels, information concerning energy, density, and capture cross-section, of recombination centers in the depletion region, can be readily obtained. It is also possible to determine the spatial distribution of defects within the crystal structure, and to distinguish between minority and majority traps; all of which permit characterization of the defect's effect on semiconductor operation. [Ref. 19:p. 1730]

Concentration profiling provides a more precise determination of trap concentration, but requires a number of scans for good resolution. Each successive scan uses a progressively larger majority-carrier pulse. To obtain the profile, a plot of signal destruction versus pulse voltage is used. Exploiting the fact that defects in the crystal lattice create energy levels within the bandgap, DLTS detects the presence of defects by monitoring the change in the junction capacitance due to the transient occupation of the defect levels by free charge carriers. In this way, the defects are said to capture free charge carriers, and since there are both majority and minority carriers available for capture in a

semiconductor junction, DLTS is capable of distinguishing between which type of charge carrier has been captured.

1. Defect Annealing

Another important aspect of a solar cell's radiation resistance is the annealing properties of the induced defects. The radiation induced defects of InP are well documented (references 10, 11, 16-19). The defects believed to be primarily responsible for radiation induced degradation in InP solar cell performance are majority carrier (hole) traps known as H3, H4 and H5, as shown in Figure 4-6. The H4 defect is associated with recoverable damage, and is believed to anneal out. The H5 trap is most often found in cells with permanent junction damage. The H3 defect behaves similarly to H4, but so close in spectrum to H4, that it is often masked H4's spectrum, and is difficult to distinguish. Majority carrier traps present a positive DLTS signal. The minority (electron) traps, designated EA through ED, present a negative signal, as shown in Figure 4-7. The sign of the DLTS signal will define the actual trap type. The damage effects of proton irradiation differ from those of electron irradiation, as illustrated in Figures 4-8 and 4-9.

By monitoring the height of the DLTS signal of the H4 defect center while injecting the diode with minority charge carriers, it was found that minority carrier injection rapidly anneals H4 even at temperatures as low as 200 K. This DLTS data is displayed in Figure 4-6. Similar measurements at

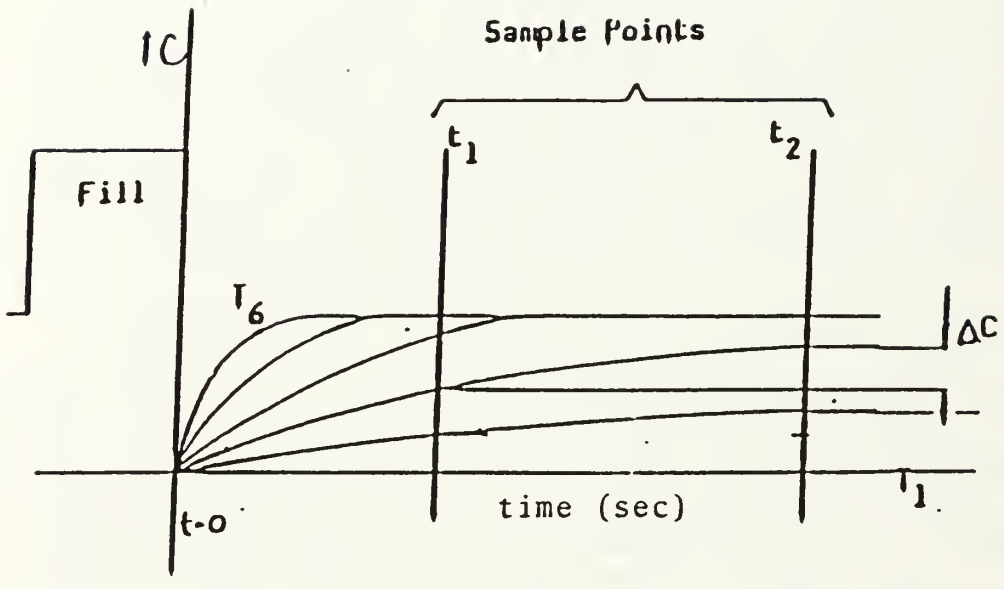

Figure 4-3. DLTS capacitance sampling sequence. The initial rise in capacitance is due to the applied fill pulse. The rate window indicates the temperature at which the transient is a maximum. [Ref. 16: p. 8]

higher temperatures showed that the annealing rate increases with increasing temperatures. Notice that injecting the diode with minority charge carriers simply means passing a current through it. These results indicate that under normal solar cell operating conditions, the major cause of the solar cell degradation is substantially annealed.

In summary, the analysis of the transient enables us to determine the trap characteristics (i.e. energy, capture cross-section, and concentration). The transient is measured between two sampling points at times t_1 and t_2 (i.e. $\delta C = C(t_2) - C(t_1)$). The rate window is defined as the inverse of the time period between the sampling points. δC will be small at high temperatures since all of the traps are readily ionized, and small at low temperatures since few will be ionized. However, when the rate window matches the maximum thermal emission rate of the deep level, δC will be a maximum. Hence an output of δC against temperature will show a DLTS peak, which is characteristic of the trap being studied.

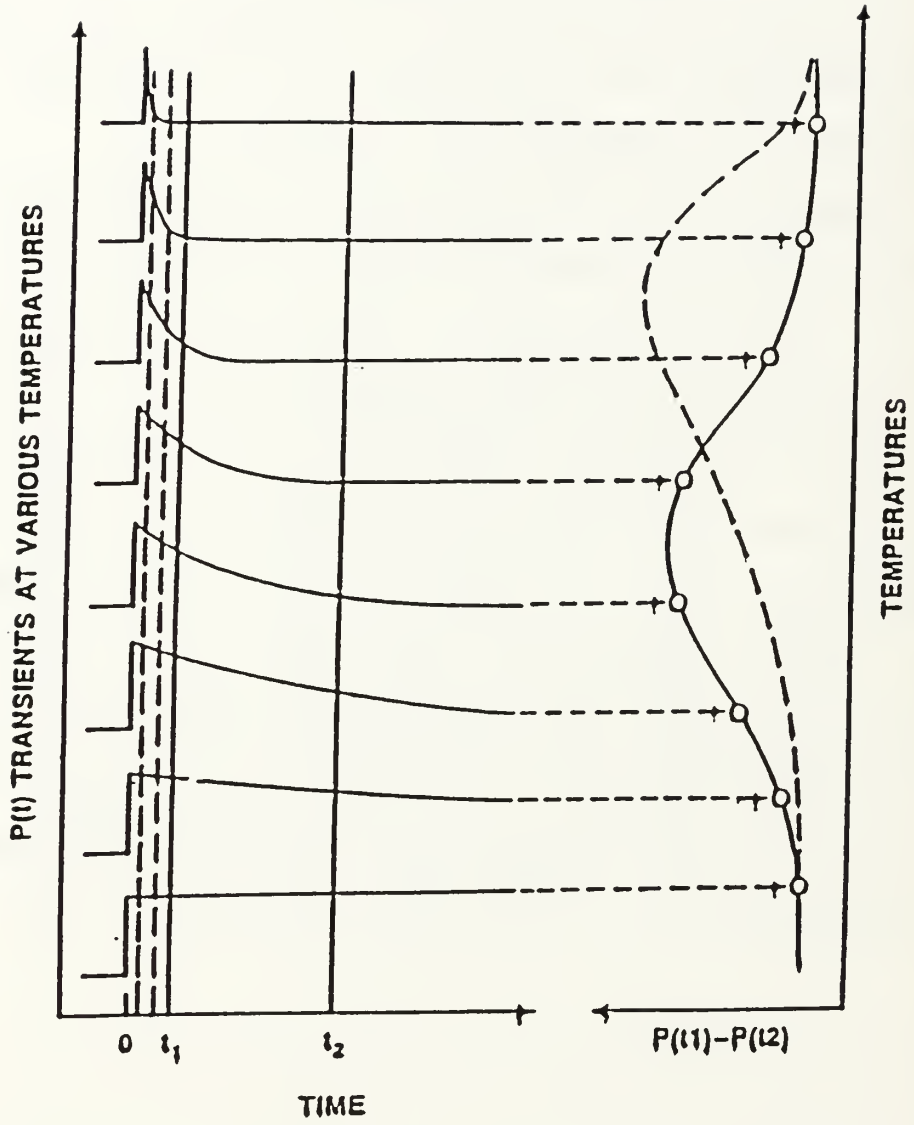

Figure 4-4. Formation of DLTS peaks. The double boxcar sampling measures the capacitance transient at two fixed times after removal of the fill pulse. [Ref. 2: p. IV-19]

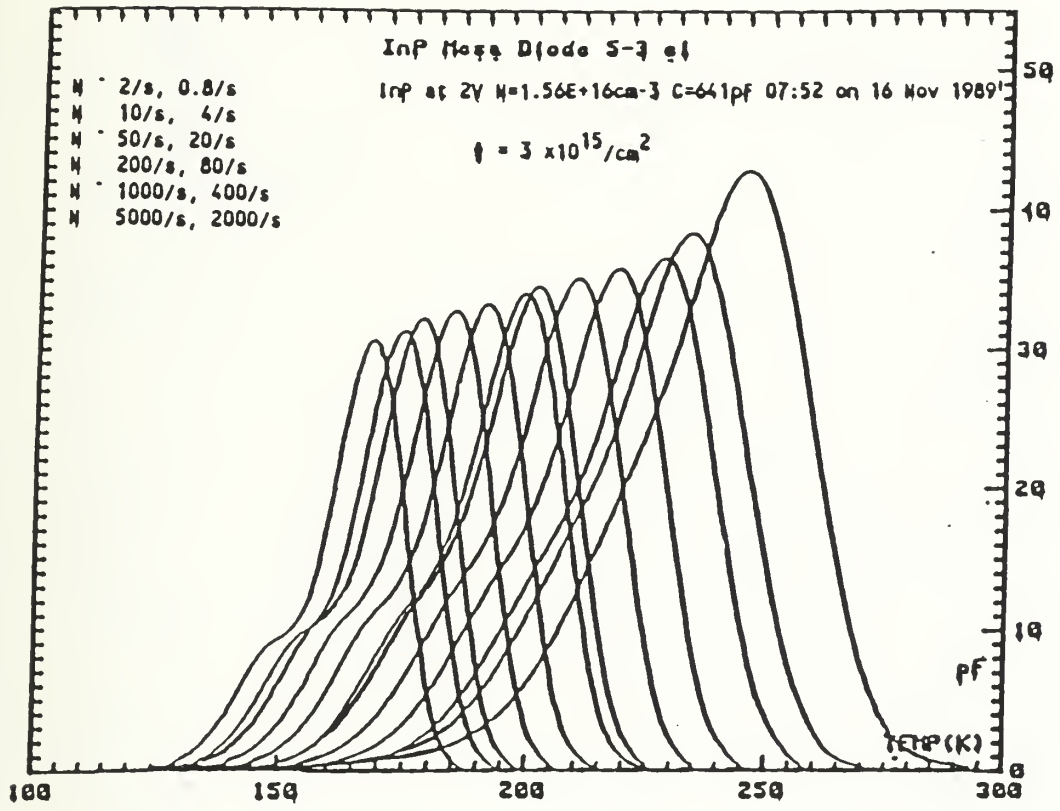

Figure 4-5. Typical DLTS spectrum generated by the temperatre sweep and the rate window. [Ref. 11:p. 16]

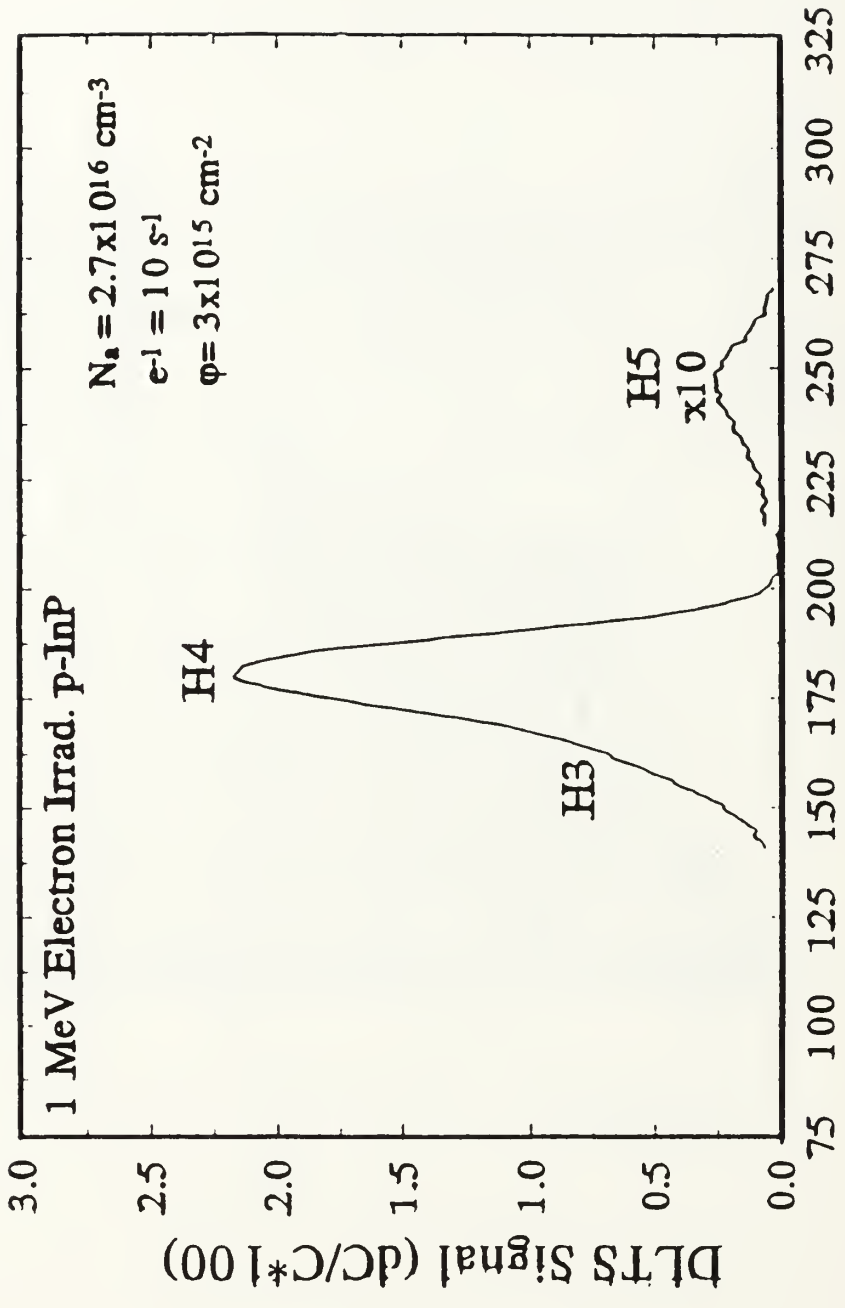

Figure 4-6. DLTS spectrum of the primary majority carrier traps (H3, H4, H5) induced by 1 MeV electron irradiation of InP. [Ref. 11: p. 42]

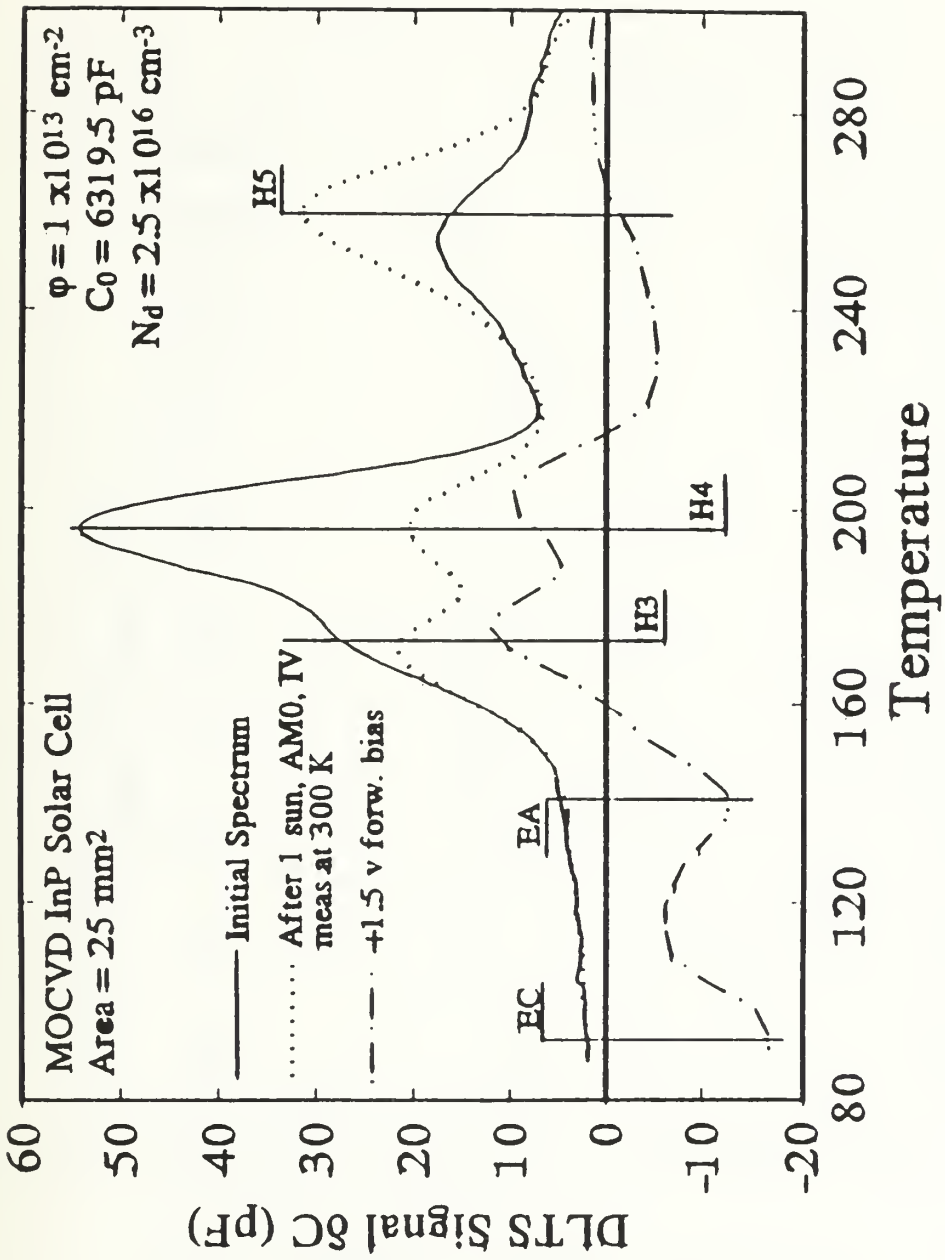

Figure 4-7. Complete DLTS spectrum of an InP solar cell , measured after exposure to 10 MeV proton irradiation. [Ref. 11: p.45]

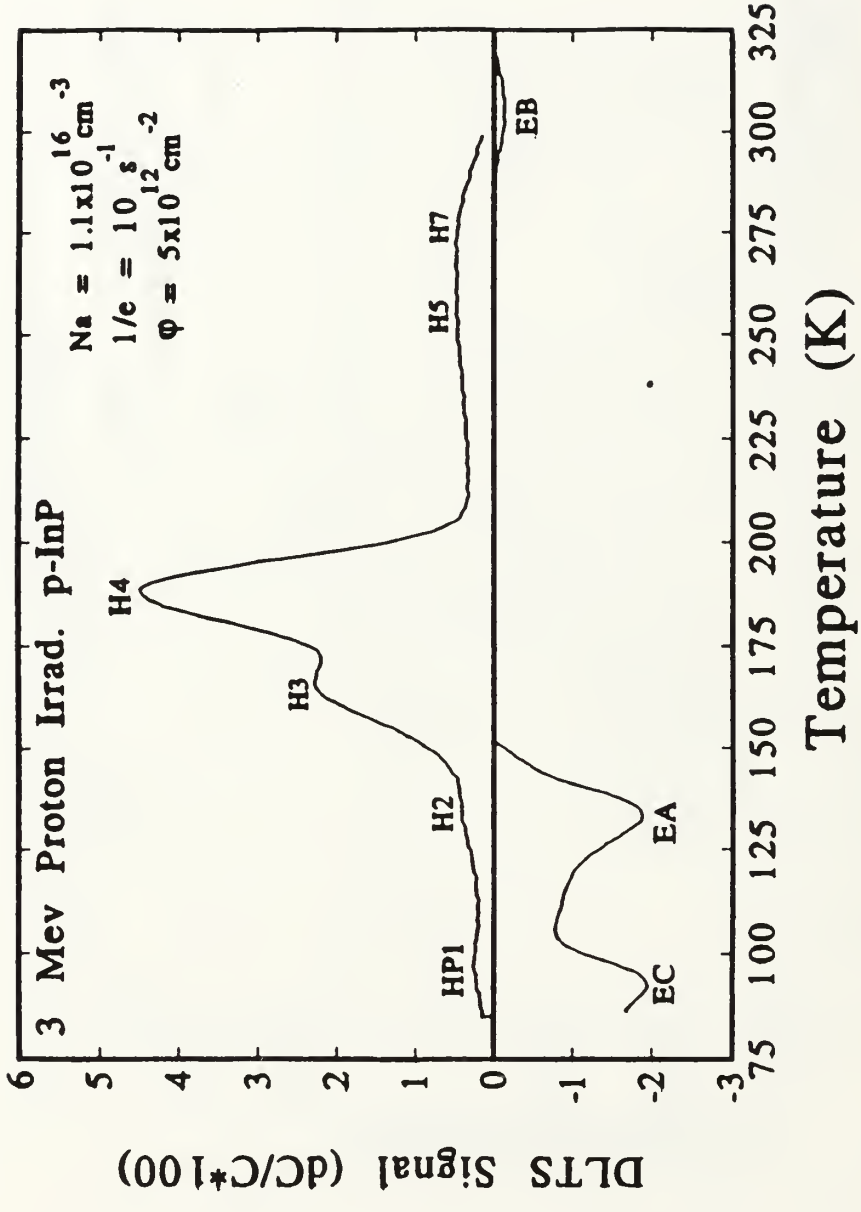

Figure 4-8. DLTS spectrum illustrating the effect of 3 Mev proton irradiation on an InP solar cell. [Ref. 18: p. 6491]

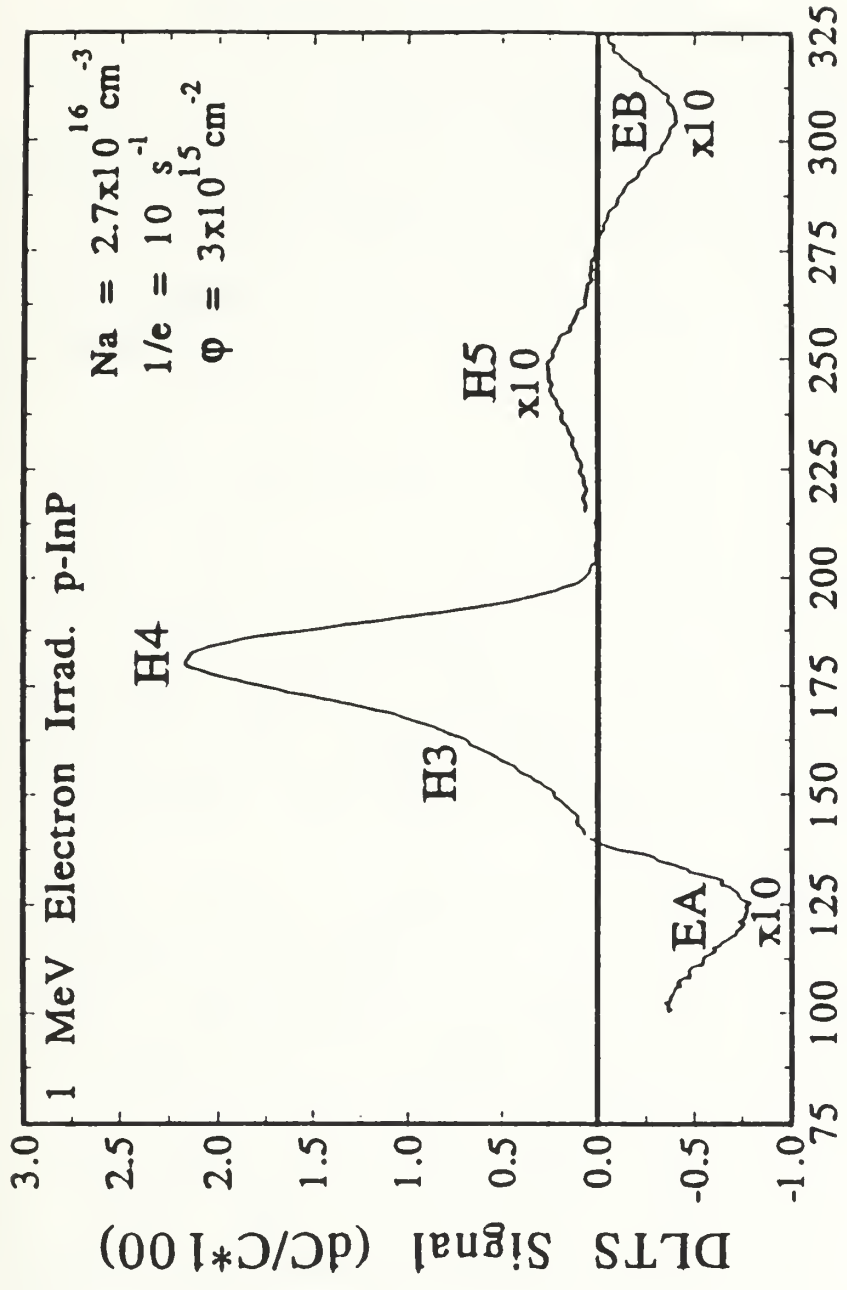

Figure 4-9. DLTS spectrum illustrating the effect of 1 MeV electron irradiation on an InP solar cell. [Ref. 11: p. 47]

V. GALLIUM ARSENIDE SOLAR CELLS

A. GaAs SOLAR CELL CHARACTERISTICS

The primary advantages of GaAs solar cells are radiation hardness and high photovoltaic conversion efficiency. Because of its nearly ideal bandgap (1.42 ev), efficiencies of up to 22 percent have been achieved. The zincblende lattice structure of GaAs causes it to be a direct bandgap semiconductor. In other words, photons are absorbed almost immediately after entering the cell. Also, the minority carriers' lifetimes and diffusion length are much smaller compared to a indirect bandgap semiconductors, such as silicon. Rapid absorption of incident photon energy by the lattice also contributes to the radiation resistance of GaAs cells. [Ref. 20]

The GaAs cells used in Cypranowski's 1989 research [Ref. 5] were grown on GaAs substrates (GaAs/GaAs). The weight density of GaAs solar cells is more than twice that of Silicon cells. Also, the GaAs/GaAs cells were found to be very brittle, and suffered high mechanical losses when handled. Originally, both silicon and germanium were considered for foreign substrates to host thin GaAs cells. Germanium substrates proved more effective, and in recent years, have replaced GaAs as a very strong, light, and thin substrate material. Advancements in germanium substrates for GaAs solar

cells have led to reduced cost, better electrical performance, and higher mechanical strength (fewer solar array assembly losses).

> The use of Ge substrates retains all the advantages of GaAs cells (high efficiency, good radiation resistance, low temperature coefficient, and increased tolerance of reverse biassing caused by shadowing), and the higher mechanical strength of Ge improves the ruggedness. The only drawback with Ge substrates is that they absorb most of the solar spectrum at wavelengths above the cut-on wavelength of GaAs (>0.87 microns), and this increases solar absorptance. However, the slight increase in orbital temperature is of less concern because of the low temperature coefficients. [Ref. 21: p. 1512]

GaAs/Ge cells are thinner than GaAs/GaAs, leading to a reduction in cell weight, and a corresponding savings in the orbital mass of the array. Pinzon's 1991 work [Ref. 6] was conducted on GaAs/Ge cells manufactured by the Applied Solar Energy Corporation (ASEC). The cells used in the research were the same (ASEC "22 Ge-200") type; 2 x 2 cm, p+ on n-type GaAs, heterojunction, with a germanium substrate (Figure 5-1). The cells were produced using metalorganic chemical vapor deposition (MOCVD) techniques.

The distinction between the homojunction GaAs/GaAs cells, and those on a Germanium substrate, is significant. The radiation tolerance of GaAs/Ge cells is superior to that of GaAs/GaAs cells [Ref. 22]. The importance of the heterojunction on the cell's electrical characteristics must be considered when the lattice is subjected to damage from radiation. "Germanium is better than silicon as a starting substrate for this heterostructure cell configuration because

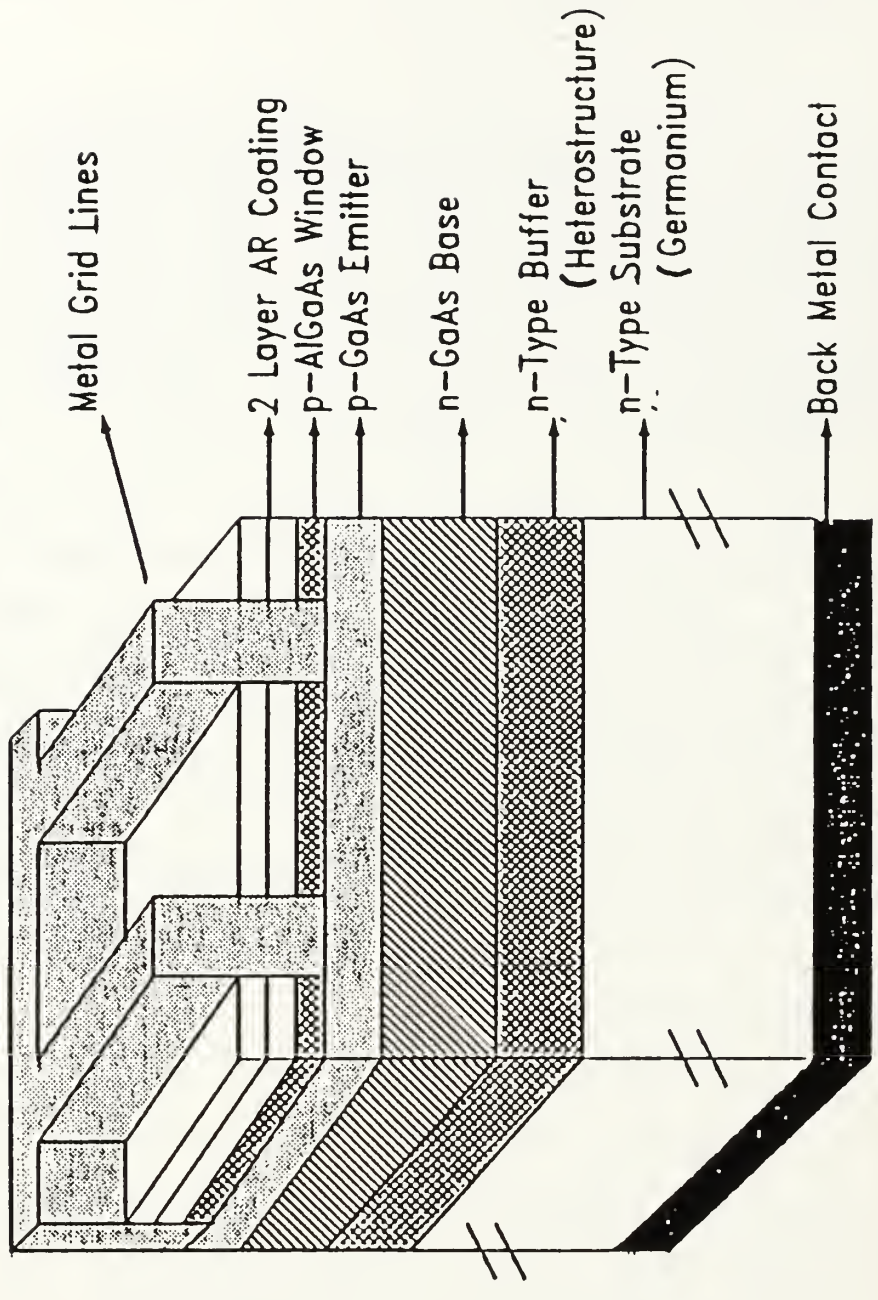

Figure 5-1. Cross sectional view of ASEC "22 Ge-200" GaAs/Ge solar cell. Actual manufactured cell dimensions: 2 cm x 2 cm x 200 microns. [Ref. 4]

GaAs and Ge have closely matched lattice constants and thermal expansion coefficients" [Ref. 23: p. 273]. The final performance of radiation damaged materials is strongly effected by the behavior of the lattice. "For GaAs, the p^+n configuration is significantly more radiation resistant than the n^+p cells. The increased degradation in this latter cell can be attributed to radiation induced increases in series resistance, decreased shunt resistance, and degradation in the p-base." [Ref. 24:p. 551] The importance of the heterojunction interface causes significant differences in behavior from GaAs substrated material.

Previous research on gallium arsenide [Refs. 5, 13 and 15] yielded extensive DLTS data after electron irradiation to GaAs/GaAs. DLTS analysis indicated three defect levels were introduced to GaAs/GaAs. The deep levels are known as the E3, E4, and E5 defects with energies of 0.31, 0.71, and 0.90 Ev, respectively [Refs. 25, 26]. Sheng, et al [Ref. 15] presented DLTS scans of these defects in electron irradiated (AlGa)As/GaAs. In this material, defect concentration decreased with increasing annealing time; in minutes at 230°C. However, the density of E5 defect increased with the 60-minute anneal time at 230°C, indicating that a greater number of defects are being created by this process, than are recovering through annealing. It is possible that the E5 defect may limit annealing recovery, and is indicative of permanent cell damage. A similar problem exists in InP for the H5 defect.

B. EXPERIMENT OBJECTIVE AND PLAN

Cypranowski [Ref. 5] determined the optimum annealing process for radiation-damaged GaAs/GaAs solar cells. The objective of Pinzon's work [Ref. 6] was to reproduce Cypranowski's results, and analyze the damage and annealing mechanisms associated with induced defects using DLTS. Pinzon's results were inconclusive, and the objective of this research was to further investigate the mechanisms of defect growth and recovery, in an attempt to optimize solar cell annealing. In order to provide a better understanding trap concentration behavior, this experiment was planned to baseline reference measure the cells, then irradiate, and measure them again. Each performance measurement was planned to require a DLTS run, and I-V curves. A full test cycle was to involve measurement, irradiate, measure, anneal, measure, irradiate, and to repeat the cycle. The intent was to have multiple cycles to establish a pattern of trap level fluctuation, demonstrating radiation damage and annealing recovery.

C. EXPERIMENTAL PROCEDURE AND RESULTS

The Bio-Rad DL4600 is equipped with a capacitance offset unit to remove the relatively large quiescent capacitance of the sample. The capacitance of the 2 x 2 cm GaAs/Ge cells greatly exceeds the offset unit's picofarad magnitude, so the cells must be cut to a small size for DLTS analysis. All cells used in this study were scored and cleaved at the NRL

Nanotechnology Lab by Mr. Stan Lewis. The success of the cell sizing is apparent in the uniform I-V curves measured on the 45 mm^2 resultant GaAs samples, Figures 5-2 and 5-3. The few samples that demonstrated reduced fill factors, as a result of defects introduced during cleaving, were discarded.

The DL4600 requires four points of electrical contact; two on each side of the junction. Mounting the sample to the cryostat stage with silver paint provides electrical contact to the cell back, the n-side of the GaAs junction. Top contact is made through two 50 micron whisker probes to the cell bus bar. In the case of the GaAs cells, the antireflective coating insulated the probes from contacting the bus bar, and prevented electrical contact. Contact could be made only by coaxing the 50 micron whiskers into the bond pads, providing tenuous contact. Thermal cycling in the cryostat frequently caused probe contraction, and lost contact. This obstacle was eventually overcome by shearing off the probe whiskers, and forcing two probe stubs into the dimpled contact pads (4) on the bus bar. All electrical contacting work was performed using a microscope, but still resulted in some damage to the bus bar plating. Forcing the probe stubs onto areas of the bus bar without contact pads scratched through the silver plating, and destroyed the bus bar. Sample segments without a bus bar could not be measured. Achieving electrical contact only through the bond pads meant

that when a 2 x 2 cm cell was sized, only two of the eight segments produced could be mounted for analysis.

Current-voltage (I-V) characteristics of the cells were measured under a Spectrolab X25 solar simulator calibrated with a GaAs reference cell. All I-V measurements were done at AMO, one sun, at 25°C. The DLTS equipment was calibrated using silicon samples with known gold defect impurities. DLTS measurements , in vacuum, over the range of 80 to 300k were to be made directly on the mounted samples through a window in the liquid nitrogen cryostat.

Experimental objective required pre-radiation exposure I-V curves and DLTS runs for a baseline reference. All samples had been cut, and I-V measurements made, before receiving any indication of a problem with the DLTS procedure. Previous research on these same GaAs/Ge cells produced extensive DLTS data [Ref. 6].

DLTS measurements could not be made on the GaAs/Ge cells due to the very low breakdown voltage experienced when a reverse bias was applied to the samples. Reverse biasing the GaAs/Ge cells causes significant current leakage. This current leakage prohibits DLTS analysis of ASEC GaAs/Ge solar cells. Section V.B.1 offers an explanation for the effect.

The samples were irradiated with 1 MeV electrons to a level of 1E15 in the Van de Graff generator at NASA Goddard Space Flight Center. An electron fluence of 1E15 was used in the belief that: 1) solar arrays in geosynchronous orbit

currently receive this level of exposure, or greater, during orbital life (Figure 1-4), and, 2) this level would show adequate I-V degradation to make annealing recovery easily apparent within the tolerance of the equipment used. The radiated sample I-V characteristics were then measured. The radiation induced degradation in I-V performance of all samples was as expected for this dose level.

Sample annealing was performed in the DL4600 cryostat for thermal control and ease of applying the selected forward bias current. Since GaAs solar arrays do not generally operate at temperatures higher than 90°C on orbit, this temperature was used to optimize all forward bias annealing attempts. The search for the optimum current level and duration was then begun in the attempt to maximize forward biased, thermal annealing. No attempt was made to illuminate the cells during annealing, since the applied forward bias current densities greatly exceed those generated during illumination. Pinzon [Ref. 6], concluded that an applied bias of 0.5 amps/cm^2 was too high for the thin (200 micron) cells, and probably caused damage to the samples. The results presented in references 5 and 6, both concluded that recovery in I-V parameters occurred after each annealing phase. In planning this experiment, following the procedures of previous work, it seemed reasonable to expect some recovery after each annealing step.

In the first annealing attempt four samples were placed in the cryostat for 48 hours at 90°C. The bias current densities applied to each sample were 0, 0.05, 0.1, and 0.2 A/cm^2, respectively. The resultant I-V curves showed no improvement in any sample. Also, the reference sample mounted at the rear of the stage, with no applied current, was destroyed. A second attempt was made, using the same conditions, on four different samples and yielded identical, negative, results; and a destroyed reference sample.

The back end of the stage probably has poor thermal control, due to thermostat location, and resulted in overheating the reference (no current) samples mounted there. The failure to produce cell recovery at the low currents initially applied led to a search for the maximum applied current that these samples could withstand before failing. New samples were forward biased with densities of 0.25, 0.3, 0.4, and 0.5 A/cm^2. These bias levels produced no recovery, but the samples were not damaged either. The 0.5 A/cm^2 biased cell showed no change in I-V characteristics, proving that the cells could withstand this current density. Figures 5-2 and 5-3 illustrate the general results of these annealing attempts for a few samples. Note that most of the post-anneal curves fall within a small tolerance margin, with little failure in fill factor. The cumulative fill factor degradation routinely inherent in solar cell testing becomes apparent in Figures 5-4

through 5-8, where a history of the annealing attempts on one sample, cell fragment #27.3, are plotted.

Samples were then mounted, three at a time, for annealing at 90 centigrade, for 12 hours, to receive the same forward bias voltage, by applying a uniform current density. The applied forward bias was increased from 0.5, in 0.1 A/cm^2 increments, up to 1.30 A/cm^2. I-V measurements were made after each increment in forward bias. Failed cells were discarded and replaced. Many cells were lost to mechanical failure during mounting, and few samples survived long enough to be measured after 1.0 A/cm^2. No recovery in I-V characteristics was evident after annealing. Figure 5-9 shows the results of one sample that survived 1.10 A/cm^2 forward bias, with little destruction in cell performance.

As in any experimental work, great care should be exercised when interpreting data results. The cumulative plots of normalized photovoltaic parameters shown in Figures 5-4 through 5-8 can be misleading if not viewed together. For example, Figures 5-5, and 5-6 would seem to indicate good recovery in fill factor, and in V_{oc} after annealing sample #27.3 for 15 hours, at 0.30 A/cm^2. The actual I-V curve that produced this data point seemed very promising, since the I-V plots are not normalized to their original, post-radiation value. However, Figures 5-4, 5-7, and 5-8, show no corresponding recovery in I_{sc}, power, or in efficiency. Successful annealing recovery would appear as an increase in

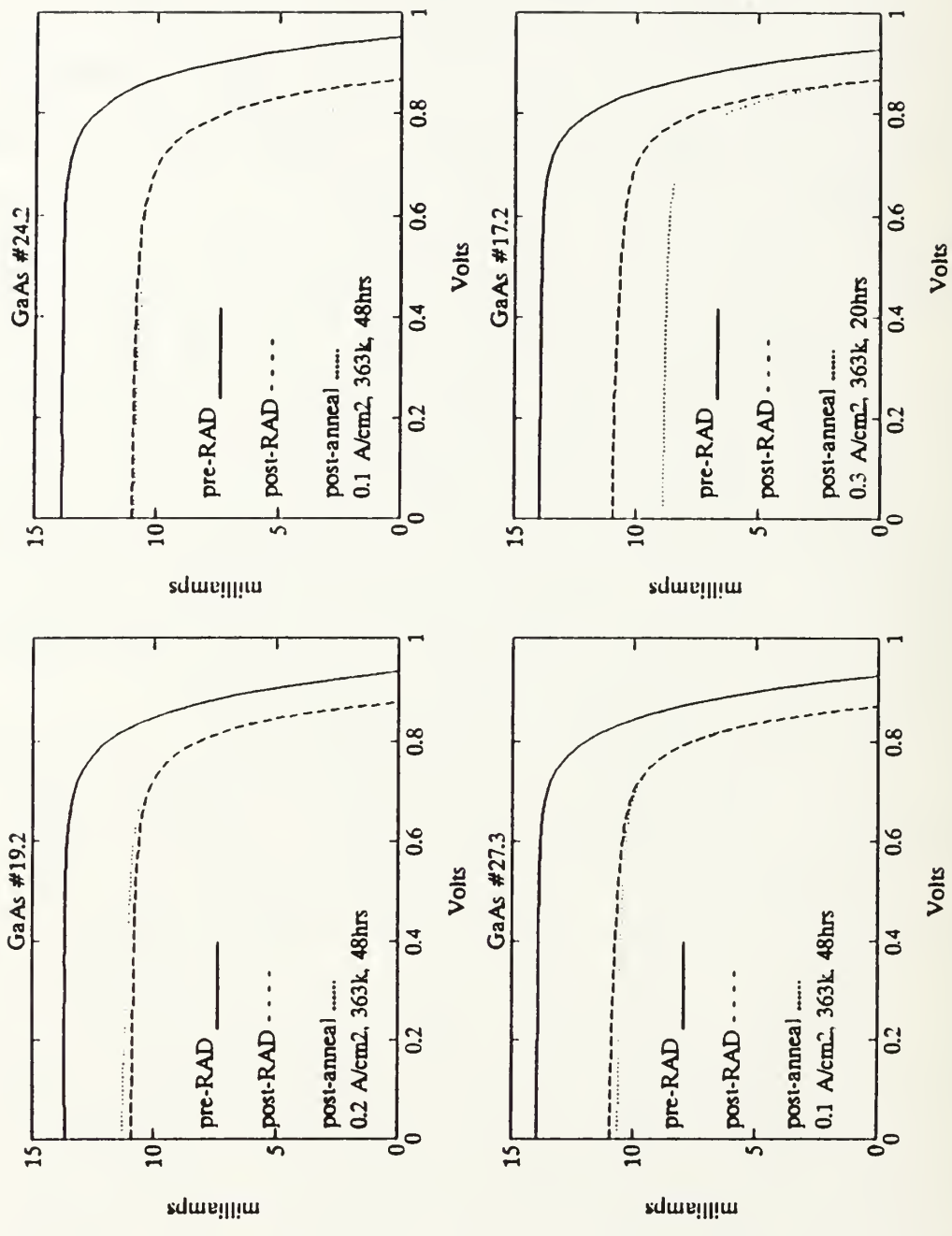

Figure 5-2. GaAs/Ge 45 mm^2 sized sample solar cell I-V curves before and after 1 MeV electron irradiation. Fluence = 1E15.

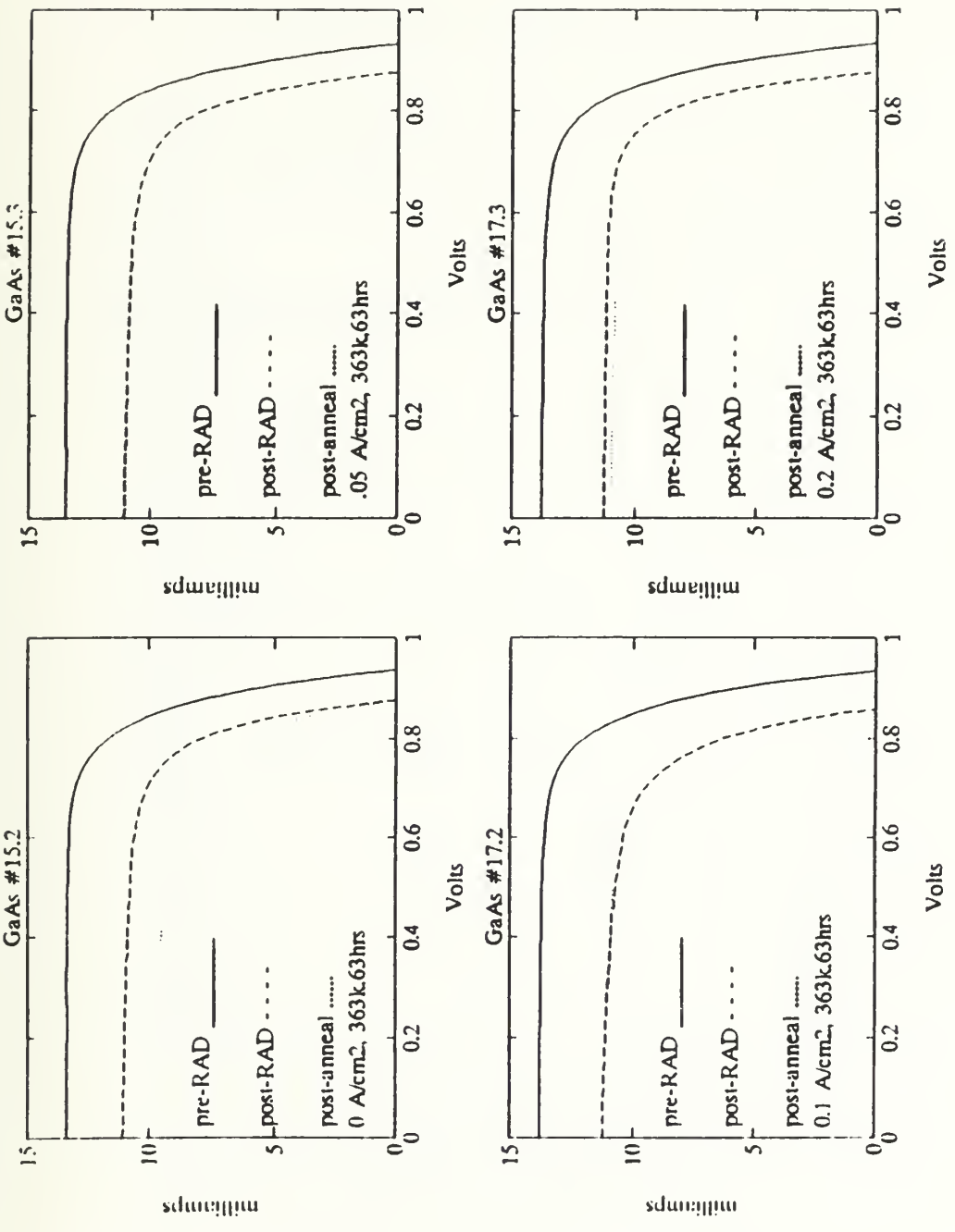

Figure 5-3. GaAs/Ge 45 mm^2 sized solar cell sample I-V curves before and after 1 MeV electron irradiation. Fluence = 1E15.

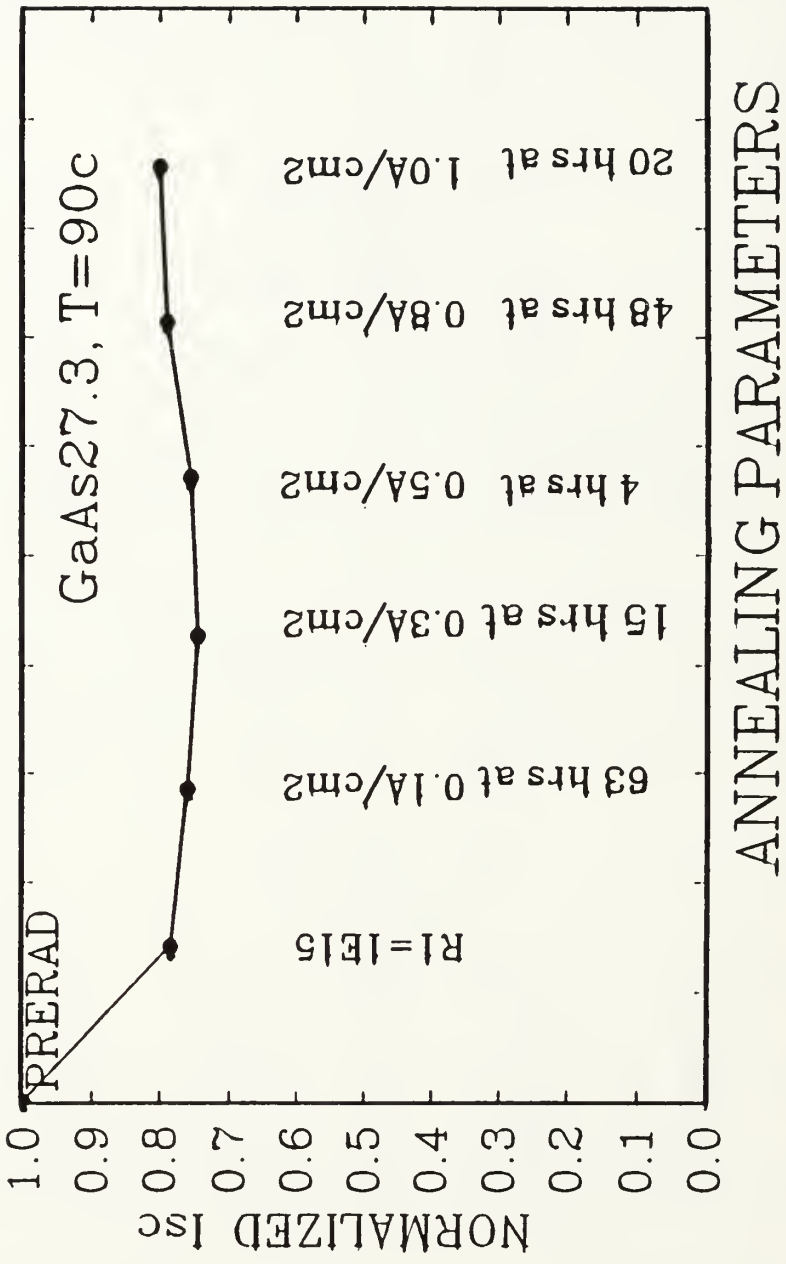

Figure 5-4. GaAs/Ge sample #27.3, effect of annealing on short-circuit current after 1 MeV irradiation to a fluence of 1E15.

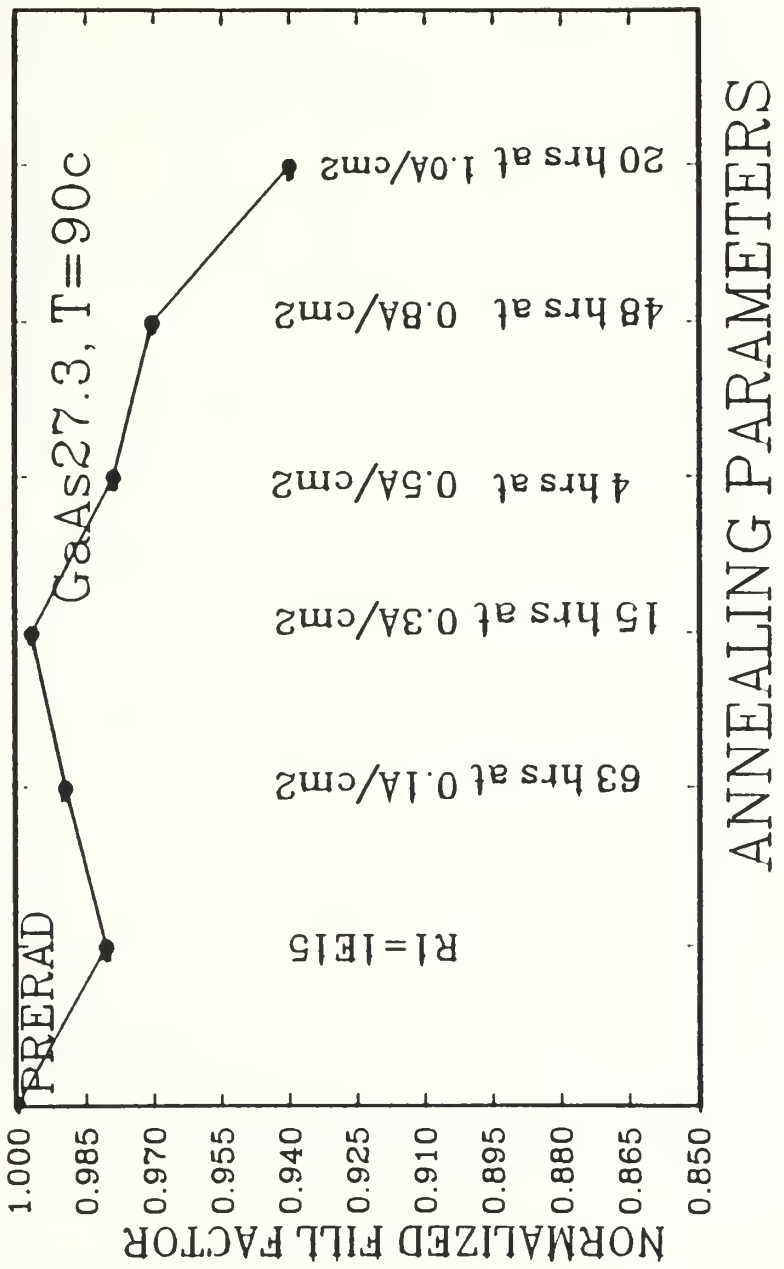

Figure 5-5. GaAs/Ge sample #27.3, effect of annealing on Fill Factor after 1 MeV irradiation to a fluence of 1E15.

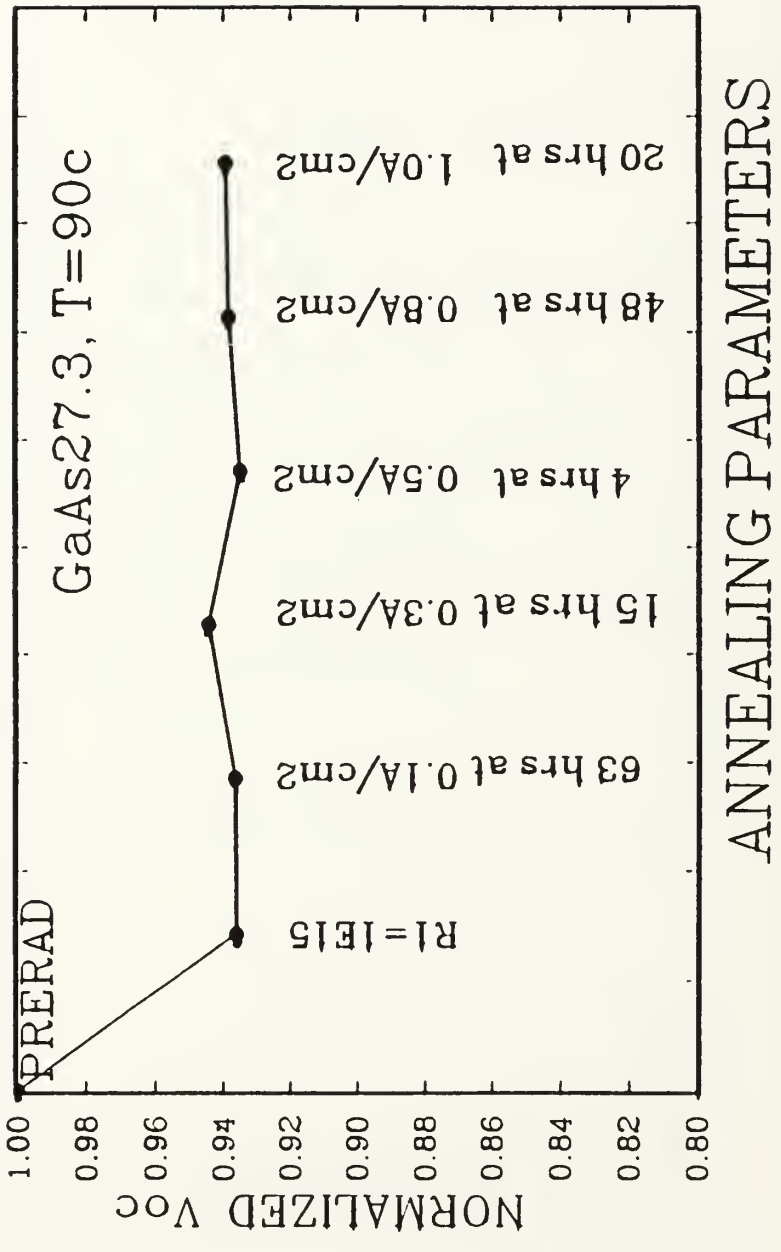

Figure 5-6. GaAs/Ge sample #27.3, effect of annealing on open-circuit voltage, after 1 MeV irradiation to a fluence of 1E15.

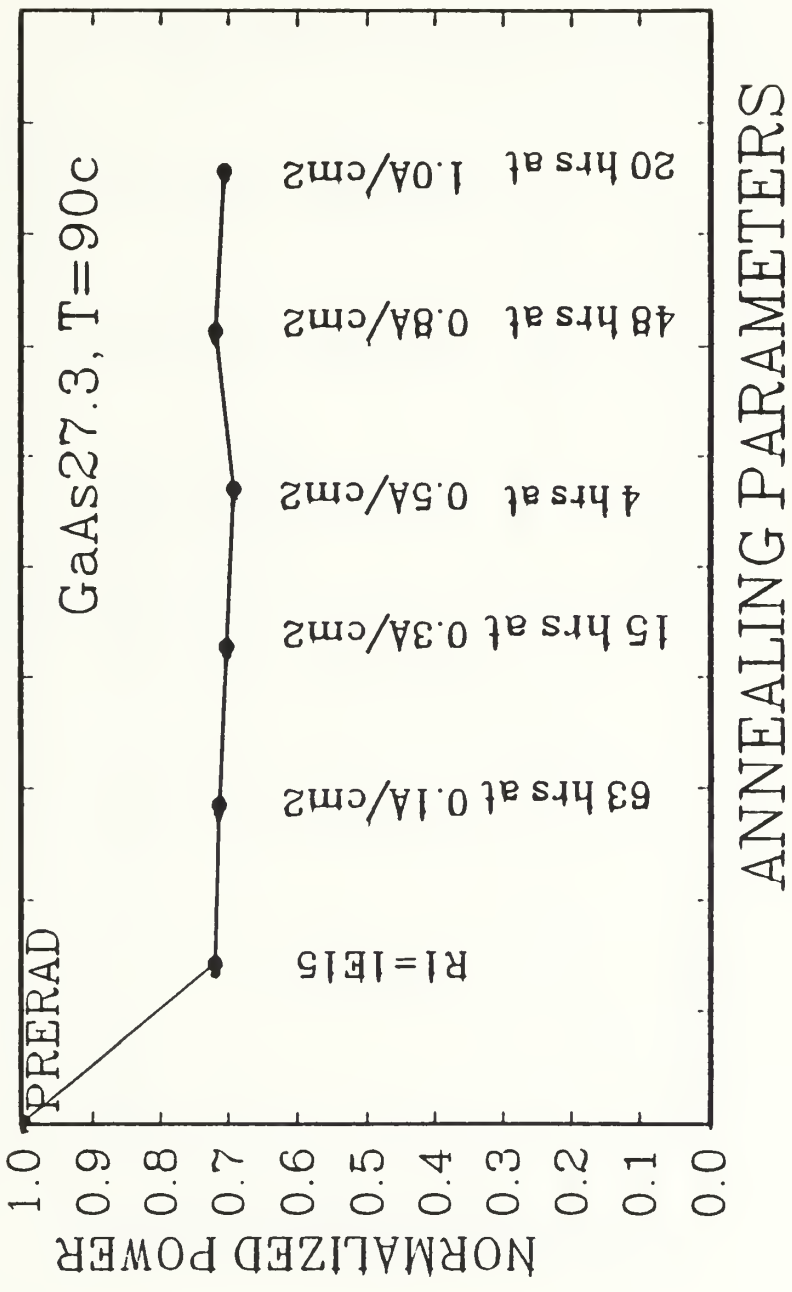

Figure 5-7. GaAs/Ge sample #27.3, effect of annealing on output power, after 1 MeV irradiation to a fluence of 1E15.

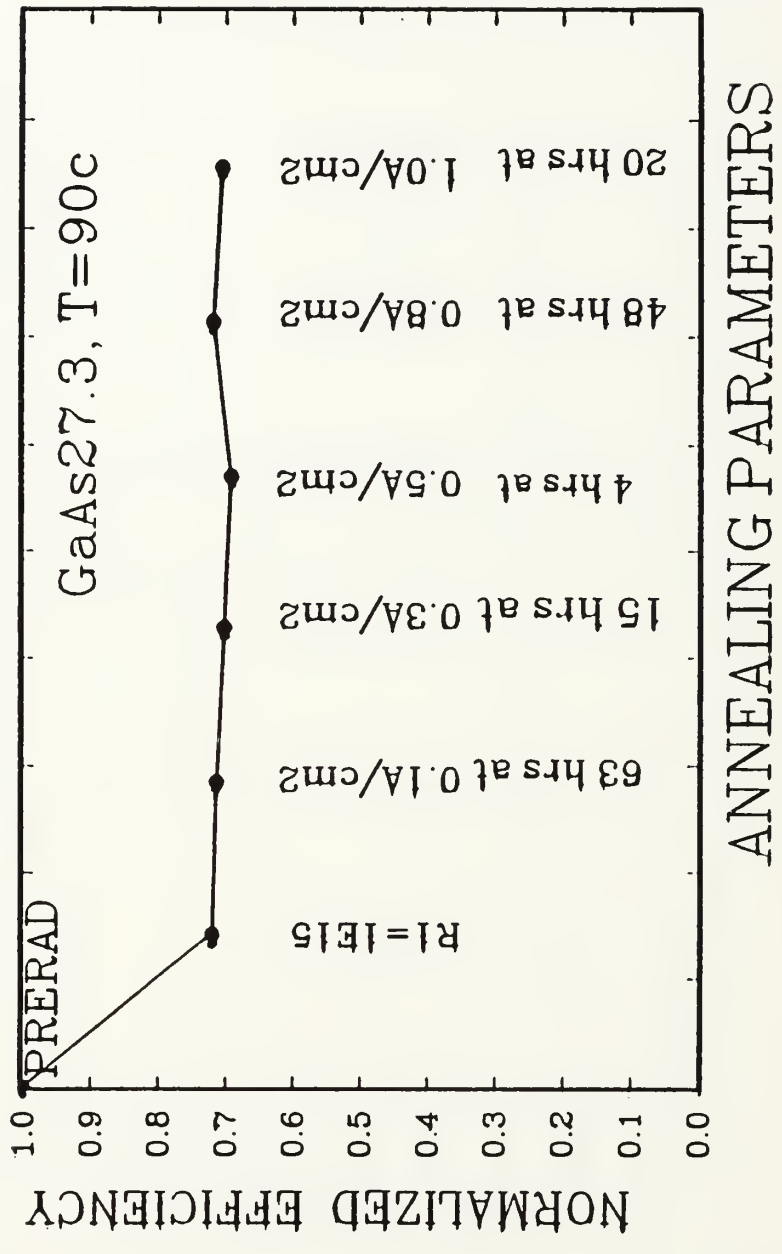

Figure 5-8. GaAs/Ge sample #27.3, effect of annealing on Efficiency, after 1 MeV irradiation to a fluence of 1E15.

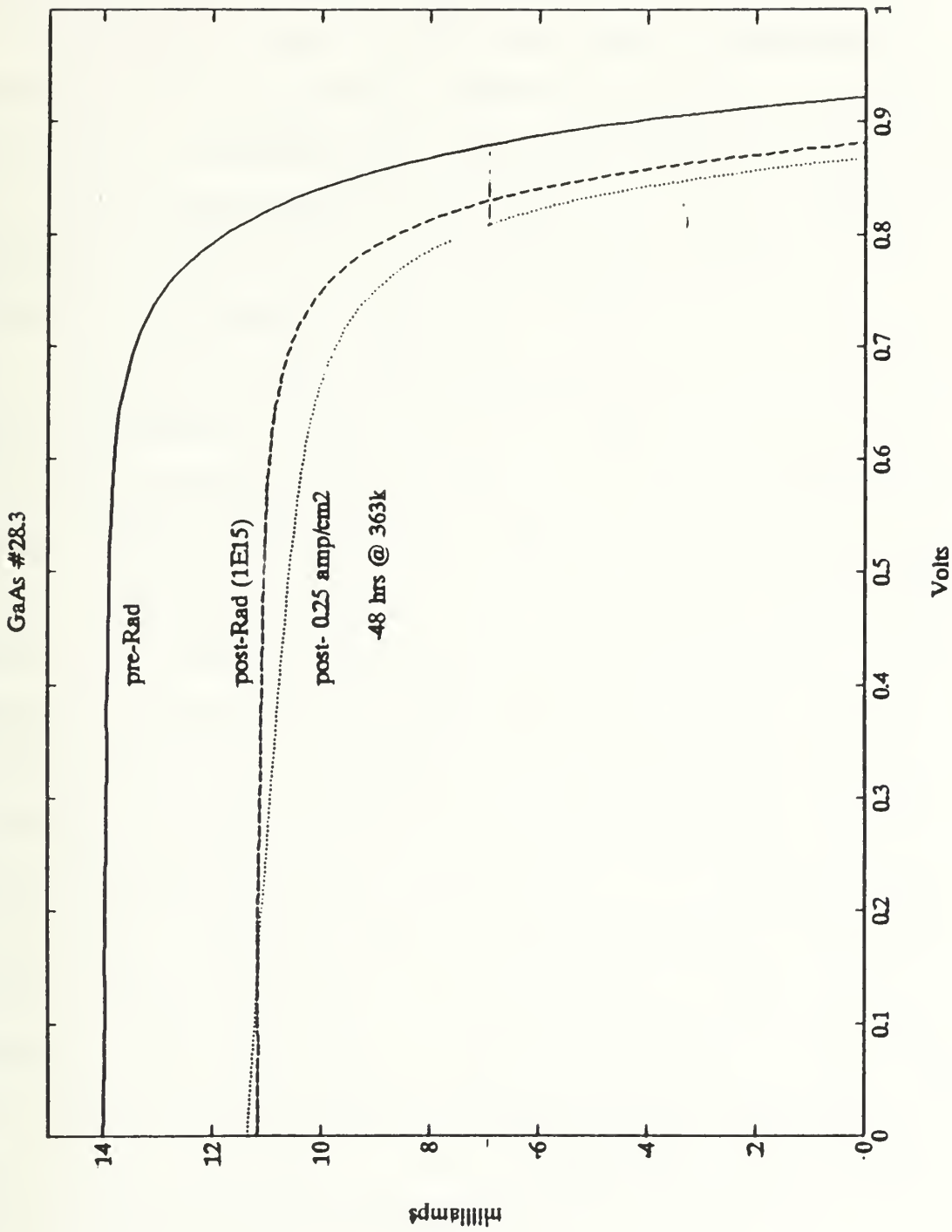

Figure 5-9. GaAs/Ge sample #28.3, after surviving forward bias annealing currents of 1.10 A/cm^2, at T=90^{0}C.

all parameters, except possibly fill factor. This data point is inconsistent, indicating some error in experimental procedure. A similar explanation should be invoked for GaAs sample #17.2, Figure 5-3, that demonstrated a temporary improvement in its I-V curve, but was not reproducible. A potential source of significant error lies in calibrating the solar source illumination. Any sudden increase in V_{oc} should indicate a need to verify illumination intensity.

An even more dramatic I-V curve was obtained after annealing sample #27.3 for 48 hours, at 90 degrees C, with 0.8 A/cm^2. The I-V curves for this annealing attempt were repeated four times to verify the uniform increase in I_{sc}, power, V_{oc}, and efficiency. The decrease in fill factor was to be expected, due to the extensive handling of this sample. As can be seen in Figures 5-4 through 5-8, even after these parameters were normalized to their post-radiation values, a definite improvement is evident. No suitable explanation is available for this event, but it is difficult to ignore.

In an effort to continue the experiment, new GaAs cells were sized and I-V curves measured. Had time and equipment permitted, continued annealing investigation intended to proceed in two directions:

1) Irradiate samples to an exposure of 1E15, then forward bias and thermally anneal them ($90^{\circ}C$, 12 hours, 0.6 A/cm^2) , cyclically, for 4 or 5 radiation/ anneal cycles. The objective would be to determine if cycling the annealing

halted degradation to a fixed percentage of efficiency.

2) Irradiate samples to 1E14, and cycle the annealing, in an attempt to determine if a dose of 1E15 introduced damage too extensive to anneal out. Repeating the cycles would also be attempted to determine if degradation could be halted by annealing after lower levels of damage were incurred.

1. Antiphase Domains and DLTS

In order to effectively conduct a DLTS analysis, the very weak capacitance transient that occurs at the junction must be measured with great accuracy. The heart of the Polaron DL 4600 Deep Level Transient Spectroscopy system is the Boonton capacitance meter. The Boonton is a capacitance bridge which matches the capacitance of the sample. This meter uses phase sensitive detection and is accurate to 0.01 fF (10E-17 Farads). Leakage currents in a sample can affect the sensitive capacitance measurements (on the order of pF to fF) which the Boonton meter detects. Too much leakage current presents the detector with a resistive shunt across the junction which prevents detection of the capacitance transient. Current leakage causes the sample to conduct and lose its capacitor effect, especially in the presence of large electric fields. If the leakage is high enough, both carrier emission and capture occur at the same time, leading to complete failure of the junction to separate charge. Current leakage increases with: (1) reverse bias, since there are more carriers introduced available to be captured, and (2)

exposure radiation, since this increases the number of carrier-emitting defects produced.

Diode edge effects, generally introduced when the sample is cut to size for analysis, can create small leakage currents. These edge effect generated currents are apparent in a decrease in sample Fill Factor during an I-V measurement. The sharpness of the 'knee' on the I-V curve peak power point collapses, indicating a loss in the junction's ability to separate charge, due to small currents that leak across. This non-recoverable loss in photovoltaic efficiency is frequently encountered during solar cell analysis, and can be seen in Figure 5-8.

Internal paths for leakage currents can develop in the crystal lattice of the cell during manufacturing. The electrical performance of solid state materials is strongly dependent on proper crystallographic orientation of the lattice. "The V_{oc}, open-circuit voltage, of a cell on exact (100) Ge is much lower than that of a cell on a 2 degree off (100) Ge. This is supposed to arise from the leak current through the antiphase boundary of the GaAs layer on exact (100) Ge. ....solar cells on 2 degree off (100) Ge substrate have extremely high intrinsic efficiency (20.3%), identical to that on GaAs substrate at AMO." [Ref.28] Since cell performance is enhanced by preferential substrate lattice orientation, manufacturers produce the favored growth orientation.

However, cell performance remains significantly affected by the heteroface (GaAs/Ge) region's influence on the p-n junction.

> When GaAs cell layers were grown on both GaAs and Ge substrates in the same MOCVD run, the reverse breakdown voltage for GaAs/Ge cells was about one-half that of the GaAs/GaAs cell. Considering that the reverse bias behavior is controlled by the GaAs P-N junction, it was concluded that one different factor in reverse bias behavior for the two substrates was the possibility of different growth properties of the GaAs layer. One hypothesis is that the Ge substrate is covalent (electrically neutral) whereas the grown GaAs layer is ionic (Ga and As atoms with opposite charges). This electrical imbalance affects the grown structure (even though the lattice spacings are well matched) and is usually considered to form antiphase domains. [Ref. 29]

The APB's provide a path for current to leak across the junction, effectively shorting the junction when a reverse bias is applied. "An antiphase boundary forms in GaAs because, although it is cubic, it does not possess a crystallographic center of symmetry; materials with the diamond-cubic structure (Si and Ge) do. Two domains can therefore grow which are related to one another by the inversion operator, i.e. the sites occupied by the Ga and As atoms in one domain are interchanged in the other domain. The interface between the two antiphase domains is then conventionally known as an antiphase boundary." [Ref. 30: p. 181]

The formation of antiphase boundaries (APB) in GaAs solar cells grown on Germanium substrates is generally considered a benign phenomenon since its affects the cell's

behavior only during reverse bias conditions. "This network, of mainly benign-growth features, does not significantly shunt the PN junction (meaning that the curve fill factors at and above one-sun conditions are not lower). However, the network could spread the reverse power dissipated when the cells are shaded and thus reduce the chance of catastrophic failure at a few defects." [Ref. 29] The APB's thus have a beneficial effect in protecting the solar array during shadowing, when the shaded cell is driven into reverse bias and must dissipate power to prevent localized hotspots that lead to thermal failure.

The reverse bias breakdown voltage of a sample is particularly critical to DLTS analysis. At reverse breakdown voltage the junction fails and conducts. This breakdown threshold occurs at 20 to 50 volts in silicon cells, and about 8 to 10 volts for GaAs/GaAs and InP. Since the GaAs/Ge cells could not be held at reverse bias, due to current leakage through antiphase boundaries, DLTS analysis could not be done on them. This unfortunate fact was confirmed by the manufacturer [Ref. 29].

The significant crystallographic differences between homojunction GaAs/GaAs and heterojunction GaAs/Ge are not the only corrections needed in this research. References 5, and 6, conducted annealing attempts for extended periods, often for days. The reaction kinetics of 1 MeV electron damage is primarily all first-order, and any defect concentration

recovery should occur within a short period of time, 60 to 90 minutes. [Refs. 9, 13, 15, 20] Thus, annealing attempts should not exceed a few hours duration. Six hours should be viewed as a maximum time for permitting recovery to become evident, and any annealing beyond this time would not significantly reduce trap concentrations enough to make them any less apparent. In other words, if recovery does not show in six hours, it probably is not occurring.

VI. INDIUM PHOSPHIDE SOLAR CELLS

A. InP SOLAR CELL CHARACTERISTICS

Indium phosphide has a bandgap of 1.35 eV, and a very high resistance to radiation damage. These properties, and an average conversion efficiency of 16.5%, make InP a superior replacement for GaAs and silicon in conventional solar cells. High radiation tolerance permits considerable thickness reduction in protective solar cell coverglass, which translates directly to reduced solar array mass. However, InP has been used in only a very few applications in the electronics industry, and is not currently in high demand. Consequently, InP material and manufacturing costs remain high. While InP solar cells can be manufactured with excellent uniformity, they are very expensive, and are not economically attractive for commercial applications. Although InP technology is not as well developed as that of silicon or GaAs, solar cells have been fabricated from InP with efficiencies of over 18% [Ref. 11]. Table 6.1 presents the important electrical properties of InP.

The InP cells used in this research are the same Nippon Mining Company, NS12B type used in Cypranowski's [Ref. 5] and Pinzon's [Ref. 6] research, Figure 6-1. The thermally diffused, n^+-on-p cells, had initial dimensions of 1 cm x 2 cm x 400 microns.

TABLE 6-1

PROPERTIES OF INDIUM PHOSPHIDE
[from Ref. 11:p. 2]

Crystal Structure	Zincblende
Lattice Constant	5.869 Å
Density	4.787 g/cm^3
Melting Point	1330-1335 K
Dielectric Constant	12.35 x ϵ_o
Bandgap	1.34 eV at 300 K
Electron Affinity	4.38 eV
Temperature Dependence of E_g	-4.6×10^{-4} eV/K
Electron Mobility	$3\text{-}5 \times 10^3$ cm^2/Vs @300 K
Hole Mobility	80-150 cm^2/Vs @300 K
Electron Diffusion Length	1 um @300 K
Hole Diffusion Length	1.6 um @300 K
Electron Effective Mass	0.05-0.07 m_e
Hole Effective Mass	0.4-0.8 m_e
Surface Recombination Velocity	(n-type) 10^3-2×10^4 cm/s
Surface Recombination Velocity	(p-type) 1.5×10^5 cm/s
Intrinsic Carrier Concentration	6×10^6 - 2×10^7 cm^{-3}

B. EXPERIMENTAL OBJECTIVE AND PLAN

Cypranowski [Ref. 5] determined the optimum annealing process for radiation damaged InP solar cells. The objective of Pinzon's research [Ref. 6] was to reproduce those results while analyzing the damage and annealing mechanisms associated with the process using DLTS. This experiment was designed to continue investigating the mechanisms of defect growth and recovery in an attempt to optimize InP solar cell annealing .

The radiation resistance of n^+-on-p InP is slightly better than the p^+-n type. This is believed to be due to radiation induced degradation to the heavily doped p-emitter region [Ref. 24: p. 551]. Although this experiment had only one type of InP cell available for study, this effect is the

type of anomaly that is generally best investigated by DLTS analysis.

The intended experimental procedure for studying the InP cells is identical to that described in section 5.B for GaAs cells: I-V measurement, DLTS, irradiate, I-V, DLTS, anneal, etc.... However, the plan was more successful for the InP samples, in that these cells respond well to the reverse bias voltage applied for DLTS. An initial DLTS measurement was to be taken on the previously irradiated cells to establish a baseline for the analyses. Once damaged, the cells would be annealed using thermal and forward biased current annealing established by previous research [Refs. 5,6]. As with the GaAs cells, the InP samples were cut to size, and tested, prior to being included in the experiment, in an attempt to exclude sources of error that complicated previous investigations.

The NS12B InP cells have n^+-p junctions ,so a positive DLTS signal, indicating a majority carrier trap, represents hole capture. Similarly, a negative DLTS signal, resulting from electron capture, identifies minority carrier traps. Indium Phosphide research by Yamaguchi, et al [Ref. 31] identifies two major defect levels associated with radiation damage (Figure 6-2). The DLTS was taken on p-InP after 1-MeV electron radiation with 1E15 electrons/cm^2 fluence and successive thermal annealings at 410°K. The defect centers in the figure are labeled H4 and H5 for hole traps, in accordance

NIPPON MINING CO., LTD

May 16, 1991

LIST OF CONTENT

PRODUCT : INDIUM PHOSPHIDE SOLAR CELLS
TYPE : NS12B
QTY : 5 PCS
USER : NAVAL POSTGRADUATE SCHOOL
P/O NO. : N62271-91-M-1904

Cell Type : NS12A

Dimentions : 1 cm x 2 cm x 400 μm
AR Coating : SiO2/ZnS
Shadow Loss : Appr. 5 %

Measured I-V Data (AM0, Ta=25 °C)

CELL ID NO.	Voc (V)	Isc (mA)	FF (%)	Eff. (%)
A400-1	0.823	64.4	83.1	16.3
A400-2	0.823	64.2	82.9	16.2
A400-3	0.822	64.3	83.1	16.2
A400-4	0.823	64.2	83.2	16.2
A400-5	0.823	64.2	82.8	16.1

* Efficienctes mesured at Nippon Mining with AM0 solar simulator named SPECTROLAB X-25 MK-II.

Spectral Response

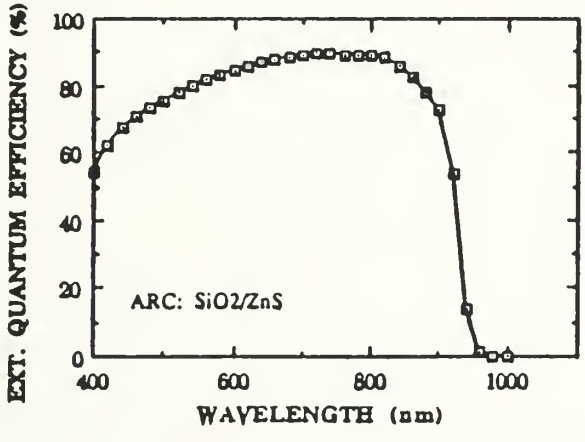

Figure 6-1. Manufactured characteristics of the Nippon Mining InP solar cells used in this research. [courtesy of Nippon Mining Company]

with Yamaguchi's [Ref. 31] findings. The major defect state introduced by electron irradiation in p-InP in the 0.37 Ev hole trap H4. This has been confirmed to be a recombination center [Ref. 10, p. 215]. This defect center is annealed out after 30 minutes of annealing at 410° K. Solar cell degradation and recovery is associated with the introduction and annealing out of the defect center.

A second hole trap, H5, is introduced with an energy level of 0.52 eV. Contrary to the beneficial effect of annealing on H4, the H5 defect density grows with increasing annealing time. This could be associated with the overall permanent degradation of the cell. H5 is considered to be a point-defect-impurity complex such as a phosphorous vacancy-zinc bond or a phosphorous interstitial-zinc bond. H4 is considered to be a point defect such as a phosphorous vacancy or phosphorous interstitial [Ref. 10].

Consistent with the findings of references 5, 6, 10, and 31, two trap levels were observed: H4 at a level of approximately 0.32 eV, and H5 at a level of 2.54 eV. As shown in Figure 6-2, H4 trap concentration increases with each irradiation, and decreases with each subsequent annealing. The higher level trap, H5, initially decreases with annealing but then grows with the second annealing cycle. It is believed that this trap will continue to grow with subsequent annealing, is indicated in on previous research. [Ref. 17, 18]

These concentrations seem to indicate that solar cell recovery is affected mainly by the H4 trap while the overall permanent degradation of the cell is associated with the high level H5 trap. In thermally diffused junction InP cells, damage introduced by irradiation anneals at room temperature [Ref. 17-19], and is also attenuated by higher impurity doping levels [Ref. 32:p. 211]. It has been reported that radiation damage in this material can be annealed by solar photons as low temperature minority carrier injection [Ref. 11]. This is a very attractive feature in any operational solar array, in that orbital environmental conditions would passively provide incident photons, at room temperature, and would thus anneal damaged InP cells, with no additional design modification.

The primary difficulty in studying thermally diffused InP junctions is the annealing response of these junctions to any energy introduced to measure cell performance. In order to determine radiation induced degradation, the cell must be exposed to simulated solar illumination. The illumination is capable of annealing the cell, introducing a degree of uncertainty in the true I-V degradation of the irradiated sample. To avoid inadvertant sample annealing (observation annealing), the irradiated samples were held at 86 K during post-radiation I-V measurements. DLTS analysis run before and after an I-V measurement at 86 K, indicated no trap density variation at this temperature. Repeated I-V measurements at

86 K demonstrated no change in solar cell parameters, verifying that accidental annealing was successfully avoided.

A similar difficulty exists in the measurement of minority carrier trapping centers by DLTS. Detection of minority traps by DLTS requires that minority charge carriers be injected into the depletion region. This is usually achieved by applying a forward bias fill pulse to the sample. The fill pulse, however, establishes a current flow at the junction, which causes injection annealing of the defect spectrum. To avoid this form of observation annealing, pulsed laser excitation is used to create electron-hole pairs in the depletion region. "The forward Fill pulse is replaced with an optical pulse focused onto the sample. Provided the optical pulse is absorbed by the semiconductor [this requires an appropriate combination of photon energy and energy gap], minority carriers will be generated. Minority carriers collected by the barrier field, which is maintained by the constant reverse bias, are available for capture and emission and so can be exploited for DLTS signal processing." [Ref. 33] These pairs are quickly separated by the junction electric field, leaving the minority carriers available for capture at defect sites.

The laser excitation unit mounts directly on the cryostat window, and permits detection of minority trapping centers without inadvertently annealing the sample. "Practical implementation of this laser excited DLTS technique is termed

Minority Carrier Trap Spectroscopy (MCTS). It is fully automated in the sense that the laser unit timing is fed from the main DL4600 unit. When the DLTS mode of the S4600 system is switched to MCTS, the diode, which is connected in the normal way, receives only the quiescent reverse bias required for the measurement phase. The logic drive and timing sequence normally used to generate the forward bias pulse now triggers the laser." [Ref. 33]

C. EXPERIMENTAL PROCEDURE AND RESULTS

In order to mount the cell in the DLTS cryostat, it was necessary to reduce them in size using the same score and cleave technique applied for the GaAs samples. The final size of the InP samples was 0.4 x 1.0 cm, after scoring in only one direction: parallel to the electrical contact metal fingers. However, the electrical contacts on the InP samples are not strongly bonded to cell surface, and many of the contact fingers were bent and dislodged from the cell face. The loss of current carrying grid occurred frequently on all InP sized samples and resulted in a greatly degraded fill factor and efficiency, similar to an series resistance introduced by edge-effects from sample cutting. This precluded effective use of changes in efficiency and fill factor, restricting sample performance evaluation to measuring changes in open circuit voltage (V_{oc}), short circuit current (I_{sc}) and maximum power (P_{max}). These parameters were normalized to initial (pre-irradiation) values, and are

presented, plotted as results, in the following discussion. The very weak structural behavior of the metalization grid bonding is, apparently, a common problem in InP solar cells. The delicate mechanical behavior of the contact grid results in a very high loss rate when InP solar cells are handled for any reason.

The I-V measurements were made under one-sun, AMO conditions at 86 K. The equipment used was the same as described in Chapter V, section C. DLTS measurements were made with a -2 volts reverse bias in order to provide an adequate fill pulse, as described in Chapter IV. The InP samples were exposed to 1 MeV electron fluences of up to 1E16 electrons/cm^2, to exploit the high theoretical radiation tolerance inherent in this material. This dose was selected to make radiation degradation and annealing recovery readily apparent.

After the sized samples were tested by I-V measurements to verify performance, a baseline DLTS analysis was conducted before irradiation. This reference spectrum indicated one minority carrier trapping center , the dashed line in Figure 6.2, but, no majority carrier trapping centers were apparent. The activation energy of this minority trap was found to be about 0.32 eV below the conduction band. This energy corresponds well with the defect labeled ED measured in electron irradiated MOCVD InP, [Ref. 18:p. 6489], and is believed to be the same.

The defect spectrum induced by 1 MeV electron irradiation is indicated by solid lines in Figure 6.2. The electron fluence was 6E15 cm^{-2} . With the exception of the relatively weak EE and EF defect signals, this spectrum is identical to that measured in irradiated MOCVD InP [Ref. 17:p. 4204]. These spectra show a clear correlation between the pre-radiation minority trap, and the ED defect. Note that the signal of trap H5 and of all minority traps is multiplied by a factor of 10, to make them more visible. Also, since the negative DLTS signal of H5 is more evident after removal of the positive bias signal, the minority trap spectrum shown was measured on a cell which had been annealed at 500 K, with AMO 1 sun illumination, for 60 minutes. The EA, EC, and ED defect centers were evident after irradiation, before annealing. The EE, and EF centers were not detected until the H4 and H5 centers had been substantially annealed. Since the EE and EF signals are weak, and located directly below the H4 and H5 spectrum peaks, respectively, their detection is difficult. The spectrum of the defect labeled H3 is too close to that of H4 center, and is thus difficult to distinguish.

The first experiment was an isochronal annealing . A 40 mm^2 size InP sample was exposed to a 1 MeV electron fluence of 1E15 cm^{-2}, and illuminated with one-sun, AMO light for one minute intervals, at increasing temperatures. During illumination, the cell was short-circuited through an ammeter. After each illumination, the majority carrier defect

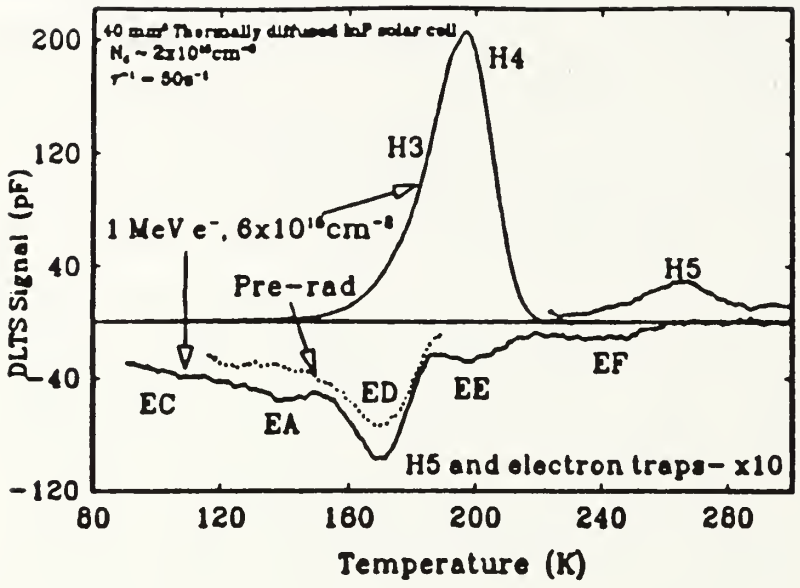

Figure 6-2. Radiation induced defects in thermally diffused InP. The H5 and minority carrier trap signal is multiplied by ten.

DLTS spectrum ,and I-V curve, was measured at 86 K. The results are shown in Figures 6-3 and 6-4. The height of the DLTS peak is directly proportional to the defect concentration. The photovoltaic parameters of Figure 6-3 are shown normalized to their pre-radiation values, and the H4 peak is normalized to its maximum , post-radiation value. V_{oc} was unaffected by this irradiation (1E15). P_{max} and I_{sc} degradation was slight after the first irradiation with clear annealing recovery at 175 K, during which the H4 peak essentially disappeared.

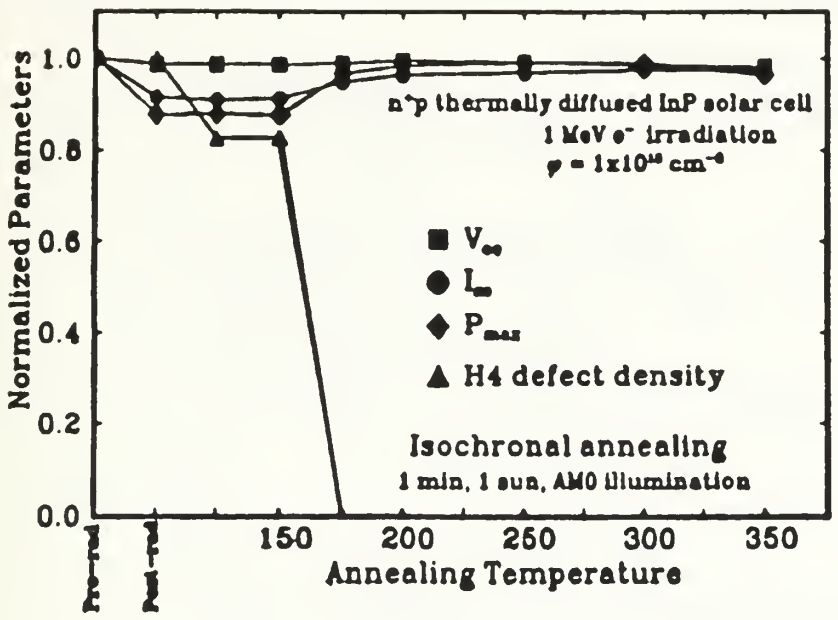

Figure 6-3. The annealing induced by solar illumination in an InP sample. Cell parameters are normalized to their pre-radiation values. Defect density is normalized to maximum.

The second experiment was isothermal photo-injection annealing of a sample exposed to a 1 MeV electron fluence of 3E15 cm^{-2} , illuminated at 225 K. I-V curves, and both the majority and the minority trap spectra were measured at 86 K. The DLTS results are shown in Figure 6-7. Irradiation degraded V_{oc} from 1.198 V to 1.151 V; followed by no observable recovery from photo-injection. The eight percent radiation induced degradation in I_{sc} recovered fully after one hour of annealing at 225 K, with AM0 one sun illumination. This hour of illumination almost completely removed the H4

defect. However, the concentration of defect H5 was unaffected by this annealing.

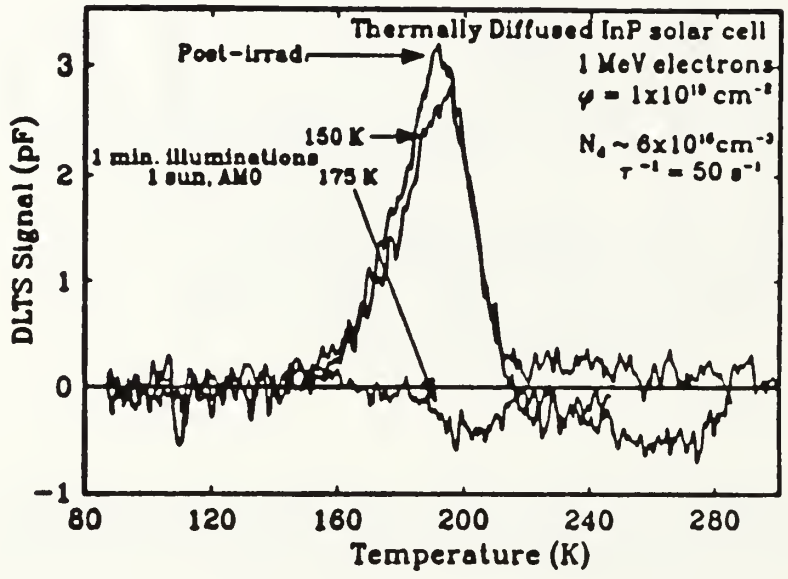

Figure 6-4. The photo-injection annealing of the H4 defect in the InP solar cell depicted in Figure 6-3.

Another isothermal annealing experiment was conducted on a sample that had been exposed to a fluence of 1E16 cm^{-2}. Annealing illumination was provided at 275 K, for a cumulative period of 4.25 hours. For the first 25 minutes of annealing, the sample demonstrated steady recovery in all parameters. The recovery continued at a much slower rate after the first 25 minutes, indicating an asymptotic limit to annealing recovery. To investigate a possible recovery limit, after 4.25 hours of one sun illumination at 275 K, the temperature was raised. Illumination for 30 minutes at 300 K, and 60

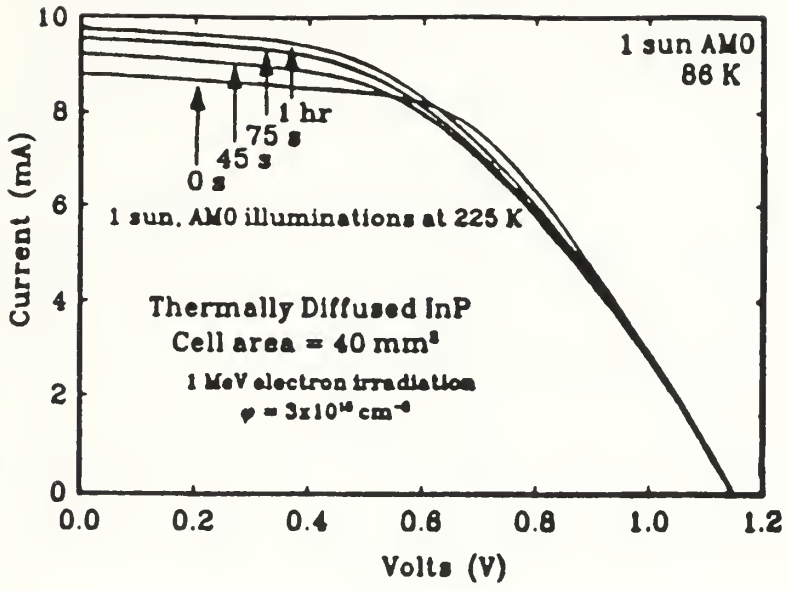

Figure 6-5. The isothermal, photo-injection annealing of the I-V curves of an electron irradiated InP solar cell. Note the increase in I_{sc}, but not in V_{oc}.

minutes at 373 K, caused further recovery in V_{oc} , but no improvement in I_{sc}. Illumination for one hour at 475 K resulted in dramatic improvement in the I-V curve. This recovery was accompanied by complete removal of all majority traps, and a reduction in minority trap concentration, Figure 6-7. Annealing attempts at 450 K were considered the most successful; in one hour of illumination provided complete recovery at this temperature. Illumination at 500 K showed a possible recovery in I_{sc}, but the sample failed before concluding a second annealing attempt. Sample failure at 500 K was caused by mechanical destruction of the electrical

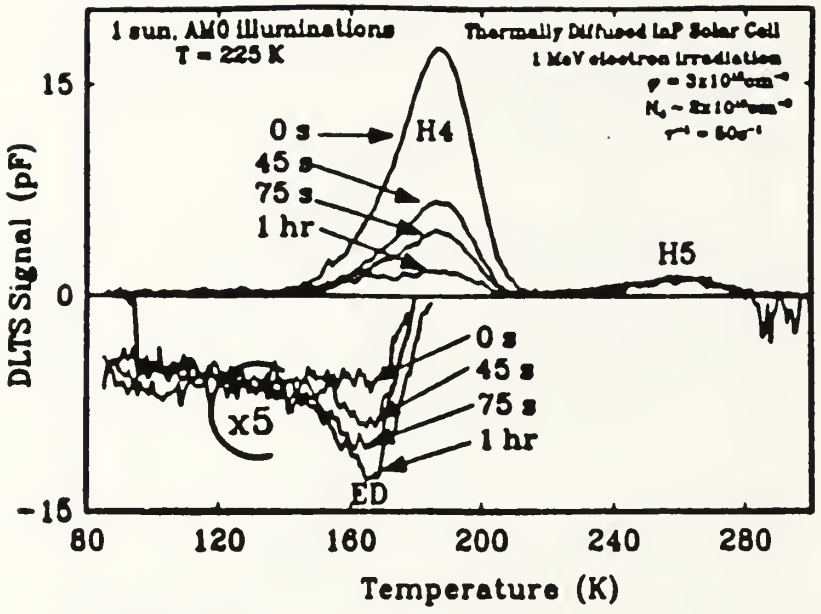

Figure 6-6. The photo-injection annealing of the DLTS spectra of the InP cell of Figure 6-5. The H4 defect concentration decreases, but H5's in unchanged.

contacts, not 500 K thermal exposure for annealing.

Figure 6-8 shows the complete sample history. InP solar cell exposure to a 1 MeV electron fluence of $1x10^{16}$ cm^{-2} caused severe degradation to all photovoltaic parameters. Photo-injection annealing at successively higher temperatures resulted in improved annealing. Note that good, not complete, recovery was achieved at 373 K , which is an acceptable upper temperature limit for a solar array in synchronous orbit. This result alone makes InP extremely attractive for spacecraft applications. Full I-V curve recovery was achieved with one hour of illumination, at 450 K.

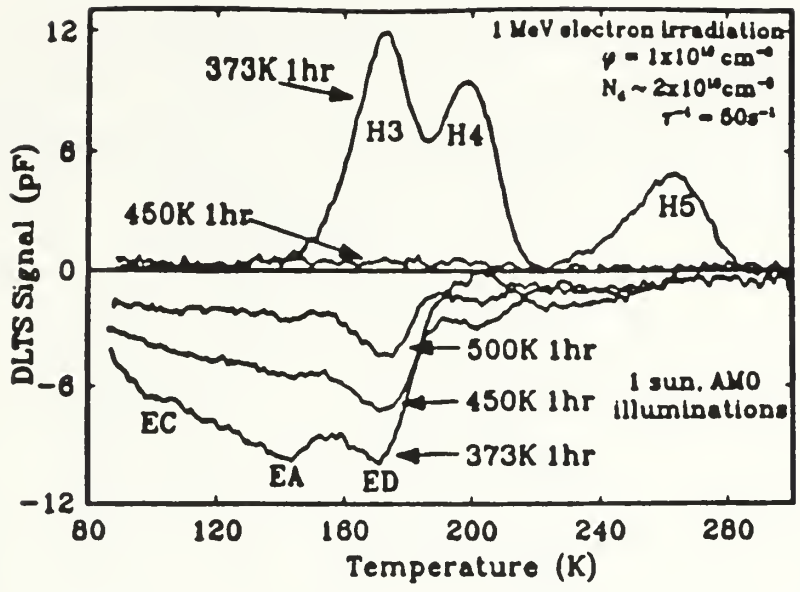

Figure 6-7. The annealing of an InP cell. Illumination at 450 K removed all of the majority carrier traps. The 500 K illumination further reduced the minority carrier traps.

The results of this annealing study indicate that radiation damaged, thermally diffused junction InP solar cells will recover their photovoltaic parameters when a current is established in the depletion region. Annealing occurs through a thermally activated process in which electron-hole recombination induces defect annealing, which causes recovery in the cell's PV parameters. Figures 6-2 and 6-3 support the conclusions of Yamaguchi that the H4 defect is the controlling trap, [Ref. 31]. However, the annealing behavior reported in reference 31 differs from the results found here in the positions of the negative peaks in the spectra, and in the behavior of the minority carrier trapping centers. While the

dramatic recovery in cell performance can be related to annealing of the H4 defect, the effect of the minority carrier traps on the asymptotic recovery limit remains unknown. After H4 is annealed out, the minority carrier traps effects dominate, and have a significant effect on complete solar cell recovery.

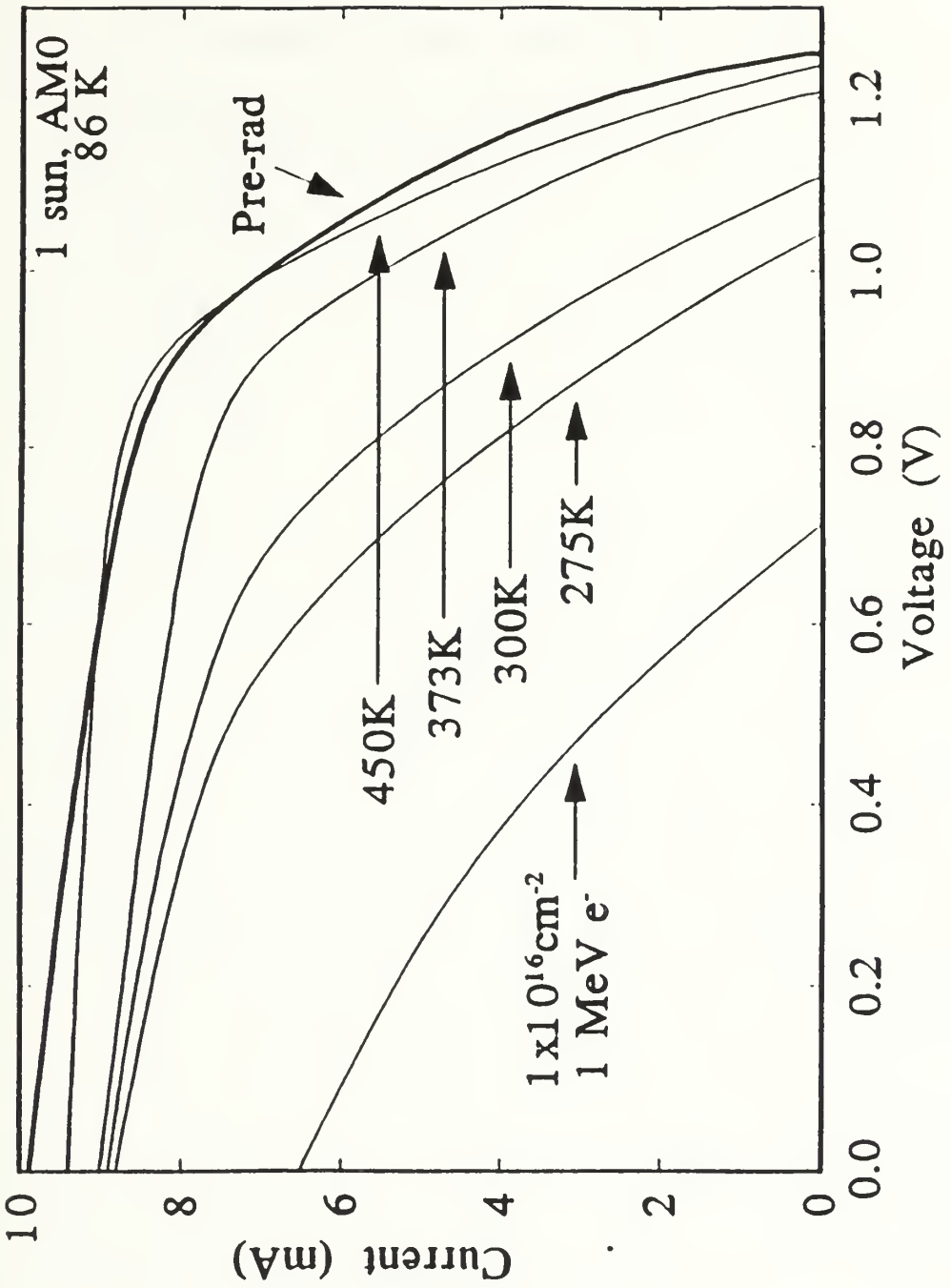

Figure 6-8. The full history of the InP cell depicted in Figure 6-7. Although 1 MeV electron irradiation almost destroyed the cell, photo-injection by illumination caused almost full recovery.

VII. CONCLUSIONS AND RECOMMENDATIONS

The significant crystallographic differences between GaAs/GaAs and heterojunction GaAs/Ge cannot be underestimated when investigating the lattice response to radiation damage. However, the premise that an effective analysis of solar cell radiation damage recovery demands an extensive understanding of the solid-state mechanisms of defect annealing is erroneous. The actual details of defect concentration growth and recovery may be of great interest to research physicists, but provide little information on the actual power losses in an orbiting spacecraft solar array. The quantum-electrodynamic behavior of lattice defects is not directly relevant to solving the power recovery problem in space quality solar cells. The economic constraints of spacecraft design severely limit the practical methods that can be applied to correct power loss. Investigating the mechanisms of defect growth may lead to improved solar cells, but will not immediately provide a solution to radiation damage. More specifically, defect annealing at 500 K is of little consequence in an application where 400 K is catastrophically excessive. The extremes of temperature and forward bias current density explored in this experiment are a good example of research in pursuit of results.

DLTS is an excellent tool for investigating defect behavior. However, cutting samples to the tiny sizes necessary to fit into a cryostat resulted in unacceptable damage to the cells; from introduced edge-defects, destroyed contact grids, and excessive handling. Use of DLTS equipment forced this experiment away from simple solar cell IV performance analysis, into a program of photovoltaic diode research not anticipated. Simply using DLTS consumed valuable solar cells, and weeks of time in learning to operate the equipment.

The poor results for the GaAs cells studied here should not preclude further investigation of this popular material. Two important sources of error here may be masking the true potential of GaAs. The first is the significance of the edge defects introduced when the samples were sized. Pre- and post-radiation IV measurements seemed consistent with expected sample behavior. The actual complication of radiation damage to junctions with these edge effects must be considered. Secondly, better recovery may be obtained by smaller increments of radiation exposure (1E14) and annealing, for many cycles. This would more realistically model the orbital life of applying annealing to a solar array.

Indium phosphide's excellent damage recovery behavior in the laboratory does not outweigh its more mundane limitations. The extremely high mechanical losses experienced during handling indicate that this material is not adequately

developed for routine spacecraft use, even if it were available. Also, even if InP were economically competitive with GaAs on a power output basis, solar array assembly losses would quickly make their flight cost prohibitive.

In considering the desired properties of a solar array, full life-cycle cost assessment must be applied. The employment of photovoltaic arrays should always be considered from an end-of-life power, and a panel weight ratio comparison. This is especially true for replacing silicon solar arrays with GaAs technology. "GaAs/Ge solar cell cost and weight are still a concern, even with significant increases in power per unit area. The cost of producing GaAs/Ge solar cell assemblies can be 5 to 6 times the cost of silicon cells. These penalties are reduced, or eliminated, at the solar array panel, or systems, level." [Ref. 34:p. 1423]

The potential savings, in both cost and spacecraft mission, of solar cell annealing are too great to overlook. Further investigation of the annealing properties of GaAs and InP should be pursued. Investigators should restrict their efforts to studying full size solar cells. Research in the annealing behavior of solar cells should begin with commercially available material (GaAs/Ge), subjected to orbital environment conditions, measured for the photovoltaic properties of interest, and annealed using realistically achievable conditions. That is, simple annealing currents of 0.5 A/cm^2, at 100 centigrade, for a few hours. Power output,

i.e. IV performance, should be the only measurement of interest for solar array engineering applications. Finally, thermal annealing, at low fluence exposures, for a high number of cycles, may be the most realistic solution for the growing GaAs/Ge market.

REFERENCES

1. JPL Publication 43-48, *Solar Cell Array Design Handbook Vol. 1*, October 1976.

2. Summers,G.P., *Displacement Damage: Mechanisms and Measurement*, IEEE Nuclear and Space Radiation Effects Conference Short Course, July 1992.

3. Agrawal, B.N., *Design of Geosynchronous Spacecraft*, Prentice-Hall, 1986.

4. Applied Solar Energy Corporation, *Space Products Catalog*, 1991.

5. Cypranowski, C., *Power Recovery of Radiation-Damaged Gallium Arsenide and Indium Phosphide Solar Cells*, Master's Thesis, Naval Postgraduate School, Monterey, CA, December 1989.

6. Pinzon,D., *Analysis of Radiation Damaged and Annealed Gallium Arsenide and Indium Phosphide Solar Cells Using Deep Level Transient Spectroscopy Techniques*, Master's Thesis, Naval Postgraduate School, Monterey, CA, March 1991.

7. JPL Publication 82-69, *Solar Cell Radiation Handbook*, Third Edition, November 1982.

8. Dalven, R., *Introduction to Applied Solid State Physics*, Plenum Press, 1980.

9. Kittel, C., and Kroemer,H., *Thermal Physics 2nd edition*, W.H. Freeman and Company, San Francisco (1980).

10. Walters, R.J., Messenger, S.R., Summers,G.P., Burke, E.A., Keaveny, C.J., *Proton and Electron Irradiation of Mocvd InP Solar Cells: Experimental Results and Modeling*, Twentythird IEEE Photovoltaic Specialists Conference, pp. 210-216, 1991.

11. Walters, R.J., *DLTS Study of Electron Irradiation Induced Defects in MOCVD Grown n^+p InP*, Master's Thesis, University of Maryland, Baltimore County, June 1990.

12. Sze, S.M., *Physics of Semiconductor Devices*, John Wiley and Sons, 1081.

13. Loo, R., Knechtli, R.C., Kamath, G.S., *Enhanced Annealing of GaAs Solar Cell Radiation Damage*, Fourteenth IEEE Photovoltaic Specialists Conference, pp. 33-37, 1981.

14. Lang, D.V., *Deep-Level Transient Spectroscopy:A New Method to Characterize Traps in Semiconductors*, Journal of Applied Physics, Vol. 45, No. 7, July 1979.

15. Sheng, S. Li, Wang, W.L., Lou, R.Y., and Rahilly, W.P., *Deep Level Defects and Annealing Studies in One-MeV Electron Irraditaited (AlGa)As - GaAs Solar Cells*, Sixteenth Photovoltaic Specialists Conference, pp. 211-215, 1982.

16. Mayes, I.C., and Robinson, M.N., *Introduction to Deep Level Transient Spectroscopy*, BioRad Semiconductor Corp. Notes, Note N0. 410, May 1987.

17. Messenger, S.R., Walters, R.J.,Summers,G.P., *The Effect of Carrier Concentration on the Properties of Irradiation Induced Defects in p-type InP Grown by MOCVD*, Journal of Applied Physics, Vol. 71, No. 9, May 1992.

18. Walters, R.J.,and Summers,G.P., *DLTS Study of Proton Irradiated p-type InP*, Journal of Applied Physics, Vol. 69, May 1991.

19. Keaveny, C.J., Walters, R.J., Drevinskiy, P.J., "Optimizing the Radiation Resistance in InP Solar Cells: The Effect of Dopant Density and Cell Thickness," paper submitted to the Journal of Applied Physics, March 1992.

20. Rahilly, W.P., *Radiation Effects in Solar Cells*, pp. 365-385, Wright Patterson Aeronautics Laboratory, 1980.

21. Chu, C., Isles, P.A., Yoo, H., Reed, B., Krogen, J., *Recent Technology Advances in Large Area, Lightweight GaAs/Ge Solar Cells*, Twentyfifth IEEE Photovoltaic Specialists Conference, pp. 1512-1517, 1991.

22. Chung, M.A., Meier, D.L., Szedon, J.R., and Bartko, J., *Electron Irradiation and Annealing of MOCVD GaAs and GaAs/Ge Solar Cells*, Twentysecond IEEE Photovoltaic Specialists Conference, pp. 924-929, 1988.

23. Chang, K.I., Yeh, Y.C.M, Isles, P.A., Tracy, J.M., Morris, R.K., *Heterostructure GaAs/Ge Solar Cells*, Nineteenth IEEE Photovoltaic Specialists Conference, pp. 273-279, 1987.

24. Weinberg, I., Swartz, C.K., Hart, R.E., Statler, R.L.,*Radiation and Temperature Effects In Gallium Arsenide, Indium Phosphide, and Silicon Solar Cells*, Twentyfirst IEEE Photovoltaic Specialists Conference, pp. 548-557, 1987.

25. Pons, D., *Charge State Effects on the Annealing of the Electron Irradiation Induced Defects in GaAs*, Institute of Physics Conference, Ser.No. 59, p. 269, 1981.

26. Peaker, A.R., *Defect Energy Levels in Electron Irradiated GaAs*, EMIS Datareview, RN=15443, December 1985, pp.13.10.

27. Barry, A.L., Maxseiner, R., Wojcik, R., Briere, M.A., Braunig, D., *An Improved Displacement Damage Monitor*, IEEE Transactions on Nuclear Science, Vol. 37, No. 6, December 1990. pp.1726-1730.

28. Mizuguchi, K. ,et al, *MOCVD GaAS Growth on Ge (100) Substrate*, International Symposium on GaAs and Related Compounds, Karuizawa, Japan, 1985.

29. Isles, P., "Reverse Breakdown Testing", Applied Solar Energy Corporation internal memorandum, 1989.

30. Carter,C.B., et al, *Characterization of APBs in GaAs Grown on Si and Ge*, Proceedings of the Materials Research Society Symposium, 1987.

31. Yamaguchi, M. and Ando, K., *Mechanism for Radiation Resistance of InP Solar Cells*, Journal of Applied Physics, vol. 63, No. 11, June 1988.

32. Walters, R.J., Keaveny, C.J., Messenger, S.R., Summers, G.P., *The Effect of Dopant Density on the Radiation Resistance of MOCVD InP Solar Cells*, Twentyfifth IEEE Photovoltaic Specialists Conference, pp. 211-215, 1991.

33. BioRad, *Applications of the Laser Excitation Unit*, BioRad Laser Excitation Unit, DL4930, Instruction Manual, 1990.

34. Datum, G.C., Billets, S.A., *Gallium Arsenide Solar Arrays - a Mature Technology*, Twentyfifth IEEE Photovoltaic Specialists Conference, pp. 1422-1428, 1991.

INITIAL DISTRIBUTION LIST

Defense Technical Information Center Cameron Station Alexandria, VA 22304-6145	2
Library, Code 52 Naval Postgraduate School Monterey, California 93943-5002	2
Prof. Sherif Michael, Code EC/Mi Department of Electrical and Computer Engineering Naval Postgraduate School Monterey, California 93943-5000	2
Prof. I. M. Ross, Code AA/Ro Department of Aeronautics and Astronautics Naval Postgraduate School Monterey, California 93943-5000	1
Chairman, Code AA/Co Department of Aeronautics and Astronautics Naval Postgraduate School Monterey, California 93943-5000	1
Space Systems Academic Group CDR Wade Duym, Code 31 Naval Postgraduate School Monterey, California 93943-5000	1
Dr. Peter Isles Applied Solar Energy Corporation 15251 E. Don Julian Road City of Industry, California 91749	1
LT Joseph A. Bruening 472 Scarborough Lane Painsville, Ohio 44077	3